Generation and characterisation of human cortical interneurons reporter stem cell lines

Thesis submitted for the degree of Doctor of Philosophy

School of Biosciences

Cardiff University

María Concepción Cruz Santos

November 2019

STATEMENT 1
This thesis is being submitted in partial fulfilment of the requirements for the degree of PhD

Signed _____
Date _____

STATEMENT 2
This work has not been submitted in substance for any other degree or award at this or any other university or place of learning, nor is it being submitted concurrently for any other degree or award (outside of any formal collaboration agreement between the University and a partner organisation)

Signed _____
Date _____

STATEMENT 3
I hereby give consent for my thesis, if accepted, to be available in the University's Open Access repository (or, where approved, to be available in the University's library and for inter-library loan), and for the title and summary to be made available to outside organisations, subject to the expiry of a University-approved bar on access if applicable.

Signed _____
Date _____

DECLARATION
This thesis is the result of my own independent work, except where otherwise stated, and the views expressed are my own. Other sources are acknowledged by explicit references. The thesis has not been edited by a third party beyond what is permitted by Cardiff University's Use of Third Party Editors by Research Degree Students Procedure.

Signed _____
Date _____

WORD COUNT _____

(Excluding summary, acknowledgements, declarations, contents pages, appendices, tables, diagrams and figures, references, bibliography, footnotes and endnotes)

Acknowledgments

First, I would like to thank deeply to my supervisor Meng for giving me the opportunity of doing my PhD in her laboratory. Thanks for supporting me since the very first moment that I decided to apply for the scholarship for my PhD studies. I am grateful for her continuous guidance, open door policy and uncountable discussions that always enriched my view in my field of study.

I thank to the Mexican government, which through CONACYT (Consejo Nacional de Ciencia y Tecnología) provided the scholarship 410994 to carry out my PhD.

I would also like to thank to all members in the lab for creating such a great environment for doing science and being always willing to help. I specially thank to Lucía for helping me in my adaptation to the lab, for being there for discussing ideas and her friendship.

Along the years, I have been so lucky to find extraordinary mentors that have nourished my scientific curiosity and without their help, I would have never pursued PhD studies. Thereby I express here my gratitude to the teacher who lighted my interest for sciences, Camelia Hernandez, the teachers who well prepared me for going to university: Fernando Sanchez, Angeles Galan and Arnoldo Bernal. I also thank to my university professors who encouraged me to do post-graduate studies Dr. Guadalupe García and especially to Dr. Juan Riesgo who gave me the first opportunity to experience a research laboratory. Thanks both for your invaluable help in crucial moments.

I finally would like to thank to my family because our history and evolution have made us strong to move forward chasing our goals. Thanks to my siblings, nephews my brother in law but especially to my parents for giving me opportunities that we would have never imagined possible for me. This is to my parents: Isabel and the memory of my father Nicolás.

Abstract

Cortical interneurons are GABAergic inhibitory neurons localised in the cerebral cortex where they establish local connections and regulate the excitatory/inhibitory input onto cortical networks. Cortical interneuron dysfunction is thought to underlie the aetiology of neurodevelopmental disorders (NDDs), such as autism, schizophrenia and epilepsy.

The ability of human pluripotent stem cells (hPSCs) to give rise to any cell type of the body make them a valuable tool to study cell fate specification. Moreover, they can provide an unlimited source of interneuron populations for diseases modelling, drug screening and regenerative medicine purposes. Nonetheless, such application can be greatly benefited by the generation of reporter cell lines that allow the identification of specific cell types, which in turn can facilitate the development of better differentiation protocols.

This thesis reports the generation of a LHX6-mCherry/PV-GFP reporter cell line for tracking hPSC-derived cortical interneurons. The reporter cells can readily acquire medial ganglionic eminence (MGE)-like identity upon in vitro differentiation, with mCherry signal restricted to the MGE lineage and faithfully labels LHX6^{+} cells. These findings validate the potential of this reporter line as a useful tool for future investigations into potential MGE-fate determinants and interneuron subtype specification. However, the poor efficiency in generating parvalbumin^{+} neurons limited the functional verification of the PV-GFP reporter.

I then exploited the LHX6-mCherry reporter cells in an investigation of TGFβ signalling in cortical interneuron development. Pharmacological inhibition of this pathway keeps the MGE-like cells as progenitors through prolonging the cell cycle, while the addition of exogenous TGFβ3 accelerated mCherry^{+} cells production (postmitotic-cells). These findings unravelled a novel function of TGFβ signalling in controlling the balance between MGE-like progenitor maintenance and neuronal differentiation.

Table of Contents

List of figures

List of tables

List of abbreviations

5HT3aR$^+$	Serotonin receptor
ANR	Anterior neural ridge
APC	Adenomatous polyposis coli protein
ASD	Autism spectrum disorders
BDNF	Brain-derived neurotrophic factor
BMP	Bone morphogenetic protein
Cas9	CRISPR-associated protein 9
CCI	Cell cycle inhibitors
CGE	Caudal ganglionic eminence
ChAT	Choline acetyltransferase
CNV	copy number variation
CR	Calretinin

CRISPR	Clustered regularly interspaced short palindromic repeats
DKK	Dickkopf proteins
FGF	Fibroblast growth factor
FZD	Frizzled proteins
GABA	Gamma-aminobutyric acid
GDF	Growth and differentiation factor
GF	Growth fraction
GFP	Green Fluorescent protein
Gli	Glioblastoma proteins
gRNAs	Guide ribonucleic acid
GSK3	Glycogen synthase kinase 3
HA	Homology arms
hESCs	Human embryonic stem cells
hPSCs	Human pluripotent stem cells
iGNs	Induced GABAergic neurons
iNs	Induced neurons
iPSCs	Induced pluripotent stem cells
Lef	Lymphoid enhancing factor
LGE	Lateral ganglionic eminence
LPR	Lipoprotein receptor-related protein
MGE	Medial ganglionic eminence
MIS	Mullerian inhibiting substance
MSN	Striatal medium spiny neurons
NDDs	Neurodevelopmental disorders
PM	Purmorphamine
Ptc1	Patched 1

PV	Parvalbumin
RA	Retinoic acid
Rock	Rho-associated kinase
SARA	Smad anchor for receptor activation
sFRPs	Secreted frizzled related proteins
SHH	Sonic hedgehog
Smo	Smoothened
SST	Somatostatin
t_c	Cell cycle length
Tcf	T-cell factor
TGFβ	Transforming growth factor β
Tle	Transducin-like enhancer protein
t_s	S-phase length
TβR	Transforming growth factor beta receptor
VIP	Vasoactive intestinal peptide
WIF	Wnt inhibitory factors

1. Introduction

1.1 Cortical interneurons and neurodevelopmental disorders

1.1.1 Cortical interneuron diversity

The neocortex is the brain region where the higher specialised functions are processed. It is assembled by cortical networks built up by cortical glutamatergic projection neurons (excitatory neurons, also known as pyramidal neurons), which transmit information from different regions of the neocortex and other brain regions. On the other hand, cortical interneurons possess axons that branch within the cortex, known as local projections, where they function to establish connections between different neuronal types to modulate network activity (Marin, 2012; Tremblay et al., 2016). Most cortical interneurons use GABA (Gamma-Aminobutyric Acid) as neurotransmitter, and hence, they are inhibitory neurons.

The inhibitory function of cortical interneurons enables them to modulate the responses of pyramidal cells to input signals, preventing over-excitation of cortical circuitries and synchronising oscillatory activity (Tremblay et al., 2016). Although all of cortical interneurons release GABA, they are diverse in morphology, connectivity and electrophysiological properties as well as in the expression of cellular markers (Kelsom and Lu, 2013; Marin, 2012; Tremblay et al., 2016). All this diversity underlies differences in synaptic kinetics and intrinsic membrane properties, which in turns results in a highly precise spatiotemporal control of the activity of local networks.

The expression of cellular markers have provided a good starting point to classify interneurons diversity, since three main interneuron types account for nearly the totality of GABAergic interneuron population in the mouse neocortex (Kelsom and Lu, 2013; Tremblay et al., 2016). These interneurons types are: parvalbumin (PV^+), somatostatin (SST^+) and serotonin receptor ($5HT3aR^+$) expressing interneurons. From these three virtually non-overlapping interneurons populations, PV^+ and SST^+ represent around 70% of total interneurons (Wamsley and Fishell, 2017), while PV^+ type constitutes 40% of the total GABAergic interneurons (Kelsom and Lu, 2013).

In addition to biochemical markers, interneurons are further classified in terms of their morphology. In case of PV^+ interneurons, two different morphologies can be distinguished: basket cells and chandelier cells, the former is characterised by targeting the soma and proximal dendrites of pyramidal neurons, while the later targets the initial axonal segment. SST^+ are subdivide into Martinotti and non-Martinotti cells. The Martinotti cells are found through cortical layers II and VI being especially abundant in layer V. The non-Martinotti reside in all cortical layers. Both of them target dendrites and function to facilitate excitatory inputs. A proportion of SST^+ also expresses calretinin (CR^+) (Kelsom and Lu, 2013).

The $5HT3aR^+$ group is especially heterogeneous but the co-expression of other proteins of neuropeptides allows their classification into two main subgroups. One subgroup expressing the vasoactive intestinal peptide (VIP^+) accounting for 40% of $5HT3aR^+$ cells, which is characterised for connecting onto dendrites, and largely co-express with CR. The remaining 60% of $5HT3aR^+$ interneurons is formed by a subgroup that does not express VIP and most of them express $reelin^+$. Within this subgroup, neuroglial form interneurons are distinguished by their ability for making synapses with other interneurons from the same subtype as well as with other interneuron types (Kelsom and Lu, 2013; Wamsley and Fishell, 2017).

The properties of the main interneuron classes including morphology, synaptic targets, distribution, electrophysiological properties and expression of other markers, are summarised in Figure 1.1. All these properties account for the identification of interneuron subtypes, which emerge from transient embryonic regions known as ganglionic eminences in the developing ventral telencephalon (Hansen et al., 2013; Lavdas et al., 1999; Ma et al., 2013). PV and SST subtypes represent between the 5 to 7% of total neurons in rodents and are derived from the medial ganglionic eminence (MGE), whereas CR^+ proportion is three times increased in primates (12 % of total neuronal population) with respect to rodents (4%), and it is largely derived from the caudal ganglionic eminence (CGE), with the exception of those CR^+/SST^+ which are thought to be generated within the MGE (Hladnik et al., 2014).

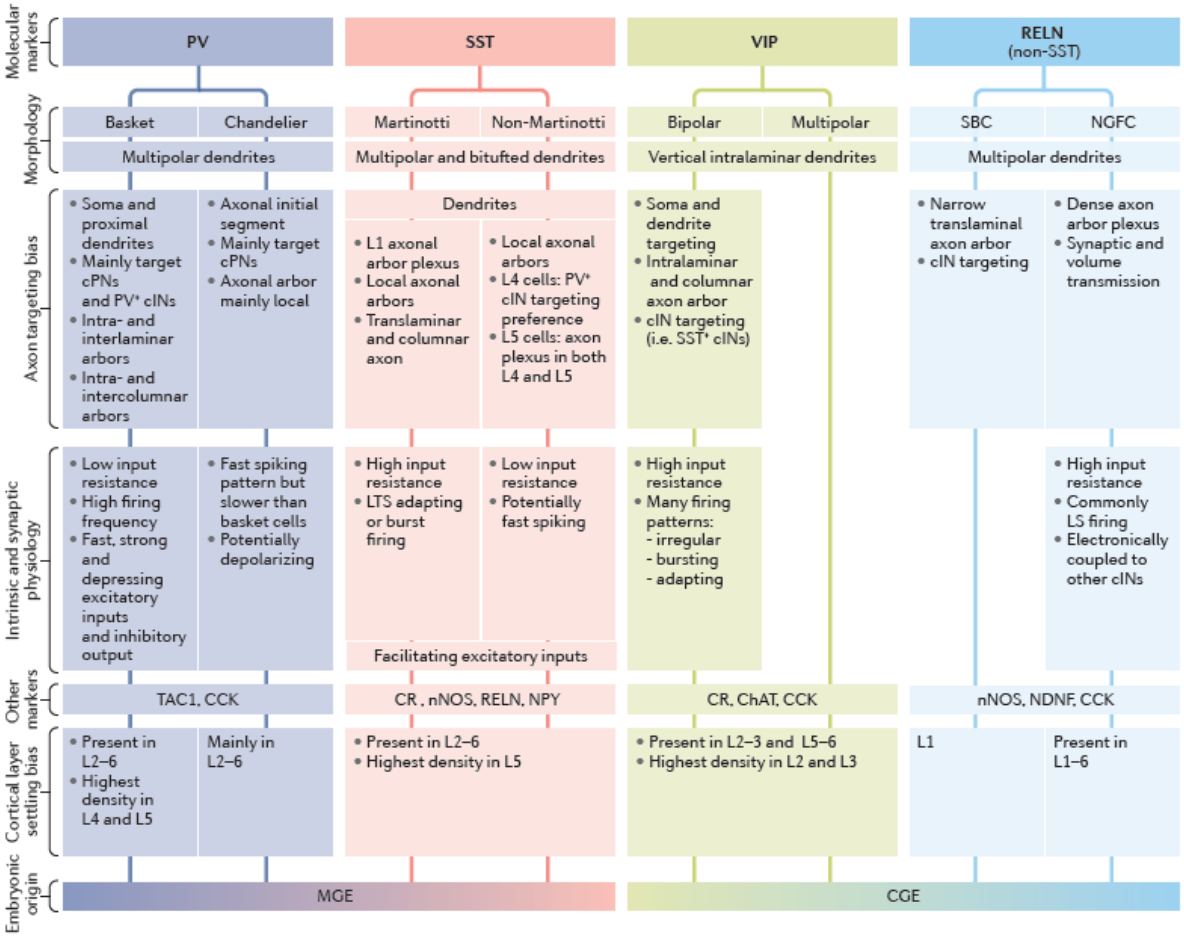

Figure 1.1| Classification of the main classes of cortical interneurons. The first level of classification is by expression of key biochemical markers, which divide cortical interneurons into three virtually non-overlapping populations. These are PV^+, SST^+ and $5HT3aR^+$ (comprising VIP^+ and $Reelin^+$ interneurons) which account for nearly the total number of interneurons. These main interneuron types are further divided into subgroups based on their morphology. These sub-classes show defined properties in terms of their synaptic targets and electrophysiological properties. From Wamsley and Fishell, 2017

1.1.2 Cortical interneuron dysfunction in neurodevelopmental disorders

The abundance and function of cortical interneurons seems to be affected in neurodevelopmental disorders such as autism spectrum disorders, schizophrenia and epilepsy (Del Pino et al., 2013; Filice et al., 2016; Tremblay et al., 2016). For instance, mouse models deficient in genes implicated in cortical interneuron development, such as *Sox6* displays reduction of SST^+ and PV^+ interneurons, defects in their laminar localisation and epileptic phenotypes (Batista-Brito et al., 2009) whereas a *PV*-null mouse recapitulates symptoms of autism spectrum disorders (ASD) in humans such as decreased social interaction, stereotyped behaviours and impairment in communication (Wohr et al., 2015). Another line of evidence comes from the studies of mutant mouse models of the *SHANK* gene family, which codes for scaffolding proteins located in the post-synaptic density of glutamatergic synapses. Mutations in this gene-family have been often found in individuals with schizophrenia and ASD, and decreased expression of *PV* has been found in *Shank1* and *Shank3* null mice that display ASD phenotype (Filice et al., 2016) .

Additionally deletion of *Erbb4* (a gene expressed in migrating cortical interneurons) in PV^+ interneurons resulted in a schizophrenia-like phenotype (Del Pino et al., 2013). These observations, along with interneuron function to dynamically modulate network activity, have suggested a correlation between interneuron dysfunction and clinical features of neurodevelopmental disorders; hence, it has been proposed that severe defects in the function of inhibitory interneurons might cause an instability of cortical networks, which leads to an excitatory/inhibitory impairment. Figure 1.2 illustrates some of defects founds in cortical networks in patients or mouse models of schizophrenia. Many more investigations have related interneuron dysfunction or gene mutations related to interneuron development with neurodevelopmental disorders, which has been summarised by Marin, 2012.

Therefore, the establishment of differentiation protocols to obtain human MGE interneurons *in vitro* hold an enormous potential to study not only the specific mechanisms of interneuron development in humans, but also to serve for modelling neurodevelopmental diseases. Although this research is focused in the study of MGE-derived interneurons due to evidences linking them to neurodevelopmental diseases,

the larger proportion of CGE-derived interneurons found in primates, is suggestive of a possible relevance of CR^+ population, which also should be considered in future studies.

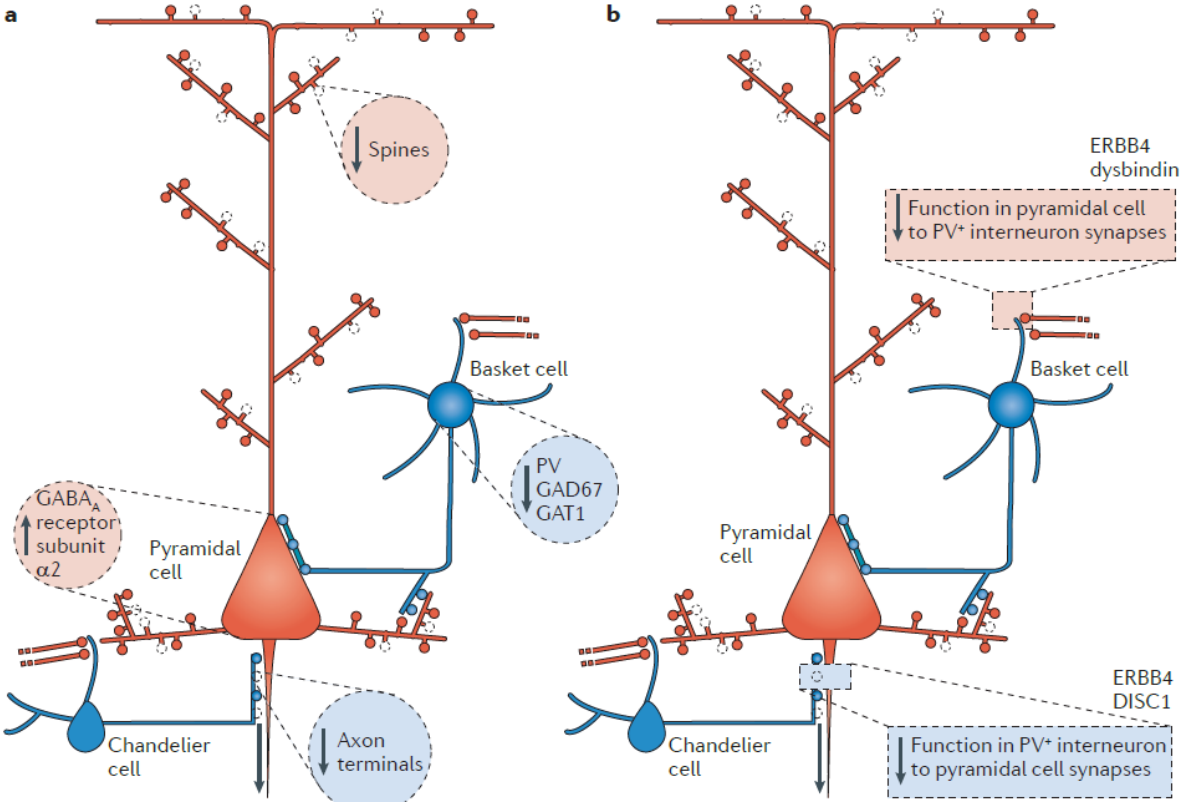

Figure 1.2| Impairments in cortical networks found in patients and animal models of schizophrenia. a) A reduction in GAD67 expression in PV interneurons is often found in this disorder. This reduction may lead to compensatory mechanisms such a reduced mRNA expression of *GAT1*, which encodes a transporter responsible for re-uptaking GABA at synapses. Other compensatory mechanisms could be an increase of GABA receptors onto pyramidal cells as well as a reduced number of spines. b) Interneuron dysfunction in schizophrenia have been related to cell-autonomous impairments in interneuron sub-types, named the presynaptic mechanism or a post-synaptic mechanisms explained by reduction of excitatory inputs to PV^+ interneurons along with a loss of inhibitory drive from PV to pyramidal cells as has been observed in a conditional mutation of Erbb4. Therefore, it is hypothesised that pyramidal cells might be hyperactive and asynchronous in the cortex of schizophrenia-patients. From Marin, 2012.

1.2 Forebrain Development

1.2.1 Emergence of the MGE in the ventral telencephalon

As result of gastrulation in the mammalian embryo, three germ layers are developed: endoderm, mesoderm and ectoderm. From studies in frogs and fish, it has been proposed that ectodermal cells acquire neural identity unless they are exposed to bone morphogenetic proteins (BMP) signalling (Vieira et al., 2010). However, studies in other species suggests that in addition to BMP inhibition, an early signalling of fibroblast growth factor (FGF) is required for the induction of neural fate (Streit et al., 2000; Vieira et al., 2010). After the neural fate is acquired, local signalling leads to the establishment of cell populations known as organizers. This organizers secret morphogens and/or growth factors to orchestrate regional patterning, which leads to the establishment of the anterior/posterior and dorsal/ventral axes in the embryonic neural tube (Vieira et al., 2010).

From the anterior neuroectoderm develops the forebrain or prosencephalon, the embryonic region that gives rise to the telencephalon, where the expression of Foxg1 is initiated around E8.5 (Hebert and Fishell, 2008) by the effect of a group of cells called the anterior neural ridge (ANR), which promotes telencephalic gene expression. The ANR carries out its function by expressing inhibitors of WNT along with active FGF8 and sonic hedgehog (SHH) signalling (Vieira et al., 2010; Wilson and Houart, 2004). As a result of the concerted action of these signalling pathways, transient embryonic structures, named ganglionic eminences are developed at E11.5 in the ventral part of the embryonic telencephalon. These ganglionic eminences are the source of GABAergic interneurons.

1.2.2 Medial ganglionic eminence: the major source of cortical interneurons

The ganglionic eminences are named depending on their localization along the rostral-caudal and dorsal-ventral axes of the subpallium: the medial ganglionic eminence (MGE) located in the rostral-ventral subpallium, the lateral ganglionic eminence (LGE) located in the rostral-dorsal and the caudal ganglionic eminence (CGE) in the most caudal region

of the subpallium (Danjo et al., 2011; Kelsom and Lu, 2013). The MGE is the embryonic structure from which the vast majority of PV^+ and SST^+ cortical interneurons arise (Corbin and Butt, 2011; Kelsom and Lu, 2013; Lavdas et al., 1999). Newborn interneurons migrate tangentially from the MGE to populate the cortex (Lavdas et al., 1999). This configuration of three ganglionic eminences, and tangential migration of MGE-derived newborn interneurons towards the cortex is conserved in human developing forebrain (Hansen et al., 2013; Ma et al., 2013). Studies in the mouse MGE revealed that Shh signalling promotes the expression of Nkx2.1 (Xu et al., 2005), a key transcription factor required to maintain regional identity in the MGE (Sussel et al., 1999) and for the specification of SST and PV cortical interneurons. Primary cultures from the cortex of the *Nkx2.1*-mouse knockout have no PV or SST interneurons (Xu et al., 2004).

Although a role of Nkx2.1 in promoting and maintaining MGE identity was stablished in 1999, a genome-wide analysis of the transcription networks controlled by Nkx2.1 was only reported in 2016. This study revealed that Nkx2.1 acts as a repressor to prevent the expression of CGE and LGE genes. However, the combinatorial activity of Nkx2.1 and Lhx6 activates gene expression in the sub-ventricular zone and mantle zone in the developing MGE. These results suggested that these two transcription factors together control gene expression in the developing MGE (Sandberg et al., 2016).

Since the expression of Lhx6 was first documented in the MGE, its role in cortical interneuron development has been extensively studied (Grigoriou et al., 1998; Lavdas et al., 1999). From these studies is known that Lhx6 is a direct target of Nkx2.1, and can rescue the lack of PV^+ and SST^+ neurons in *Nkx2.1* null mice (Du et al., 2008). Additionally and in line with the proposed cooperative action of Nkx2.1 and Lhx6, the latter is also required for the specification and migration of SST+ and PV+ interneurons (Liodis et al., 2007; Vogt et al., 2014).

Downstream of Nkx2.1 and Lhx6, other transcription factors and genes such as Dlx5/6, Sox6, Arx, CXCR7, SATB1, Sp9 have been demonstrated to have a role in the development of MGE-derived cortical interneurons (Kelsom and Lu, 2013; Liu et al., 2019; Vogt et al., 2014). For instance, *Dlx5/6* mutant mice have defects in the tangential migration of cortical interneurons and a 3-fold reduction in the number of PV^+ interneurons (Wang et al., 2010), while *Sox6* null mice display decreased numbers of PV^+ and SST^+ interneurons, defects in laminar localisation and epileptic phenotype (Batista-

Brito et al., 2009). Human MGE is also characterised by NKX2.1 and SOX6 expression. Although Nkx2.1 is necessary for the establishment of the MGE, it must be downregulated in progenitors fated to become cortical interneurons (Nobrega-Pereira et al., 2008). Human PV^+, CB^+, SST^+, $nNOS^+$ and NPY^+ interneurons co-express SOX6, suggesting that they are derived from human MGE (Ma et al., 2013). Figure 1.3 depicts gene networks controlling the development of MGE-derived lineages.

Recent findings from single cell RNA-seq have demonstrated the existence of highly heterogeneity of progenitors within the MGE. Such heterogeneity is thought to contribute explaining the diversity of interneuron subtypes developed from the MGE. In addition, these studies also allowed the identification of cell populations that prospectively would develop as SST^+ or PV^+ interneurons. Such molecular distinction could be found as early as 12.5 and 13.5 (Mayer et al., 2018; Mi et al., 2018). Therefore, it has been suggested that cell type-specific genetic programs might be established by the time interneurons become post-mitotic, however through migration and allocation to a laminar position, these cells will be exposed to different environments that allow the unfolding transcriptional programs to shape the final features of interneurons (Lim et al., 2018).

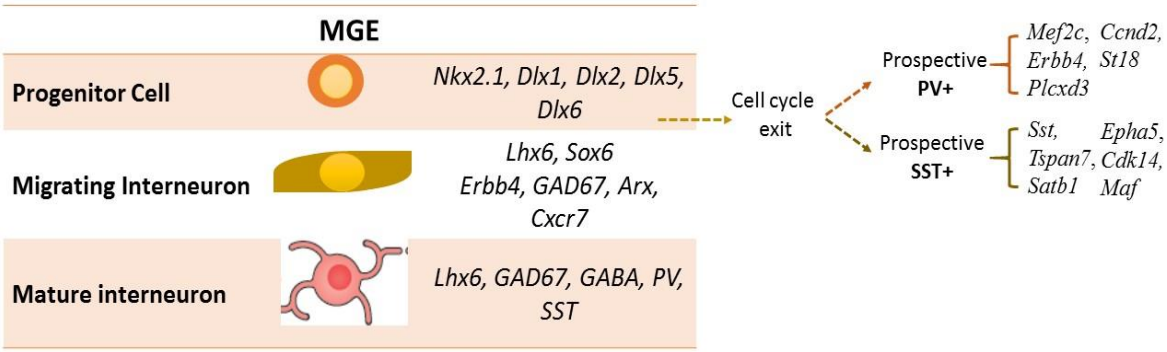

Figure 1.3| Genes involved at different states of interneuron development. Dlx genes have been shown to be necessary for GABAergic fate specification and repression of glial fate. Nkx2.1 instructs and maintains the MGE identity by repressing the expression of CGE and LGE genes. Nkx2.1 transcriptionally activates Lhx6, together they promote a transcriptionally permissive chromatin to transcriptionally activate downstream genes involved in the migration and acquisition of mature features of PV^+ and SST^+ interneuron. Recently, it has been suggested that soon after cell cycle exit, a distinctive set of genes can be identified in cell populations that will later develop into PV or SST interneurons. From these candidate genes *Mef2c* and *Maf* had been validated for having a role in PV and SST specification.

1.2.3 Emergence of interneuron diversity from the MGE

From the MGE emerges diversity of PV^+ and SST^+ interneurons. Such diversity is determined by the position of the progenitors within the MGE as well as by the time at which an interneuron is born (Hu et al., 2017b; Lim et al., 2018). For instance, it has been shown that the MGE can be subdivided into dorsal, intermediate and ventrocaudal domains, where the first two domains are specialised to give rise to cortical interneurons whereas the ventrocaudal domain produces PV^+ projection neurons destined to the globus pallidus (Lim et al., 2018). Moreover, several lines of evidences suggested that progenitors from the caudal MGE have a tendency to differentiate as SST^+ interneurons, whereas the rostral MGE-progenitors preferentially differentiate as PV^+ interneurons. The bias on interneuron fate is dependent on the expression of Coup-TF2 in the caudal MGE that binds the putative *Sox6* enhancer. *Sox6* transcriptional activation controls the ratio of SST^+ and PV^+ interneurons generated by the caudal MGE (Hu et al., 2017a). A bias for generating SST^+ and PV^+ interneurons has also been shown along the dorsal-ventral axis of the MGE, where SST^+ interneurons are preferentially generated by the dorsal MGE while PV^+ are generated by progenitors in the ventral MGE (Wonders et al., 2008).

Paradoxically, even though there is a bias for the generation of distinct class of interneurons, the dorsal MGE still produces PV^+ interneurons and vice versa. Moreover, the existence of a tendency to generate either fate at certain time in neurogenesis suggest that interneuron fate is guided not only by progenitor localization but also by the time of interneuron birth (Inan et al., 2012; Lim et al., 2018). Therefore, model of interneuron generation should take into account both spatial and temporal control of interneuron fate.

A model proposed by Oscar Marin's laboratory is based on the theory that MGE progenitors progress through intrinsic changes in their competence to produce MGE-derived lineages. In this model, molecular specification of progenitors occurs in the ventricular zone of the MGE, where progenitors are assigned a probability to generate certain number of neurons at sequential competence states. Consequently, the capability of MGE-progenitors to sequentially generate projection neurons, SST^+ and PV^+ interneurons is biased. This model is illustrated in Figure 1.4, and it is consistent with

the reported works showing that molecularly distinct progenitor cells are present in the developing MGE. In previous works, the heterogeneity within the MGE was interpreted as sub-regional specification of the MGE rather than a result of changes in the capability of progenitors to generate different kind of neurons at different competent states.

However, this model predicts the existence of a transcription factor network, which would control the progression from one competent state to another. Recently Coup-TF2 has been related to the control of SST and PV ratio in a time-dependent manner (Hu et al., 2017a), but more investigation remains to be done in order to find other transcription factors that regulates interneuron fate specification temporally.

Recently, interneuron diversity in terms of biochemistry markers, morphology, connectivity and physiological properties have been explained by the implementation of specific transcriptional programs, that can be either intrinsic to cell populations or driven by the interaction with environment. These programs, named transcriptional modules are proposed to control each of the characteristics that contribute to interneuron diversity. Hence, interneuron diversity is conceived as the result of the combinatorial assembly of different transcriptional modules through development (Lim et al., 2018). This concept might explain how interneuron subtypes can share certain characteristics, like biochemistry markers, while being different in morphology or connectivity.

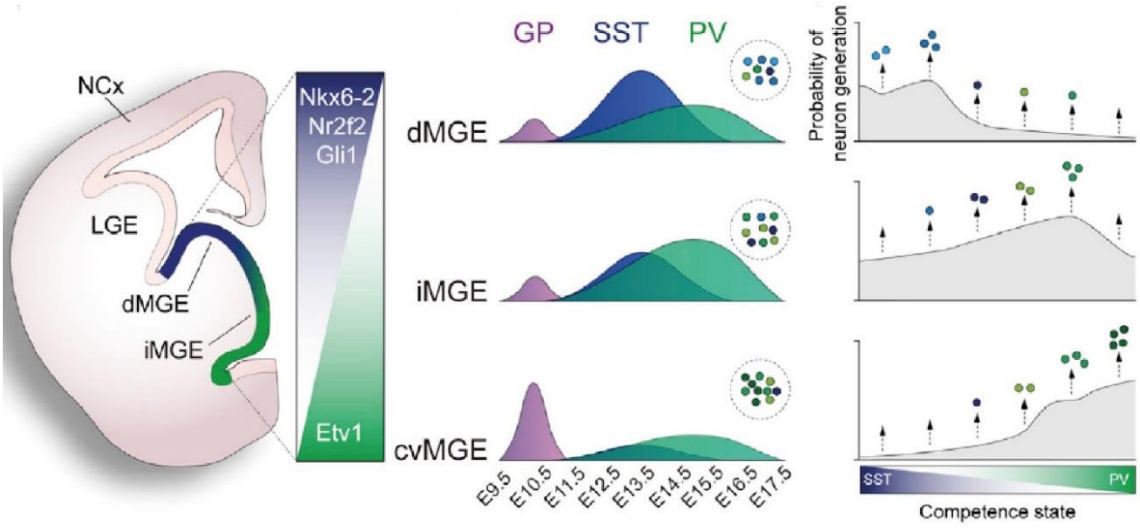

Figure 1.4| Integrated spatiotemporal model for neurogenesis in the MGE. This model considers a differential expression of transcription factors controlling the spatial patterning of the MGE into three different domains: dorsal MGE, intermediate MGE and caudo-ventral MGE. Secondly, these domains generate different numbers of neurons in a temporal sequence, where projection neurons are generated first, followed by SST interneurons and PV interneurons later on. Finally, interneurons are generated within each domain through progressive intrinsic changes in their competence to differentiate as a specific class of neuron. Where the generation of different numbers of each class of neuron is determined by the probability to generate these neurons at each competence state. From Lim, et al., 2018.

1.2.4 Key signalling pathways directing MGE development

As described in section 1.2.1, once telencephalic primordium was specified, signalling pathways and their associated effectors are implicated in the patterning and neurogenesis of the telencephalon. Below brief reviews of the mechanisms of these signalling pathways are presented. Recently activity of TGFβ signalling has been documented in the sub-pallium (Maira et al., 2010). Specifically TGFβ3 is expressed in the ventricular and sub-ventricular zone of the MGE, where its expression seems to be controlled by Nkx2.1 and Lhx6 (Sandberg et al., 2016).

1.2.4.1 Sonic Hedgehog signalling

The establishment of the dorsal-ventral fate in telenchephalon is determined by the expression of Shh and Gli3 (glioblastoma proteins). Gli3 is broadly expressed in the telencephalic anlagen and is downregulated in the ventral portion, the disruption of *Gli3* expression impairs the development of the dorsal telencephalon. In contrast, Shh is expressed in the ventral neural plate and its expression is preserved along the ventral midline of the developing central nervous system. In the ventral telencephalon, Shh restricts the dorsalising effects of Gli3 (Hebert and Fishell, 2008). Shh is one of the three vertebrate hedgehog genes (Indian, Desert and Sonic), homologous to one of the *Drosophila* segment polarity genes, the *Hedgehog* gene (Nusslein-Volhard and Wieschaus, 1980) and belongs to a family of secreted glycoproteins. Shh has been widely reported to act as a morphogen, inducing different cell fates depending on the concentration of Shh to which cells are exposed.

Shh is secreted as a precursor protein of approximately 45 kDa, which undergoes an autocatalytic cleavage that renders (approximately) a 20 kDa amino-terminal domain and a 25 kDa carboxylic terminal domain. The amino terminal domain is responsible for the known biological activity whereas the carboxylic domain is necessary for the precursor processing acting as an intramolecular cholesterol transferase, which produces a lipid-modified-amino-terminal fragment that acts as an active Shh, and such modification seems to be necessary for the restriction of the localisation of Shh in tissues (Porter et al., 1996b). After cholesterol addition to the N-terminal, a palmitoyl residue is additionally added by the acyl- transferase Ski (Porter et al., 1996a).

Cells expressing the transmembrane receptor Patched1 (Ptc1) are able to respond to Shh. In the absence of Shh, Ptc1 inhibits the activity of the co-receptor Smoothened (Smo). Binding of Shh to Ptc1 relieves this repression. Activated Smo initiate downstream signalling which leads to the activation of Gli transcription factors (Choudhry et al., 2014). Three Gli proteins are found in vertebrates, Gli1 and Gli2 have activator functions, while Gli2 and Gli3 can undergo proteolysis to produce repressor forms (Choudhry et al., 2014; Ruiz i Altaba et al., 2002). Finally, Gli proteins exert their action on Shh-target genes as transcriptional activators or repressors. In the context of the MGE, Shh activity is necessary for the expression of Nkx2.1 (Xu et al., 2005),

therefore in this thesis recombinant Shh and purmorphamine (PM), a Smo agoinst (Sinha and Chen, 2006), were employed for the in vitro derivation of MGE-like cells.

1.2.4.2 WNT signalling

Wnt signalling and its relevance in anterior patterning is well demonstrated by a Tcf3 (T-cell factor 3) mutant zebrafish, which lacks eyes, forebrain and part of the midbrain. It was shown that Tcf3 function as a repressor of Wnt signalling is critical for head formation (Kim et al., 2000). Additionally, Wnt/β-catenin signalling participates in the establishment in the dorsoventral axis in the telencephalon, which is activated in the telencephalic roof and constitutes a Shh-independent pathway controlling pallial specification. Foxg1 is a central player in the coordination of Shh and Wnt signalling activities. Foxg1 is an effector of Shh and inhibits Wnt signalling in the sub-pallium by direct transcriptional repression of Wnt8b; as a result pallial identities are excluded from the ventral telencephalon (Danesin et al., 2009).

The human genome contains 19 WNT cysteine rich glycoproteins proteins that are around 40 kDa of size and are post-translationally modified by glycosylation and palmitoylation. Wnt ligands are secreted through interaction with the GPR177 protein and transduce their signal through a heterodimer receptor formed by a protein of the Frizzled (FZD) family and LRP5 or LPR6 (lipoprotein receptor-related protein). Binding of the Wnt ligands to the FZD-LPR5/6 receptor recruits Dishevelled and Axin-GSK3 (glycogen synthase kinase 3) –APC (Adenomatous polyposis coli protein) complex. The recruitment of this complex to Wnt receptors inhibits β-catenin phosphorylation and prevents its degradation. These events leads to a subsequent accumulation of β-catenin, which is translocated to the nucleus to exert its action as a transcriptional co-activator by binding Tcf/lef (T-cell factor/lymphoid enhancing factor). In absence of β-catenin nuclear accumulation, Tcf/lef repress Wnt targets by interacting with Groucho/Tle (transducin-like enhancer protein) co-repressors (Steinhart and Angers, 2018; Yamaguchi, 2001).

Several mechanisms are known to restrict Wnt signalling in the embryonic regions where it should be suppressed as in the case of anterior/ventral telencephalon. For instance, Wnt ligands can be inhibited by direct interaction with Wnt inhibitory factors (WIF), which prevent their association with the receptor complex. A similar mechanisms is shared by the secreted frizzled related proteins (sFRPs). Other class of inhibitors are the Dickkopf (DKK) proteins, which act as competitive inhibitors by binding to the LRP5/6 receptors. An additional inhibitory mechanism is via negative feedback by axin proteins. Axin2 (a *Wnt* target gene) is the limiting component of the β-catenin destruction complex. Therefore, increased activity of Wnt signalling enhance *Axin2* transcriptional activation, which rises the availability of the β-catenin destruction complex and β-catenin degradation (Huang et al., 2009; Steinhart and Angers, 2018). Specifically, this mode of Wnt signalling inhibition was exploited in the differentiation paradigm employed in this thesis, where the XAV939 inhibitor was added during the neutralisation of hPSCs. This inhibitor acts through the inhibition of poly-ADP-ribosylating enzymes tankyrase1 and tankyrase2. These enzymes promotes Axin degradation by the ubiquitin-proteasome system. Hence, the inhibition of tankyrases stabilises Axin and increases β-catenin degradation (Huang et al., 2009). In this thesis, XAV939 was chosen because it has been shown that the proportion of $FOXG1^{+}$ cells generated by XAV939 addition was larger than the generated by recombinant DKK1. Moreover the effect if XAV939 was consistent across multiple hESCs and iPSCs(Maroof et al., 2013).

1.2.4.3 TGFβ signalling in MGE development

1.2.4.3.1 Involvement of TGFβ in neural development

Throughout the central nervous system development, TGFβ family has been documented to regulate several steps of neurodevelopment, starting by the establishment of the neural plate, which is allowed by the inhibition of TGFβ family members, such as BMPs and nodal. Afterwards members of TGFβ superfamily have also been implicated in neural tube patterning, neuronal migration and synaptogenesis (Extensively reviewed by Meyers and Kessler, 2017). In the context of patterning, members of TGFβ family, along with Wnts and Shh, orchestrate the formation of

ventral/dorsal axis in the neural tube (Choudhry et al., 2014; Meyers and Kessler, 2017; Yamaguchi, 2001). BMPs are inducers of the roof plate stablishing the dorsal identity, where Wnt activity is also displayed (Danesin et al., 2009), whereas the activity of Shh, potentiated by Nodal, instruct the establishment of the floor plate and with it, the ventral identity (Meyers and Kessler, 2017).

At the stage of neuronal specification in the forebrain, TGFβ superfamily members, specifically BMP4 signalling has been reported to have a role in the acquisition of PV interneuron fate in mouse. Primary cultures of interneuron precursors from the MGE, treated with BMP4 displayed an accelerated maturation and acquisition of PV fate at the expenses of SST^+ interneurons (Mukhopadhyay et al., 2009). The authors proposed that BMP4 does not have a role in primary GABAergic fate specification, however it has differential effects on terminal differentiation of PV^+ and SST^+ interneurons in GABAergic precursors already specified by SHH. Their results suggested that interneurons precursors derived from the MGE expressing BMPR1a receptors respond to high levels of cortical BMP4 during their migrating towards the cortex, promoting PV^+ interneuron differentiation while reducing the number of a subset of SST^+ interneurons. (Mukhopadhyay et al., 2009).

With respect to migration and axonal guidance, TβRI (transforming growth factor beta receptor 1) has been reported to be expressed in the developing and postnatal mouse cortex along radial glial fibres. Moreover TFGβ1 signalling has been implicated in the regulation of neural cell-adhesion molecules, such as N-CAM and integrins sub-units (Meyers and Kessler, 2017). TGFβ superfamily has been related to the control of the migration of sub-pallial derivatives towards the cortex. In an *ex-vivo* approach the expression of dominant negative SMAD4 (a mediator of TGFβ signalling) impaired cell migration from the subpallium towards the cortex (Maira et al., 2010). This effect on migration was suggested to be in control of redundant function of the BMP/GDF (growth and differentiation factor) and the TGFβ/Activin/Nodal branches of the TGFβ superfamily.

TGFβ signalling has also been shown to interact with transcription factors important for murine MGE development. Specifically, TGFβ3 is proposed to be a component of the transcriptional network regulated by Nkx2.1. Since TGFβ superfamily has been documented to control several stages of neural development, and that the putative

enhancer of TGFβ3 is preferentially active in the SVZ of the developing MGE where can be regulated by Nkx2.1 and Lhx6, it is possible that TFGβ3 might control other aspects than migration of MGE development.

1.2.4.3.2 An overview of TGFβ signalling

The TGFβ superfamily proteins comprises over 30 members in humans, TGFβ signalling transduction starts when the ligand binds to their receptors, which are Ser/Thr protein kinases: Type I and type II receptors (TβRI and TβRII). Ligand/receptor binding allows TβRII to phosphorylate TβRI in its GS (Glycine-Serine kinase domain), which is a characteristic feature of TβRI but not present in TβRII. The phosphorylation of TβRI leads to a change in its affinity to bind the inhibitor FKBP12. The change in affinity activates TβRI and creates a binding site in its GS domain for the receptor regulated Smad-proteins (R-Smads: Smad 1,2,3,5 and 8) (Huse et al., 2001). The access of the activated receptor complex to R-Smads is enhanced by SARA (Smad anchor for receptor activation) proteins, which immobilise Smad2 and Smad3 close to the cell membrane.

The phosphorytated R-Smad then dimerizes with the co-mediator Smad (Co-Smad: Smad4) and translocated to the nucleus, where along with others co-activators or co-repressors transcriptionally regulate TGFβ-target genes. A third class of Smad proteins, known as inhibitory Smads (I-Smads: Smad6 and Smad7) function to negatively regulate TGFβ signalling through a variety of mechanisms such as, competing for receptors, inducing receptors degradation and competing for interaction with Co-Smad (Shi and Massague, 2003). Further regulation of TGFβ signalling occurs by the action of proteins regulating the access of the ligands to their receptors, such proteins are generally known as ligand traps (Massague, 2012; Shi and Massague, 2003).

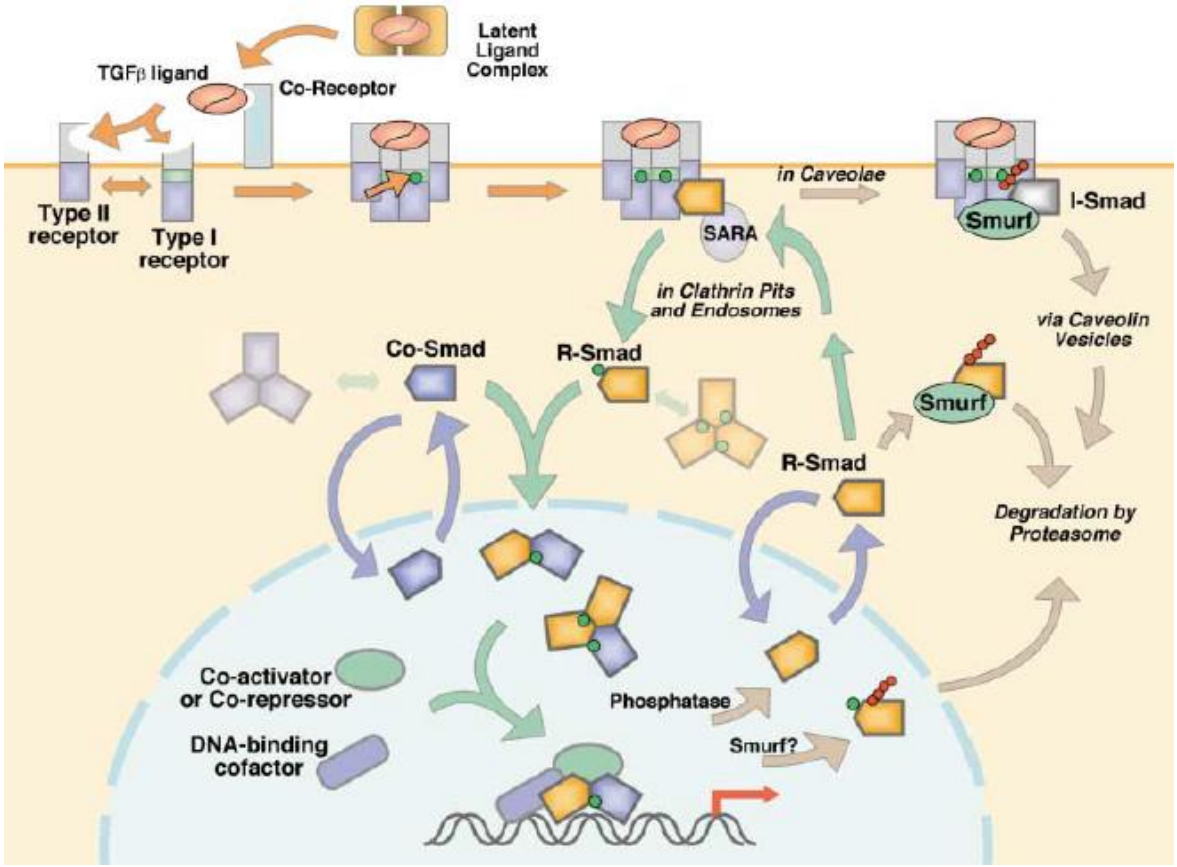

Figure 1.5| Diagram of TGFβ signalling. TGFβ binds the TβRII receptor which in turns phosphorylates the TβRI in its GS domain, creating a change in the affinity of TβRI to bind inhibitor FKBP12, leading to the recruitment and phosphorylation of R-Smads. Active R-smads dimerizes with co-Smads and together are translocated to the nucleus where they can interact with co-activator or co-represors to mediate transcriptional regulation on TGFβ targets. From Shi, 2003

The TGFβ superfamily is divided into two branches or subfamilies, the TGFβ/Activin/Nodal subfamily and the BMP/GDF/MIS (Mullerian inhibiting substance) subfamily (Massague, 2012; Shi and Massague, 2003). In spite of the variety of TGFβ ligands, they share common features in their primary and tertiary structure. Briefly, an active TGFβ ligand is a dimer formed by disulphide bridges and stabilised by hydrophobic interactions. It displays specificity to bind to a certain combination of the seven type I receptors and five type II receptors existing in humans (Massague, 2012; Shi and Massague, 2003). Table 1.1 shows the combination of receptors that different members of TGFβ superfamily binds, the R-Smads that each member phosphorylates and the

Traps proteins that regulates them. All the combinations through which TGFβ superfamily transduces signals enable it to display a plethora of, sometimes opposite, effects; which are highly context dependent, as extensively explained in Massague, 2012.

Table 1.1| Classification of TGFβ superfamily ligands, receptors and inhibitors.

Family member	Receptor I	Receptor II	R-Smad	Traps
TGFβ	TβRI (ALK5)	TβRII	Smad2/Smad3	LAP, Decorin
Activin	ACVR1 (ALK2), ACVR1B (ALK4), ACVR1C (ALK7)	ACVR2A, ACVR2B	Smad2/Smad3	Follistatin
Nodal	ACVR1 (ALK2), ACVR1B (ALK4), ACVR1C (ALK7	ACVR2A, ACVR2B	Smad2/Smad3	Cerberus
BMP	BMPR1A (ALK3) BMPR1B (ALK7)	ACVR2A, ACVR2B	Smad1/Smad5 /Smad8	Cerberus, Chordin, Follistatin, Noggin

1.3 Human pluripotent stem cells as model to investigate cortical interneuron development

hPSCs includes the human embryonic stem cells (hESCs) and the induced Pluripotent Stem Cells (iPSCs). These cells are characterised by their potential to give raise to any cell type in the body and unlimited self-renewal capability. hESCs are derived from the inner cell mass of the human developing embryo at the blastocyst stage, while iPSCs are induced *in vitro* by forced expression of the transcription factors OCT4, SOX2, KLF4, and C-MYC, whose combined expression is highly specific to the pluripotent state (Takahashi

and Yamanaka, 2006). In this thesis the term hPSCs is used to refer to hESCs, which can be identified by expressing specific cell surface markers such as stage-specific embryonic antigen (SSEA-3 and SSEA-4) (Thomson et al., 1998), as well as by the expression of pluripotency-related transcription factors: OCT4, NANOG, SOX2 among others (Brandenberger et al., 2004). Due to their differentiation potential, they have been used as an *in vitro* model of somatic cell differentiation (Reubinoff et al., 2000) for analysing several steps of commitment towards a particular cell fate (Murry and Keller, 2008).

The culture system for maintaining hPSCs has evolved over the years, moving from the use of mitotically inactivated mouse or human embryonic fibroblasts as feeder cells and chemically undefined media to feeder-free and chemically defined media. These changes led to an increases in experimental reproducibility as well as making hPSC works relatively less labour intensive (Dakhore et al., 2018). Extensive research has been done in understanding the mechanisms that govern pluripotency of hPSCs, which helped the development of improved culture media and substrates for maintaining hPSCs. Most of the currently available media contains bFGF, TGFβ, insulin and transferrin. bFGF was one of the first growth factor identified to be indispensable for pluripotency and self-renewal of hESCs. This factor was found to be released to the media from hPSCs, suggesting the presence of an autocrine signalling. The inhibition of this autocrine signalling by pharmacological inhibition of FGF receptor using SU5402 resulted in cell differentiation (Dvorak et al., 2005)

The TGFβ/activin/Nodal branch of the TGFβ superfamily, which signals through the activation of SMAD2/3 transducer, was also shown to be activated in hPSCs self-renewal condition. Upon early differentiation, SMAD2/3 activity was decreased. This pathway is required for the maintenance of pluripotency-related-markers and was also required downstream of WNT signalling activation for the maintenance of PSCs in an undifferentiated state (James et al., 2005).

1.3.1 Directed differentiation of hPSCs to cortical interneurons

1.3.1.1 Neural induction of hPSCs

Knowledge gained from developmental biology allowed understanding of basic mechanisms guiding embryonic development towards neural fate. This knowledge has been applied to stem cell research for *in vitro* derivation of cell lineages of interest. Initially, differentiation of stem cells was carried out via the formation of three-dimensional structures called embryoid bodies, which mimic a developing embryo where the three germ layers are form. However, this approach has a major drawback due to the variability between embryoid bodies and experiments (Tao and Zhang, 2016). During embryonic development, neural induction from the ectoderm requires the inhibition of SMAD signalling, as BMP inhibitors such as chordin, follistatin and noggin are known neural-inducing factors in vertebrates (Pera et al., 2014). This knowledge was applied in designing improved neural induction protocols for hPSCs. Following the initial finding that Noggin can efficiently induce neural fate conversion of hESCs (Gerrard et al., 2005), Chambers and colleagues developed a more efficient monolayer based approach using small molecule Smad inhibitor SB431542 on top of Noggin, which became a popular neural induction method known as the dual-SMAD inhibition protocol (Chambers et al., 2009). Later, it was discovered that LDN-193189 can efficiently affect all signalling cascades induced by BMP (Boergermann et al., 2010), offering a replacement option for Noggin in more recent published works.

Since neuronal subtype is dependent on the exposure to morphogens, the potential of the neural stem cells (NSCs) generated via the dual-SMAD protocol to respond to further patterning factors was tested. By exposing them to SHH and FGF8, the generation of TH^+ neurons was achieved, while motoneurons were derived after exposure to BDNF (brain-derived neurotrophic factor), ascorbic acid, SHH and retinoic acid (RA) (Chambers et al., 2009). These results were highly valuable since a monolayer culture in combination with chemically defined culture medium allow the addition of the required combination of patterning factors, where cells are thought to be exposed to uniform concentration of these factors, thus promoting a more homogeneous method for *in vitro* differentiation. Later on, other laboratories (including ours) have designed differentiation protocols to generate several classes of neurons, such as dopaminergic neurons (Jaeger et al., 2011;

Nolbrant et al., 2017), striatal medium spiny neurons (MSNs) (Arber et al., 2015) and cortical interneurons (Cambray et al., 2012; Maroof et al., 2013).

In the field of developmental neuroscience and despite the clinical relevance of cortical interneurons, most of our knowledge about human cortical interneurons relies on post-mortem studies of the human brain and animal models. Therefore, *in vitro* differentiation of hPSCs can be used to gain insights into specific mechanisms guiding cortical interneurons development in humans or modelling neuropsychiatric diseases. Currently there is not an efficient protocol for generating human cortical interneurons *in vitro.* However, the establishment of an efficient protocol for the *in vitro* derivation of human interneurons is an area of intense research. An overview of the published methods is provided in the following section.

1.3.1.2 Generation of cortical interneurons from hPSCs

Several protocols for inducing cortical interneuron fate have been published to date. These protocols were based on the combinatorial activation or inhibition of key signalling pathways aiming to mimic cell signalling conditions in the ventral telencephalon, where the MGE arises. Within this region, a concerted action of SHH activation along with WNT inhibition takes place. In the mouse embryo, the Wnt inhibitior Dkk1 gradient is opposed to the Wnt/β-catenin and together mediates anterior-posterior patterning, hence the designed differentiation protocols employ WNT inhibitors to bias cell fate towards a rostro-ventral character, which is further ventralised by activating SHH pathway (Tyson et al., 2015).

By applying the current understanding of cell signalling within the MGE, in 2013 Nicholas and colleagues showed that differentiation of hPSCs into functional interneurons required an extended timeline mimicking human development. They differentiated the hPSCs NKX2.1-GFP reporter via embryoid bodies treated with SB431542, DKK1, along with an early activation of SHH pathway (using purmorphamine). This approach resulted in 74.9±2.1 % of GFP^+ cells. Most of the cells co-expressed FOXG1. By day 35 GFP^+ cells were sorted and cultured on adherent conditions onto mouse glial cells. This method

gave rise to 40.6% of SST^+ cells after 30 weeks of differentiation, 1.5% of PV^+ and 77.7% of CR^+ (Nicholas et al., 2013). The data presented by Nicholas suggests that 37.1% of the CR^+ population was uniquely labelled CR^+. Although it has been reported that NKX2.1 is co-expressed with COUPTF-II in the dorsal MGE in mouse and humans (Cai et al., 2013; Hansen et al., 2013), and this region has been suggested as the source of SST^+/CR^+ interneuron population in mouse (Fogarty et al., 2007). Therefore data reported by Nicholas and co-workers suggest that 37.1% of uniquely label CR^+ cells were derived from $NKX2.1^+$ cells, which raises the question of whether the human MGE gives rise to CR^+ interneurons. Future investigations should be directed for answer this question.

One year later, another differentiation protocol was reported using the embryoid body approach and a different WNT inhibitor (IWP2) and SHH agonist SAG (Kim et al., 2014). A novel aspect of this work was the addition of FGF8. The authors found that the activation of SHH signalling was accompanied by induction of a rostralising factor FGF8, along with induction of FGF15/19 which counteracts FGF8-effects. The authors proposed that exogenous FGF8 would further promote anterior character, thus enhancing MGE fate and supress CGE identity. They reported 1.53% of SST^+, 0.87% of PV^+ and 22.23% of CB^+ (calbindin) cells out of total cell population (Kim et al., 2014). However, as this work did not involve a pre-selection of NKX2.1 cells prior to neuronal differentiation, it was not possible to directly compare the efficiency of this protocol with that of Nicholas et al., 2013.

Also using NKX2.1-GFP reporter cells, a similar patterning approach was also experimented on monolayer culture by Maroof and Colleagues (Maroof et al., 2013). This protocol induces neutralisation of the NKX2.1-GFP reporter by applying LDN-193189, SB431542 (dual-SMAD inhibition) along with promoting anterior-ventral character by using XAV939 during first ten days of differentiation. They showed that the combination of these three small molecules robustly induced forebrain fate in hPSC and iPSC lines. In contrast to the two other methods above, this work demonstrated that early SHH activation was not required for inducing ventralisation, as the addition of SHH and purmorphamine from day 10 of differentiation (after neuralisation) strongly induces $NKX2.1^+$ expression in more than 80% of cells and more than 90% of this population co-expressed FOXG1. GPF^+ cells were isolated and plated onto a layer of mouse embryonic

cortical cells (E13.5) to promote terminal differentiation and maturation. At day 62 of differentiation 40% of GFP^+ population was SST^+ and 5% PV^+ (Maroof et al., 2013).

The three protocols described above all generate a high proportion of NKX2.1 population, suggesting that the initial patterning towards the MGE-like fate is relatively easy. However, terminal differentiation and maturation of interneuron subtypes were generally poor efficient and require an extended timeline. Therefore, more research is needed in order to improve the yield of interneuron classes, their maturation and possibly to shorten the time necessary for their generation. Due to efficiency, differentiation timeline and monolayer culture, in this thesis a modified version of the protocol of Maroof and colleagues (reported in Noakes et al., 2019) was employed.

1.3.1.3 Direct programming of human cortical interneurons

One of the most intriguing questions in developmental biology was concerned to whether cell differentiation depends on changes in the gene expression program. This question started to be addressed when Sir John Gurdon transferred the nuclei of intestinal epithelium cells into an enucleated *Xenopus* egg, thereby generating embryos capable of developing into tadpoles (Gurdon, 1962). Later on this technique, known as nuclear transfer enabled animal cloning (Wilmut et al., 1997). These studies demonstrated that a differentiated state might be reversed by the activity of certain molecular regulators. More recently, reprograming of mouse and human fibroblast into iPSCs was achieved by forced expression of key transcription factors (Takahashi and Yamanaka, 2006). Since these works were published, a plethora of research has evidenced that although embryonic development is a unidirectional process, cell fate is not, since by exposing the nucleus to the action of specific factors, cell fate can be manipulated (extensively reviewed in Cruz-Santos et al., 2016).

Soon after establishment of the first iPSC line, searching for factors to allow direct reprogramming from one somatic lineage to another became a very active research field. Amongst these, combinatorial expression of *Ascl1*, *Brn*2 and *Myt1l* (neural-lineage-specific transcription factors) has been shown capable of directly reprograming mouse

fibroblasts into neurons (namely induced neurons, iNs) (Vierbuchen et al., 2010). One year later, *MYT1L, BRN2* and *miR-124* were successfully used for reprogramming postnatal and adult human fibroblasts to iNs (hiNs) (Ambasudhan et al., 2011).

Initially, cell reprogramming was achieved through lentiviral expression of selected transcription factors; however, the field has evolved to use other molecules, such as micro-RNAs or small molecules. Technical approaches have also evolved in a way that enhanced expression of selected genes can be achieved by using a modified CRISPR/Cas9 (Clustered regularly interspaced short palindromic repeats/ CRISPR-associated protein) system (Kabadi et al., 2014). This system employs a mutated Cas9, which contains an inactive nuclease domain (named dCas9). In addition, dCas9 is fused to two trans-activators domains (Vp64-dCas9-Vp64) to promote transcriptional activation of the targeted gene. This modified version of the CRISPR/Cas9 system has been used to mediate direct reprogramming of fibroblast into neuronal cells by targeting the promoter of *Brn2, Ascl1* and *Myt1l* (Black et al., 2016). This report exemplifies the use of CRISPR/dCas9 system to directly regulate gene expression for the purpose of "programming" a desired cellular fate.

The application of the generated of hiNs is limited by lacking regional specificity identity. Therefore, the next step forward is the derivation of specific neuronal fates. Which is particularly relevant for neuronal types that are late-born and require long term maturation as the case of PV^+ interneurons. By establishing reprogramming conditions it might be possible to bypass the laborious process of differentiation of interneurons by their direct conversion from other cell types. A first attempt to convert human iPSCs into GABAergic neurons was reported in 2015 by forced expression of *Foxg1, Sox2, Ascl1, Dlx5 and Lhx6* (Colasante et al., 2015). Using this approach around 30% of hiPSCs turned into GABAergic neurons with a large number of them expressing PV^+. However, the authors did not detect fast spiking activity in these PV^+ iNs neurons, which is a key characteristic of PV^+ interneurons. Moreover, PV^+ neurons reprogrammed from mouse fibroblasts (using the same set of transcription factors) lost PV expression after transplantation (Colasante et al., 2015).

Although the above set of genes have been shown as important players in the development of MGE-derived cortical interneurons, their failure to produce fast spiking neurons and maintain PV^+ phenotype might suggest that other factors may be lacking in

the programming cocktail. However, this report serves a proof of concept that by manipulating gene expression using the CRISPR/dCas9 system, interneuron reprogramming can be achieved, and opens a new path to functionally identify unknown-interneuron-determinants.

Later in 2016, Sun and co-workers found that lentiviral expression of three transcription factors *ASCL1, DLX2* and *LHX6* along with microRNA9/9* and micro-RNA-124 generates an enriched population of cells displaying characteristics of GABAergic cells from hPSCs. These induced GABAergic neurons (iGNs) exhibit mature properties within 6-8 weeks. iGNs generated by this approach were co-cultured with rat glia to promote functional maturation. After 42 days post-transduction, 84.5 ± 3.5% of the cell population was $GABA^+$. Further characterisation of the interneuron classes obtained by this approach revealed that 24.3 ± 4.6% were SST^+, 11.6 ± 3.0% CR^+, 6.5 ± 2.4 % CB^+ and 5.4 ± 2.0% NPY^+ (Sun et al., 2016).

In addition to the reports above, a non-integrating transgene expression system for generating iNs has been tested in mouse fibroblast. This might be a promising reprogramming strategy to minimise safety risks for generating human interneurons for clinical purposes. In this approach, the adenoviral overexpression of *Ascl1* along with the addition of forskolin at 20 µM, turned 77.2% of cells into PV^+ and the vast majority co-expressed Tuj1 by 7 days after adenoviral transduction. By 14 days, 99.6% of them were $GABA^+$ (Shi et al., 2016). However, this approach needs to be tested in human cells.

In summary, although several transcription factors and micro-RNAS have been employed for programming cortical interneuron-fate from hPSCs, the generation of cortical interneurons remains poor efficient, with unstable phenotype and particularly time consuming. However, the works outlined above provided proof of principle that gene transcriptional activation, enforced expression of transgenes, microRNAS and addition of small molecules, or combination of these factors is a valid approach for generating defined neuronal subtypes, such as cortical interneurons. Additionally recent findings of genes expressed in prospective PV or SST populations provide a starting point for identifying new interneurons determinants in order to design improved differentiation paradigms.

1.4 Aims

Human cortical interneurons derived *in vitro* provide a powerful tool for modelling normal development and interneuron associated diseases. However, current methods for producing these cells are low efficient and their functionality remains poorly characterised.

The first aim of this thesis concerns the generation of a LHX6–mCherry reporter for tracking the development of human cortical interneurons with a long term goal for using it as a screening platform for the identification of unknown interneuron determinants. Such new insights into the control of MGE differentiation would in turn facilitate the design of improved interneuron differentiation protocols.

The second objective was to apply the generated reporter in investigating the role of TGFβ signalling in MGE induction and interneuron differentiation.

2. Methods and materials

2.1 Cell Culture

Cell culture was carried out following aseptic techniques under a laminar flow hood (Maxisafe 2020, Thermo Scientific). Cultures were incubated at 37 °C, 5% CO_2 (Galaxy 170 R, New Brunswick).

2.1.1 hPSCs maintenance

Human pluripotent stem cells used in this study include H7cells and the dual reporter line (PV-gfp/LHX6-mCherry) derived from H7. Cells were cultured on 6-well multi-dishes (VWR) coated with Matrigel (VWR). Culture media was changed daily and cells were passaged when they reach around 80% confluence. For passaging, E8 media was aspirated, cells were washed once with 2 ml of PBS (Invitrogen). Cells were then incubated 4 min at room temperature (RT) in 1 ml of 0.02% EDTA (sigma). EDTA was then aspirated and 1.5 ml of E8 media added. Cells were gently scraped with a 5 ml serological pipette and seeded into Matrigel-coated 6 well plates in a 1:6 ratio.

2.1.2 hPSCs freezing and thawing

For freezing hPSCs, each well at 80% confluence was treated for 30 min with Rock (Rho-associated kinase) inhibitor (Stem Cell Technologies). Cells were detached as described in 2.1.1, except that cells were kept in larger clusters. Cells were centrifuged at 940 rpm for 4 min and resuspended in 1 ml of E8 media with 10% DMSO (Sigma). 1 ml of cell suspension was placed in a cryovial (VWR) and transferred to -80 °C freezer temporarily. Afterwards, cells were kept in liquid nitrogen for long-term storage.

To thaw hPSCs, a cryovial was taken from the liquid nitrogen and gently swirled in a water bath at 37 °C. Cell suspension was placed into a 15 ml conical tube (Fisherbrand) and 9 ml of E8 media were slowly added, followed by centrifugation at 940 rpm for 4

min. Cells were resuspended and plated into a 6-well plate previously coated with matrigel.

2.1.3 Neural differentiation of hPSCs

To induce MGE differentiation, two wells containing hPSCs 80% confluent were used. Cells were detached as described in 2.1.1 and plated into a 12-well plate, which was previously coated with reduced growth factor matrigel (VWR) for 2 hours at 37 °C. Cells were kept in E8 media (Day 0) and next day the media was aspirated, washed once with D-PBS and media was replaced by N2B27 (Day 1). 150 ml of N2B27 was prepared as following: 100 ml DMEM-F12 (Gibco), 50 ml Neurobasal (Gibco), 1 ml N2 supplement (Invitrogen), 1 ml B27 without retinoic acid (Invitrogen), 2 mM L-glutamine (Gibco), 1x Mycozap (Lonza), 0.1 mM β-mercaptoethanol (Gibco).

From day 1 to day 10, cells were treated with: LDN-193189 (100 nM, Tocris), SB-431542 (10µM, Tocris) and XAV-939 (2 µM, Stratech). For cortical differentiation cells were treated only with LDN-193189 (100 nM, Tocris) and SB-431542 (10µM, Tocris). At day 10 cells were passaged as next described: 1 hour before passaging, cells were treated with Rock Inhibitor and incubated a 37 °C. After incubation media was collected in a 15 ml centrifuge tube and cells detached applying EDTA for 3 min at RT. EDTA was aspirated and the previously collected media was returned to the cells. Using a 5 ml serological pipette, cells were gently scratched keeping them as big clusters. Cells were plated in a 2:3 ratio in 12-well plates coated with fibronectin (15 µg/ml, Sigma) for 1 hour at 37 °C. Next day, media was changed and replaced by N2B27 plus SHH (200 ng/ml; R&D) and purmorphamine (1µM; Millipore). SHH and PM were added to the media from day 11 until day 20. For Cortical differentiation cells were seeded onto fibronectin in N2B27 media without inhibitors or growth factors.

On day 19, a second passage was carried out, as above described but this time dissociating cells as single cells using Accutase (Life Technologies). Cells were counted and plated onto poly-D-lysine/laminin-coated plates. 200,000 cells/well were plated onto 24-well plates, double number of cells were plated onto 12-well plates. From day 20 to day 25 cells were grown in N2B27 without any growth factor or inhibitor, afterwards the media was replaced by N2B27 with retinoic acid plus BDND (10 ng/ml;

Peprotech). For kinetic of mCherry experiment cells were treated with demecolcine (Sigma) at 1 µg/ml and incubated for 2 hours at 37 °C, 5% CO_2.

For TGFβ signalling modulation, cells in MGE differentiation conditions were either treated with the dual kinase TβRI/II inhibitor LY2109761 (Santa Cruz) at 5µM from day 11-20., or with TGFβ3 (R&D systems) at 1ng/ml from day 14-20. To promote exit of the cell cycle cells were treated with 2 µM PD0332991 (Sigma) and 10 µM DAPT (Tocris) from day 35 to day 60.

2.2 Gene targeting

To generate the dual reporter stem cell line, a multiplex CRISPR/Cas9 assembly system kit (Addgene kit 1000000055) was employed to express up to 3 gRNAs (guide RNAs) along with the Cas9 enzyme. This plasmid was co-delivered to the cells with a targeting vector to mediate homologous recombination. The targeting vector encodes the sequence of GFP or mCherry flanked by homology arms (HA) as described in detail in next section.

2.2.1 Plasmids generation

Three gRNAs were designed around the last coding codon of *PV* and *LHX6* loci using the CRISPR design tool (crispr.mit.edu). The complementary sequence of each gRNA was designed and BbsI overhangs were added. The sequence of the gRNAs for *PV* and *LHX6* knock in generation is listed in Table 2.1. The gRNAs were phosphorylated with T4 PNK (New England Biolabs, NEB) and annealed using the following program: 37 °C- 30 min, 95 °C-5 min, ramp down to 25 °C at 5 °C/min. Each annealed and phosphorylated gRNA was cloned separately into the pX330A-1x3, pX330S-2 and pX330S-3 plasmids. Briefly 1.5 µg of each plasmid were overnight digested with BbsI (NEB) at 37 °C. After digestion, BbsI was inactivated at 65 °C for 15 min. 1 µl of the phosphorylated and annealed gRNAs duplex was ligated with 100 ng of the BbsI digested plasmid using Quick ligase (NEB). The ligation reaction was treated with plasmid safe exonuclease (epicentre) 30 min at 37 °C. 5µl of the ligation was transformed into the *E. coli* strain XL1-Blue (agilent

technologies); plated onto LB with the corresponding selection antibiotic and overnight incubated at 37 °C.

Next day eight colonies were picked and cultured in LB media with the antibiotic selection and cultured overnight at 37 °C. Plasmidic DNA was extracted by miniprep and screened by double digestion with BbsI and EcoRI to identify the clones with the inserted gRNAs, in which the BbsI site was destroyed resulting in a linearised plasmid. One clone of each plasmid with the inserted gRNA was selected and assembled into the pX330A-1x3 plasmid by a golden gate reaction. For this, 300 ng of pX330S-2 and pX330S-3 was mixed with 150 ng of pX330-1x3, BsaI (NEB) and Quick ligase (NEB). The reaction was carried out with the following program: 25 cycles of 37 °C-5 min, 16 °C-10 min; hold at 4 °C. 5µl of the ligation were transformed into XL1-Blue strain and overnight cultured at 37 °C onto LB plates plus antibiotic. Clones were picked and cultured in LB media with antibiotic. Plasmids were extracted and screened by double digestion with AflIII (NEB) and KpnI (NEB). Clones containing three assembled gRNAs released a fragment around 1.4 kb.

In parallel, targeting vectors were designed encoding the reporter gene and a selection cassette, flanked at each end by 3' and 5' homology arms respectively. Diagrams showing the design of both targeting vectors are showed in Figures 3.2 and 3.3.

Table 2.1| Sequence of the gRNAs use for targeting *LXH6* and *PV* genes

Guide	Forward sequence	Complementary sequence
LHX6 Guide 1	TTTTTCAGTACTAACGCTGC	AAAAAGTCATGATTGCGACG
LHX6 Guide 2	CACTTCCGCATCTGCCCGT	GTGAAGGCGTAGACGGGCA
LHX6 Guide 3	TCAGCCGCTGAGATCCAGTG	AGTCGGCGACTCTAGGTCAC
PV Guide	TAAGAAGCACTGACTGCCCC	ATTCTTCGTGACTGACGGGG

2.2.2 Nucleofection and hPSCs lines derivation

hPSCs were treated with Rock Inhibitor one hour before nucleofection. Cells were detached with gentle cell dissociation reagent (Stem Cell Technologies) and dissociated as a single cell suspension. The gRNAs encoding plasmid was co-transfected with the targeting vector using the amaxa 4D-nucleofector protocol (Lonza), in a 1:3 (gRNAs: targeting vector) proportion for *PV* targeting and 1:7 for *LHX6*. Transfected cells were plated onto matrigel and cultured in TeSR-E8 media (Stem cell technologies) plus RevitaCell (Life technologies). 48 hours after nucleofection, the appropriate antibiotic was added to start the selection of nucleofected cells. After selection process, cells were plated in limiting dilution to obtain clonal populations. Two weeks after nucleofection, individual clones were picked, cultured and genotyped by PCR. Correctly targeted clones were subjected to a second round of nucleofection. Expression plasmids encoding FLP or CRE recombinase were nucleofected as above described. Individual clones were picked and genotyped. To test the loss of CMV-HygroTK, a portion of each clone was cultured in presence of hygromycin. The clones which died with the antibiotic treatment were selected, expanded and frozen.

The loss of resistance to neomycin was tested by PCR and confirmed by adding neomycin to the media to a portion of the clones. The clones which died with neomycin treatment were selected, expanded and used for differentiation.

2.2.3 PCR-based genotyping

2.2.3.1 Genomic DNA extraction

Media was aspirated and cells were treated with lysis buffer consisting of 10 mM tris, pH 8.0, 50 mM EDTA, 100 nM NaCl , 0.5% SDS (all components from sigma) and supplemented with proteinase K to a final concentration of 0.5 mg/ml. Cells were returned to the incubator for at least 4 hours. The lysate was transferred into an Eppendorf tube and an equal volume of isopropanol was added and the tube carefully mixed and centrifuged for 20 min, 4 °C at full speed. The supernatant was removed and the pellet washed with 70% ethanol and centrifugated for 10 min, 4 °C at full speed.

Pelleted DNA was air-dried and resuspended in milli-Q water, DNA concentration was measured with a Biospectrometre from Eppendorf.

2.2.3.2 PCR and electrophoresis

PCR was carried out to genotype clones transfected with the PV- targeting vector, LHX6-targeting vector or after removing the selection cassettes. A particular program was designing for each product to be amplified and the reaction was setting up following the guidelines for the specific polymerase in use. The main parameters changed among programs were temperature of extension, which is the temperature at which the polymerase in use works, extension time that considers the time needed for the polymerase to amplify the product of interest, as well as the annealing temperature depending on the primers in use. All the primers used for genotyping are listed in Table 2.2. The polymerases used were Taq polymerase from New England Biolabs or the SequalPrep long PCR kit from Thermofisher. The PCR product was analysed on an agarose gel between 1-2% of concentration depending on the amplicon size.

Table 2.2| Sequence of the primers used for genotyping

Purpose	**Forward Oligo**	**Sequence**	**Reverse oligo**	**Sequence**
WT LHX6 locus	Out5'HA_LHX6_F	TCAGCCACTATGGTCACGGT	3'HA_LHX6_R	TGGATGCGGAGGTGGGT
5' LHX6 genotyping	Out5'HA_LHX6_F	TCAGCCACTATGGTCACGGT	mCherry_F	GGGCGAGGAGGATAACATGG
Selection cassette	Neo_F	GCATCGCCTTCTATCGCCTT	SA_LHX6_R	CATTCCCTGTCTATCCCCGC
3' LHX6 genotyping	SV_40_R	GGGAGGTGTGGGAGGTTTTT	3'HA_LHX6_R	TGGATGCGGAGGTGGGT
5' PV genotyping	PVALB-p7F	TTGGCCAGGCTGGTCTCAAACTCC	5'HYGRO_R	TCGACAGACGTCGCGGTGAGTTC

2.3 Cell analysis

2.3.1 Immunocytochemistry

Cells were washed with PBS (Sigma) and fixed with 3.7% PFA (Sigma) for 15 min at 4 °C. Cells were permeabilised by washing twice with PBST (0.3% Triton X-100 in PBS) for 10 min at RT. For nuclear proteins, cells were washed for 5 min at RT with 33% and 66% methanol respectively, then with 100% methanol for 20 min at -20 °C, before being returned to PBS washing in the reverse order. Cells were blocked in blocking solution (1% BSA/3% serum in PBS) for one hour at RT, and then incubated with the primary antibody in blocking solution overnight at 4 °C. Table 2.3 lists all primary antibodies used for immunocytochemistry experiments.

Next morning cells were washed three times with PBST for 5 min each at RT, following with incubation with the secondary antibody in blocking solution for 1 hour at RT. From this point cells were kept in dark. After secondary antibody cells were washed three times with PBST for 5 min at RT with DAPI (1:3000 in PBST) added in the last wash for nucleus counterstain. Cells were washed again three times with PBST for 10 min at RT. PBST was removed and a drop of fluorescence mounting medium (Dako) was added. A coverslip was placed and images acquired using an inverted microscope (Leica DMI6000B). Images were processed using the Leica Application Suite software, ImageJ and CellProfiler.

2.3.2 Flow cytometry

For flow cytometry experiments, cells were dissociated with accutase (Life Technologies) for 5-10 min (depending on the differentiation stage) at 37 °C. After incubation, cells were washed in cold PBS and centrifuged at 960 rpm for 4 min. Cells were resuspended in 100 µl cold PBS and 100 µl of cold DAPI/PBS (1:3000) and collected in a FACS tube with cell strainer (VWR). Data was acquired using a Fortessa analyser (BD). H7 cells at the same stage of differentiation were using in each time point as a negative control, DAPI staining was used to discard dead cells from the analysis.

Table 2.3| Antibodies used for immunocytochemistry

Antigen	Species	Supplier	Code	Dilution
ChAT	GOAT	MILLIPORE	AB144P	1:100
COUPTF II	Mouse	Perseus & proteomics		1:100
CALRETININ	Rabbit	Swant	CR 7697	1:500
CTIP2	Rat	Abcam	Ab18465	1:500
FOXG1	Rabbit	Abcam	ab18259	1:250
GAD67	Mouse	Millipore	mab5406	1:500
LHX6	Rabbit	Santa cruz	sc98607	1:500
mCherry	CHICKEN	ABCAM	ab205402	1:500
NeuN	RABBIT	MILLIPORE		1:500
NKX2.1	Rabbit	Abcam	Ab76013	1:1000
OCT4	Goat	Santa cruz	Sc8628	1:500
OLIG2	Goat	R&D systems	AF2418	1:200
PAX6	Mouse	DSHB		1:1000
PARVALBUMIN	Mouse	Sigma	P3088	1:100
SATB2	Mouse	Abcam	ab51502	1:50
SOMATOSTATIN	Rat	Millipore	MAB354	1:50
TBR1	Rabbit	Abcam	ab31940	1:500

2.3.3 Gene expression analysis

2.3.3.1 RNA extraction

Cells in 12 well plate were lysed with 1 ml of Tri reagent (Sigma), then 200 µl chloroform were added and the samples were vigorously shaken for 15 seconds. Samples were then allowed to stand for 10 min at RT before centrifugation at 12,000 x g for 15 min at 4 °C. Aqueous phase was transferred into a new tube and thoroughly mixed with 500 µl isopropanol. Samples were left to stand at RT for 10 min and centrifuged at 12,000 x g for 10 min at 4 °C. The liquid was removed and the pellet was washed with 1 ml 75% ethanol followed by centrifugation at 7,500 x g for 5 min at RT. The RNA pellet was left to dry and then dissolved in 20 µl nucleases-free water.

2.3.3.2 DNAse treatment

RNA concentration was measured using a Spectrometer (Eppendorf) and 10 µg were treated with 1µl of turbo DNase (Ambion). Samples were incubated at 37 °C for 30 min. After incubation 2 µl of DNase inactivation reagent was added and incubated for 5 min at RT mixing samples regularly. Then samples were centrifuged at 10, 000 x g for 1.5 min. The supernatant, containing the RNA was transferred to a new tube.

2.3.3.3 Reverse transcription

After DNase treatment, reverse transcription was carried out using the qScrip cDNA synthesis kit (Quanta). With that purpose 1 µg RNA was mixed with 1 µl qScript R plus 4 µl qScript Reaction Mix (5X), the volume was adjusted to 20 µl with nuclease-free water. The reaction was performed with the program next detailed: 22 °C -5 min, 42 °C-50 min, 85 °C-5min. After completion of the reaction, cDNA was diluted 1:10 in nucleases-free water for qPCR amplification

2.3.3.4 Real time PCR

Once cDNA was obtained, the SYBR Mesa Green master mix (Eurogentec) was used for qPCR. Briefly 5 µl reaction buffer was mixed with 100 nM of the forward and reverse primers and made up to 10 µl with endonucleases free water. 9 µl of the mix was placed into each well of a 96 well-plate and 1 µl of diluted cDNA was added. Each sample was assayed in triplicate. The reaction was perform using the Bio-rad CFX Connect Real-Time System and next program: 94 °C for 4 min, followed by 40 cycles of 94 °C -30 sec, 60 °C- 15 sec and 72 °C- 30 sec. Melting curve analysis was performed from 65 to 95 °C to corroborate the specificity of the of the PCR product. Oligos were designed using the online PrimerBLAST tool from NCBI and their efficiency evaluated following the guidelines from Bio-Rad. Primers used for qPCR experiments are listed in Table 2.4.

Table 2.4| Sequence of primers used for qPCR

Gene	Forward	Reverse
FAPB7	GGATTGGGAGGAACTCGACC	AGGGTGGGCAAAAATCCAGT
GAD67	CGTCTTCGACCCCATCTTCGT	CGCAGATCTTGAGCCCCAGTT
LHX6	GACGACATCCACTACACCCC	GGCCCATCCATATCGGCTTT
SOX6	CTGCCTCTGCACCCCATAAT	CGCTCTGGGGTTCCAAAAGT
STMN2	CTCAGAAGCCCCACGAACTTT	TCGCTCGTGTTCCCTCTTCT
TOP2A	ACCAAGAATCGCCGCAAAAG	ACAGATTTTGCCCGAGGAGC
β-Actin	TCACCACCACGGCCGAGCG	TCTCCTTCTGCATCCTGTCG

2.3.3.5 Fold change calculation

Data collected by the CFX Manager Software (Bio-rad) and exported to Microsoft excel for analysis. To calculate the relative difference in expression level of the target gene, data was normalised to the housekeeping gene β-actin and compared to the gene expression at the pluripotent state, using the Livak method where the normalised expression ratio= $2^{-\Delta\Delta Ct}$. Fold change at each time is presented as the mean of 2 biological replicates ± SEM.

2.3.4 Chromosome preparation for karyotyping

Sub-confluent cells were treated with demecolcine (Sigma) to a final concentration of 1 µg/ml and incubated for 1 hour at 37 °C, 5% CO_2. Cells were then dissociated to a single cell suspension using Gentle Cell Dissociation reagent (Stem Cell Technologies), incubating 8 minutes at 37 °C. Cells were collected and washed twice with PBS (Invitrogen) and centrifuged for 4 min at 1000 rpm. Cells were resuspended in 2 ml of PBS and 6 ml of hypotonic 0.075 M KCl (Sigma) were added, then cells were incubated for 15 min at 37 °C. After incubation, additional 4ml of 0.075 KCl were added and cells were collected by centrifugation 4 min at 900 rpm. The supernatant was aspirated leaving 300 µl to resuspend the cell pellet by flicking. Dropwise and flicking simultaneously, 4 ml of pre-chilled (-20 °C) methanol/acetic acid (3:1, VWR chemicals) were added. Cell suspension was incubated for 30 min at room temperature. Cells were centrifuged for 4 minutes at 800 rpm and resuspended with additional 4 ml of methanol/acetic acid. Cells were collected as previously and resuspended in the remaining 300 µl of methanol/acetic acid. Cell suspension was dropped onto a slide (pre-chilled and laid on angle) from a height of 30 cm. Slides were air dried and chromosome spread was stained and mounted using a mix of mounting media (DAKO) with DAPI (1:3000). Images of chromosome spreads were obtained with an inverted microscope (Leica DMI6000B). Images were processed using the Leica Application Suite software and counted on ImageJ.

2.3.5 EdU labelling assay

Cells going through the S-phase of the cell cycle were labelled using the Click-iT EdU Assay kit from Invitrogen. Control cultures or LY-treated cultures were plated at 200000 cells per well onto a four well-plate and incubated in EdU at a final concentration of 10 µM, at 37° C. For pulse analysis cells were incubated for 2 hours or for increasing periods of time (2, 4, 8, 16 and 24 hours) for cell cycle length determination. Cells were fixed in 3.7% PFA (Sigma) for 15 min at 4 °C, following with permeabilisation with 0.5% of Triton X-100 in PBS. Cells were incubated at room temperature for 20 minutes in the reaction cocktail, prepared as per manufacturer's protocol. If co-staining is needed, it was carried out before the EdU detection. After EdU detection, nuclei stain with DAPI was performed and mounting media added. At least 3 fields/well were imaged in an inverted microscope (Leica DMI6000B). Images were processed using the Leica Application Suite software and manually counted using ImageJ.

2.3.6 Cell cycle length estimation

To estimate the length of the cell cycle, six fields from 2 biological replicates were counted at each time point of the EdU cumulative labelling. The percentages of the $NKX2.1^{+}\_EdU^{+}$ and $NKX2.1^{-}\_EdU^{+}$ in control and LY conditions were plotted against time. A linear regression was performed, and the values of the slope (m) and y-intercept (b) of the linear equation were used to calculate the values of cell cycle length (t_c) and S-phase length (t_s), using the Nowakowski equation:

$$GF(t) = (GF/t_c)t + GF(t_s/t_c)$$

Where:

GF= Growth fraction in cell population

$m=GF/t_c$ thus $t_c=GF/m$

$b= GF(t_s/t_c)$ thus $t_s=(b*t_c)/GF$

2.3.7 Statistical analysis

Data from immunocytochemistry was processed by counting positive cells from 3 fields of two or three independent differentiations (n=9 or n=6), unless otherwise stated. Data is presented as the mean percentage ± SEM. Flow cytometry was presented as the mean of the cell percentage± SEM. For flow cytometry analyses cells were collected from 3 wells of at least 2 independent differentiations (n=6 or n= 9). Gene expression profile is expressed as mean fold change ± SEM from RNA extracted at each time-point, for control conditions and LY-treatment from two independent differentiations (n=2). Fold change calculation was performed as described in section 2.3.3.5. For comparing means of two groups a two-tailed t-test was performed after analysing normal distribution with the Shapiro-Wilk test and equality of variances with Levene's test. When no normal distribution was found, a Mann Whitney U-test (non-parametric test) was carried out. To compare more than two groups a one-way ANOVA was conducted with a post-hoc Tukey. Significant differences were labelled as follows: * $P < 0.05$, ** $P < 0.01$, ***$P < 0.001$.

3. Generation of LHX6-mcherry/PV-GFP dual reporter hPSC line

3.1 Introduction

The ability of hPSCs to give rise to any cell of the body promises their application as an *in vitro* model for studying cell differentiation in health and disease (Murry and Keller, 2008; Reubinoff et al., 2000). Such application is especially useful to study the development of clinically relevant cell linages, which are not easily accessible. One such example is cortical interneurons, the dysfunction of these cells and/or mutations in key genes for their development have been related to neurodevelopmental disorders (Batista-Brito et al., 2009; Del Pino et al., 2013; Marin, 2012; Wohr et al., 2015). Nonetheless, the potential of hPSCs could not be fully exploited unless specific cell populations can be faithfully identified. The creation of knock in reporter lines allow the visualisation in real time of the dynamic expression of genes of interest (Goulburn et al., 2011; Zwaka and Thomson, 2003). Moreover, reporter cells can facilitate the identification of cell populations committed to a certain fate, the optimization of efficient differentiation protocols as well as the isolation of pure cell populations for downstream applications, such as transplantation and drug screening.

The generation of knock in reporter lines involves the use of gene editing technology called gene targeting. This technique utilises the endogenous DNA repair mechanism of the cell through homologous recombination, which requires a targeting vector containing the desired genetic modification to be introduced into the locus of interest. As gene targeting involves homologous recombination, the targeting vector should contain two segments of DNA homologous to the genomic region to be targeted (referred as Homology Arms HA) (Thomas et al., 1992; Thomas et al., 1986). Although homologous recombination has been extensively used in generating mouse models via the generation of engineered mouse embryonic stem cells, classic gene targeting in hPSCs has proved challenging and hence less exploited (Zwaka and Thomson, 2003). However, the landscape has changed in recent years due to the rapid advance of the CRISPR/Cas9 genome editing technology (Li et al., 2015b; Zhu et al., 2015). In contrast to the conventional gene targeting methods, which rely on the rare events of

recombination, the use of the Cas9 nuclease along with sgRNA to generate double strand breaks in the target DNA increases the efficiency of gene targeting (Li et al., 2015b). CRISPR/Cas9 system in combination with classic replacement targeting vectors has allowed the generation of reporter cell lines via homologous recombination, that carrying fluorescent reporters recapitulating the expression of endogenous genes of interest.

Only few neural lineage/cell type defining genes have been targeted in hPSCs to date (Li et al., 2015a; Li et al., 2015b; Xue et al., 2009). Among them, the NKX2.1-GFP knock in line has been used for facilitating the development of cortical interneurons differentiation protocols (Maroof et al., 2013). Although NKX2.1 is necessary to maintain regional identity in the MGE, this transcription factor promotes both GABAergic cortical interneurons and cholinergic fates in the basal forebrain (Fragkouli et al., 2009; Sussel et al., 1999). Therefore, the percentage of NKX2.1^{+} cells in a differentiation culture does not provide an accurate readout for cells fated to become GABAergic cortical interneurons. NKX2.1 promotes GABAergic cortical interneuron and cholinergic neuron fate via transcriptional activation of LHX6 and *LHX8* (also known as *LHX7*), respectively (Sussel et al., 1999). While NKX2.1 expression remains in cholinergic neurons (NKX2.1^{+}/LXH8^{+}), it is downregulated in a subset of MGE- derived interneurons once they exit the cell cycle (NKX2.1^{-}/LHX6^{+}). (Lopes et al., 2012; Sandberg et al., 2016; Sussel et al., 1999). Moreover, it has been proposed that post-mitotic downregulation of NKX2.1 distinguishes cortical interneurons from striatal interneurons. Post-mitotic NKX2.1 expression in striatal interneurons represses the expression of semaphorin3 receptors (Neuropilin2), and in consequence NKX2.1^{+} interneurons become insensitive to semaphorin3 repulsive signals in the striatum which allows them to settle in there. In contrast, NKX2.1^{-} interneurons, express Neuropilin2^{+} which makes them responsive to the repulsive cues from the striatum, hence guiding their position towards the cortex (Nobrega-Pereira et al., 2008). Thus NKX2.1 expression could be used as good reporter for detecting the acquisition of MGE fate and later on for striatal interneurons, whereas MGE-derivatives committed to cortical interneurons could be identified by lacking NKX2.1 expression (NKX2.1^{-}/LHX6^{+}).

Since LHX6 expression is highly specific to the MGE derivatives fated to become cortical interneurons and that its expression is maintained in these cells, a LHX6 reporter would

provide a better tool than the *NKX2.1-gfp* knock in for identifying factors regulating GABAergic cortical interneurons fate.

Out of the MGE, *Lhx6* transcript is detected within subdomains of the first branchial arch, such as the oral aspect of the mandibular process and part of the maxillary process in the developing mouse at E10.5, where LHX6 expression is confined to the neural crest-derived mesenchyme (Grigoriou et al., 1998). With regard to adult tissues, LHX6 has been suggested as a tumour suppressor in some kind of cancers, particularly lung cancer tissue displays *LHX6* downregulation compared with its expression in adjacent lung normal tissues (Liu et al., 2013). Additionally the hypermethylation in CpG islands of *LHX6* serves as a sensitive methylation marker in carcinomas such as head and neck and in early diagnosis of cervical cancer (Liu et al., 2013). Since the presence of the *Lhx6* transcript during embryonic development is highly restricted to the head as above described, it is particularly important to ensure that LHX6-mCherry expression is assayed in an enriched MGE-like population, otherwise the evaluation of mesenchymal markers alongside MGE related-markers will be essential to establish that our studies are restricted to MGE-like cells.

Furthermore, a hPSC reporter that defines specific cortical interneurons subtypes is currently not available, although a strategy to identify generic GABAergic neurons derived from hPSCs has been developed (VGAT-mCherry knock in line) (DeRosa et al., 2015). Hence, I also aim to target the *PV* gene to label the PV^+ interneurons, a clinically relevant interneuron subtype due its implications in autism and schizophrenia (Marin, 2012; Wohr et al., 2015).

PV function as a Ca^{2+}-binding protein, therefore it is not surprising that PV is detected in muscles of higher vertebrates playing a role as a relaxation factor. PV is also found in other tissues such as bone, teeth, skin, prostate, seminal vesicles, testes and ovaries of rats. PV^+ cells are also identified in developing human spinal cord mammals (Arif, 2009). While the presence of pan neuronal markers such as Tuj, NeuN or doublecortin would help to differentiate PV^+ interneurons from non-neuronal cell types, the distinction between PV^+ cortical interneurons and PV^+ neurons localised in the spinal cord needs the consideration of the developmental origins of both PV^+ populations. Since cortical interneurons are forebrain-derived, the evaluation of anterior markers (e.g. FOXG1) is

critical to discard the generation of the spinal cord neural types, which have caudal origin through the concerted action of *Hox* genes (Davis-Dusenbery et al., 2014).

The available data of the expression of *Lhx6* during development shows that LHX6 transcript is found in head but, unlike the *PV*, it is not detected in the spinal cord (reported in Grigoriou, 1998 and in http://www.eurexpress.org/); hence, it is expected that within neural lineages, the combined expression of LHX6 and PV will label specifically MGE-derived cortical interneurons.

In this chapter, I describe the generation of a dual reporter hPSC line (LHX6-mCherry/PV-GFP) using the CRISPR/Cas9 genome editing technology. The long-term goal is to use this cell line as a tool to identify factors regulating cortical interneuron differentiation and associated molecular mechanism.

3.2 Results

3.2.1 Targeting the *LHX6* gene

3.2.1.1 LHX6-targeting vector design and sgRNA assembly

The *LHX6*-targeting vector was designed to contain the *p2A-mCherry* coding sequence and a floxed neomycin drug selection cassette flanked by a 5' (500 bp) and 3' (500 bp) homology arms, respectively, which correspond to the 500 bp flanking the stop codons of *LHX6*. The p2A sequence was placed between the last coding codon of *LHX6* and the start codon of mCherry. P2A codes for a self-cleavage peptide, which enables multicistronic expression by promoting the ribosome to skip the polypeptide bond between the last glycine and proline in the C-terminus of the p2A, yielding two proteins. The upstream protein linked to most of the p2A peptide, and the downstream protein bound to a proline in its N-terminus (Kim et al., 2011; Wang et al., 2015). This targeting vector design allows bicistronic expression of LHX6 and mCherry.

The self-cleavage peptides offers two remarkable advantages compared to IRES (Internal Ribosome Entry Site). Firstly, self-cleavage peptides render an equimolar yield of the proteins flanking the peptide. Secondly, the small length of the 2A peptides (around 63 bp) is almost 9 times smaller than IRES sequences (around 500 bp) (Kim et

al., 2011). This is particularly advantageous, as the small length of p2A allows the design of smaller targeting vectors which are easier to manipulate. Due to the working-mechanism of the self-cleavage peptide, there are two essential considerations to ensure the targeting vector to be functional. Firstly, there must not be a stop codon between the LHX6 sequence and the p2A-mCherry sequence, and secondly the insertion must be *in frame* into the locus. This will ensure the targeted locus to be transcribed as a single transcript, which will be cleavage at the translation (Zhu et al., 2015). Both considerations were taken into account for the targeting plasmid design.

In spite of the multiple advantages of self-cleavage peptides, the length of the peptide affects the cleavage efficiency, having a good efficiency when using a 19-aminoacid version and showing increased efficiency when employing longer versions (Donnelly et al., 2001). However, in heterologous context, the 2A peptide remains attached to the c-terminal of the upstream gene, which may affect protein conformation or interfere with post-translational modifications when the authentic c-terminal is crucial for such modifications. In consequence shorter version of 2A peptides have been used at expense of cleavage efficiency Additionally, in shorter 2A sequences the cleavage efficiency may be affected by the C-terminal of the upstream protein coding-gene or by sequences added for cloning purposes (Minskaia and Ryan, 2013). Therefore, the efficiency of the cleavage seems to be context-dependent and difficult to predict in advance whether a particular gene targeting might affect the cleavage efficiency of the 2A peptide.

For CRISPR assisted genome editing, three sgRNA were designed using the online tool (https://zlab.bio/guide-design-resources). These sgRNAs target the last coding exon (exon 9) of the human *LHX6* gene. This gene has 12 transcripts, 9 of which are protein coding which use two different stops codons. Therefore the gRNAs were designed to target both stop codons. (Figure 3.2A). The selected sgRNAs were those displaying higher score of target efficiency and low potential off-targets. Using the multiplex CRISPR/Cas9 assembly system kit (Sakuma et al., 2014), each gRNA was cloned into independent vectors and subsequently assembled through a golden gate reaction into the destination plasmid, which also encodes the Cas9 nuclease (Figure 3.1A). Cloning of sgRNAs into individual plasmids was verified by double digestion with BbsI/EcoRI. This

double digestion should produce a linearised plasmid when the sgRNA was inserted as the single BbsI site was destroyed following the insertion of the gRNA (Figure 3.1B). The assembly of the three gRNAs was screened by double digestion with KpnI/AlfIII, which releases the 3 assembled gRNAs in a 1.4 kb fragment (Figure 3.1C). The resulting plasmid was named as Cas9/3xsgRNAs.

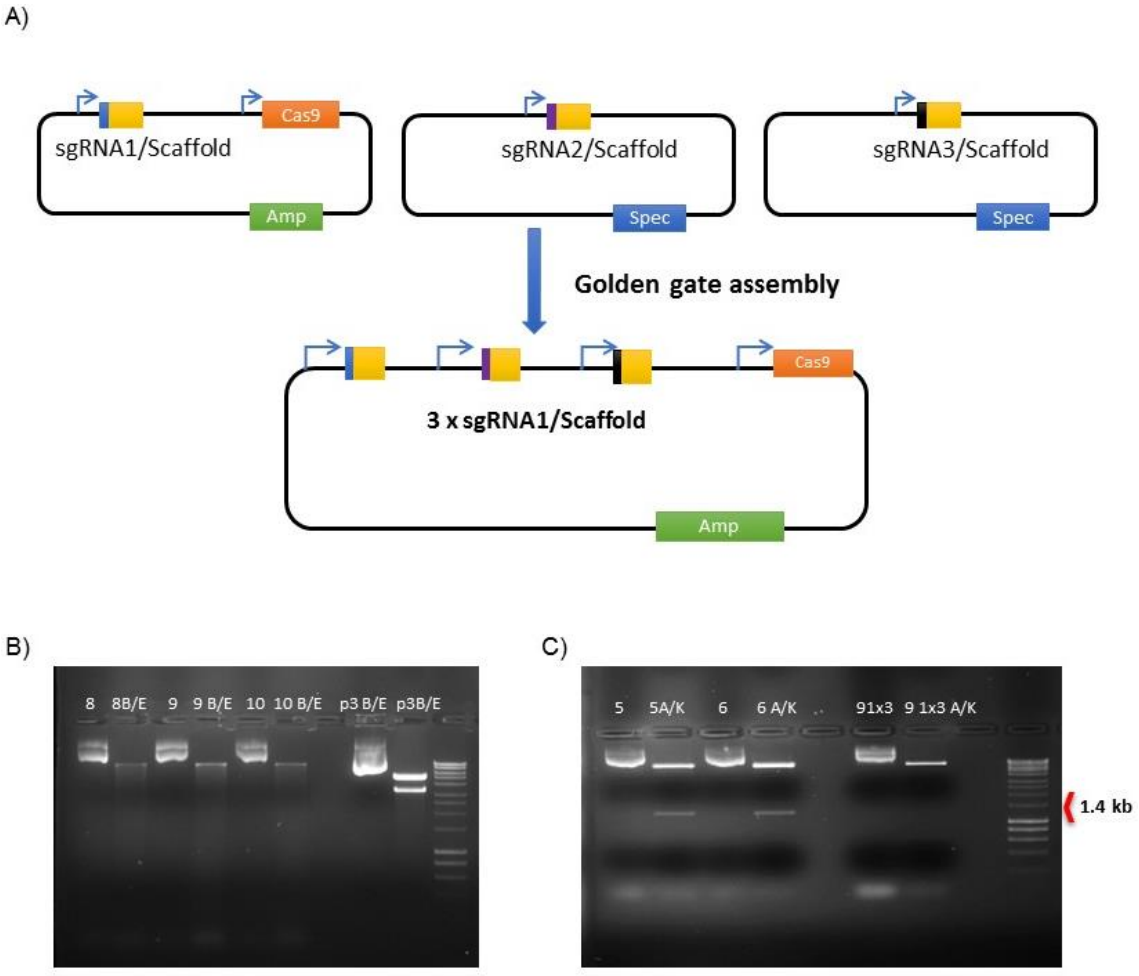

Figure 3.1| *LHX6*-sgRNA cloning A) For targeting *LHX6* gene, three sgRNA were designed to direct Cas9 around the stop codons in the exon 9 of *LHX6.* The gRNAs were added BbsI sites for cloning them into independent plasmids; which were assembled into a Cas9 expression plasmid. B) Individual clones were assayed by double digestion of plasmidic DNA with BbsI/EcoRI. The gel is showing plasmids harbouring a gRNA were the BbsI site was destroyed. Plasmids without sgRNA insertion display two bands indicating that BbsI site is preserved. C) The 3 gRNAs were assembled into the cas9 expression plasmid. Succesfully assembled plasmids were screening by double digestion with KpnI/AlfIII; which releases the region containing 3 sgRNAs. The resulting plasmid is named Cas9/3xsgRNA.

3.2.1.2 Generation of LHX6-mCherry reporter

The LHX6-targeting vector and the Cas9/3xsgRNAs plasmid were co-transfected at 7:1 ratio into the previously derived PV-GFP (Described in section 3.2.2). 24 hours after nucleofection G418 (analogue of neomycin) was applied to nucleofected cultures at a 100 µg/mL. The concentration of G418 was gradually increased to 200 µg/mL by day 3 post- nucleofection. Five days after nucleofection, the cultures were dissociated and re-plated as single cell solution at $1x10^4$ or $4x10^4$ cells/ per well onto a 6 cm plate. The antibiotic treatment continued and around one week after plating colonies emerged. At a size of around 100 cells/colony, colonies were picked and screened for homologous recombination by genomic PCR.

The wildtype allele is predicted a 650 bp band using the forward primer (O5'_HA_LHX6_F) located upstream the 5'homology arm and the reverse primer (3'HA_LHX6_R) located within the 3'UTR of *LHX6,* whereas if homologous recombination event occurred at the 5' end, I would expect to see a 765 bp amplicon from PCR using the same 5'forward primer and the reverse primer (mCherry_R) within the *mCherry* sequence (See Figure 3.2A for primers localisation). Following a similar PCR screening design, 3'homologus recombination was assayed by the amplification of a 963 bp PCR product by using a forward primer located within the resistant cassette (Neo_F) and a reverse primer located outside the 3'homology arm (SA_LHX6_R).

The 5' targeted band (765 bp) was produced by 4 out 37 clones (Figure 3.2C). Two of which (clone 4 and 7), did not amplify the wild type PCR product (Figure 3.2B), suggesting that targeting occurred in both alleles of *LHX6*. 3' homologous recombination was verified only in the clones that underwent targeting at the 5' end, all of the 4 clones produced the predicted 963 bp mutant band (Figure 3.2D). Homologous recombination of these four hPSCs clones was further verified by DNA sequencing of the 5' PCR amplicon which confirmed *in frame* insertion of p2A and *mcherry* downstream of the last *LHX6*-coding codon (Figure 3.2E).

During a pilot interneuron differentiation of the derived LHX6 reporter line, I did not detect mCherry signal either by flow cytometry or by fluorescence microscopy at day 45. I therefore removed the floxed neomycin resistance cassette by transient *Cre*

recombinase expression followed by clonal isolation and expansion (Figure 3.2A). In order to identify clones, which lost the resistance gene, primers flanking the neomycin cassette were designed. These primers give rise to a 1.9 kb amplicon when the selection gene (*Neo*) is present or a 276 bp product if removed (Figure 3.2F). Clones identified with the small product were further assayed for neomycin sensitivity. The vast majority of the cells in cultures died after 2 days exposure to neomycin (Figure 3.2G).

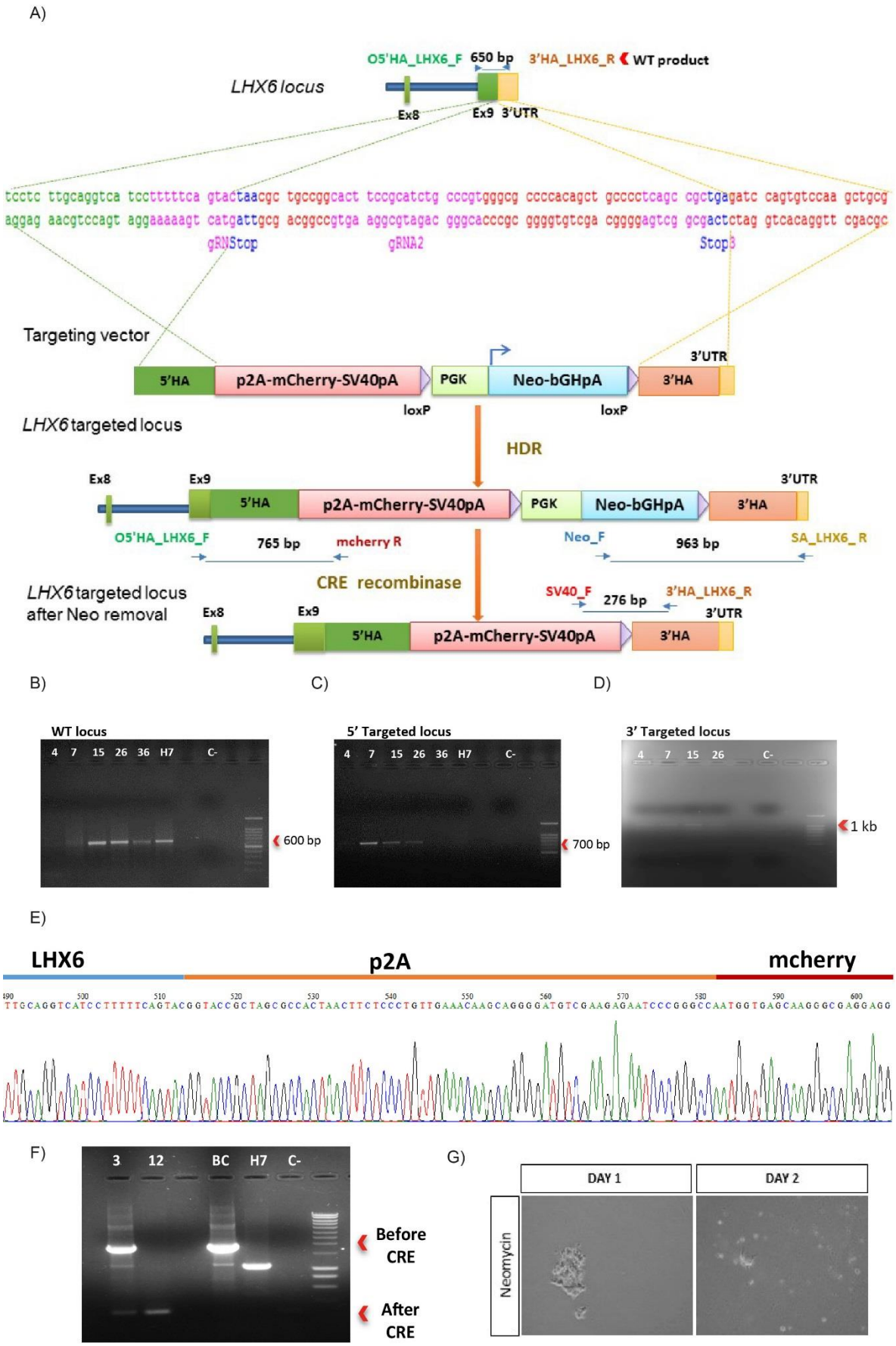

Figure 3.2| *LHX6-mcherry* hPSC line generation. A) For targeting *LHX6* locus, 3 gRNAs (sequence in magenta) were designed to direct Cas9 to the cutting site. DNA repair by homologous recombination was promoted by co-transfection of a targeting vector along the plasmid Cas9/3x

sgRNAs. The targeting vector is flanked by homology arms at the 5' and 3' end respectively, which correspond to the genomic sequence of *LHX6* 500 bp upstream (Sequence in green) and 500 bp downstream of the cutting site (Sequence in red). Between the homology arms, the targeting vector encodes *mCherry* and a resistance cassette for selection of targeted clones. B) Gel is showing the PCR to detect the WT *LHX6*-allele (650). B) Gel is displaying the 765 PCR product to detect the targeted allele in the 5' end by using a forward oligo outside of 5' homology arm with a reverse oligo inside of *mcherry* sequence. C) Gel showing the 963 bp amplicon produced by the targeted allele in the 3' side using the oligos Neo_F and SA_LHX6_R D) Sequencing verification of 5'targeted-PCR amplicon. PCR products from positive clones were purified and sequenced. Downstream of *LHX6* last coding codon, p2A and *mcherry* was integrated *in frame* in the locus. F) PCR base genotyping after CRE recombinase transfection to remove the resistance cassette. A large product (1.9 kb) is amplified from genomic DNA of the cell line before CRE recombinase transfection in contrast to the small product (276 pb) amplified from clones after CRE transfection. G) After removing the neomycin resistant gene, cultures from selected clones where exposed to 150µg/ml G418 to confirm their sensitivity to neomycin. Virtually all cells in the culture were dead after 48 h of exposure to G418.

3.2.2 Targeting the *PV* locus

This part of the work was initiated by a former member of the laboratory and Dr. Lucia Cardo and was carried out prior to LHX6-mCherry targeting. I performed the PCR genotyping of the PV targeting, the cloning of PCR products for sequencing and transient expression of FLP recombinase to remove the selection gene followed by the clonal isolation and phenotype verification of the selection gene removal. Since LHX6 targeting was 100% my work from design to execution I decided to present the LHX6 part first and in greater detail.

3.2.2.1 PV-targeting design

The *PV* a targeting vector was designed and constructed by a former member of the laboratory Dr. Xinsheng Nan. An eGFP reporter was employed and was placed downstream of an IRES sequence. IRES provides a binding site for the 40S ribosomal subunit (Chan et al., 2011), for this reason the stop codon of *PV* is included in the5' homology arm of the targeting vector, as depicted in Figure 3.3A. The *Ires-eGFP* is followed by a FRT flanked antibiotic resistance cassette (CMV-HygTK-SV40pA). These sequences were inserted between the 5' and 3' homology arms, which correspond to

the *PV* gene encompassing 700 bp upstream and 500 bp downstream of the Cas9 cut-site (Figure 3.3A).

To minimise any impact in the expression of the target gene, one sgRNA was designed to target the exon 5 of human *PV* gene encompassing the stop codon. Employing the Cas9 expression plasmid from the multiplex CRISPR/Cas9 assembly system kit (Sakuma et al., 2014), the sgRNA was cloned into the human optimized Cas9 expression plasmid. The resulting plasmid is named Cas9/1xsgRNA

3.2.2.2 PV-GFP cell line derivation

The Cas9/1xsgRNA plasmid was co-electroporated with the PV-targeting vector into the H7 cell line. Both plasmids were delivered as circular plasmids in a ratio of 1 µg Cas9/1xsgRNA: 3 µg PV-targeting vector. Individual hygromycin resistant clones were isolated, expanded and screened for homologous recombination.

Genotyping was firstly carried out by PCR amplification using a forward primer upstream of the 5'homology arm and a reverse primer in hygromycin-TK resistance cassette, 4 out 40 clones gave rise to the expected PCR product for successful targeting (1.6 kb, Figure 3.3B). All four clones were heterozygous as the WT PCR product was also detected (617 bp, Figure 3.3C). Homologous recombination was further confirmed by DNA sequencing of the PCR amplicon (Figure 3.3D). Due to the length of the amplicon, partial sequencing results are shown. The upper panel shows a portion of the 5'HA while the lower panel displays partial CMV promoter sequence.

Once targeted *gfp* integration into the *PV* locus was validated, an expression plasmid encoding *FLP* recombinase (Figure 3.3A) was transfected to remove the CMV-HygroTK-SV40pA cassette upstream of iresGFP.

The excision of the antibiotic resistance cassette should allow the transcription of GFP in PV^+ cortical interneurons. Ganciclovir was used for enriching cells that lost the TK gene (Thymidine Kinase), as in the presence of TK, ganciclovir would be phosphorylated; interfering with DNA replication resulting in cell toxicity, and hence, clones in which the selection cassette was excised became resistant to ganciclovir (Figure 3.3E).

Individual clones resistant to ganciclovir were isolated expanded and assayed for sensitivity to hygromycin. The majority of cells died after 6 days exposure to hygromycin (Figure 3.3E). Clones displaying resistance to ganciclovir and sensitivity to hygromycin were expanded and one of them was selected for a second round of targeting in the *LHX6* locus as described in section 3.2.1.

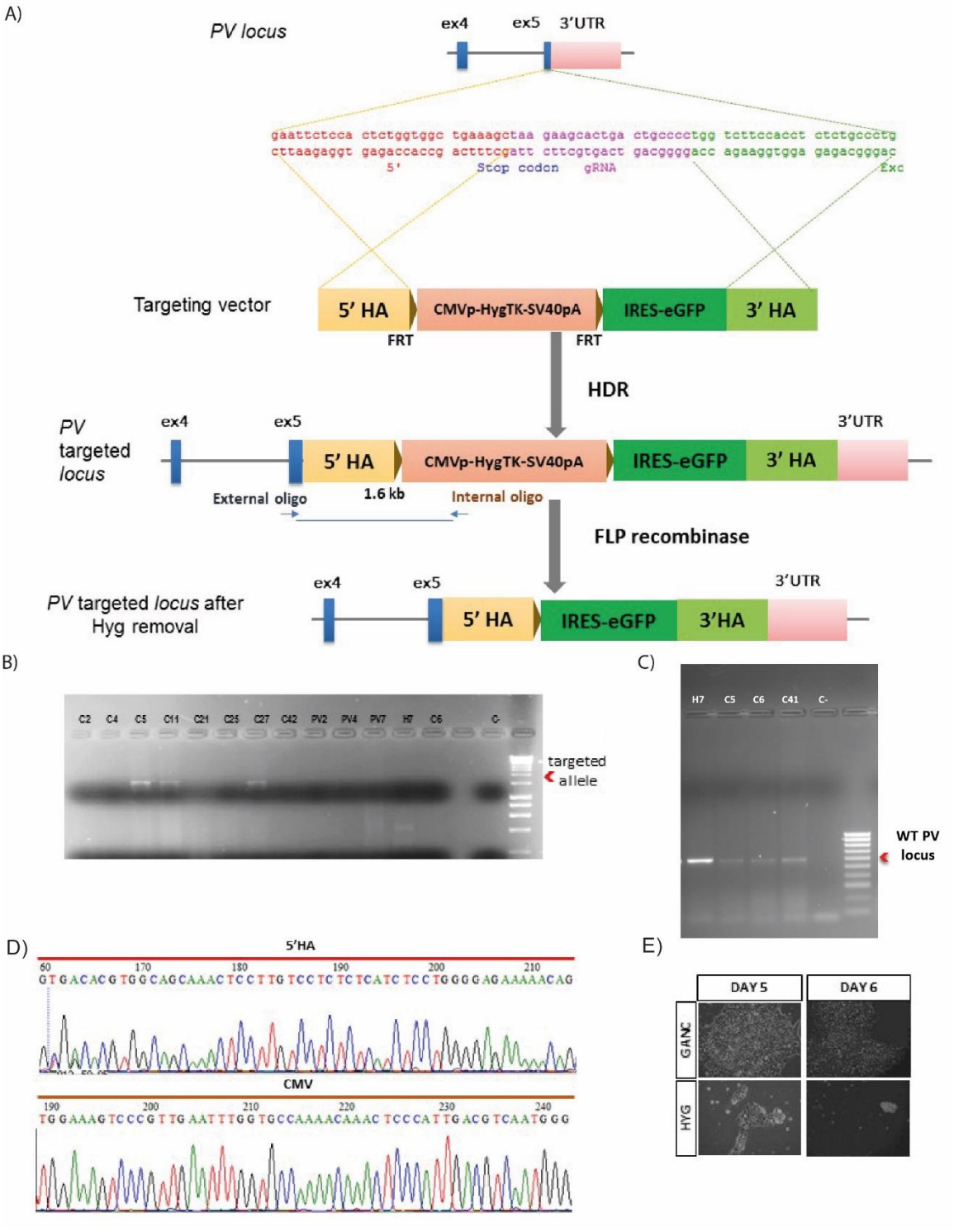

Figure 3.3| *PV-gfp* hPSC line generation. A) For targeting *PV* locus, a gRNA (sequence in magenta) was designed to direct Cas9 to the cut site in the exon 5 of *PV*. A targeting vector was co-transfected along with Cas9/1xsgRNA to promote DNA repair by homologous recombination. The targeting vector contains GFP coding sequence and a positive/negative dual selection cassette (CMVp-HygTK-SV40pA) flanked by homology arms, which correspond to the genomic sequence of PV. Sequence upstream of the Cas9 cutting correspond to the 5'HA (sequence in red) and sequence downstream is the3'HA (sequence in green. B) PCR based genotyping using a pair of primers flanking the 5' homology arm. PCR product (1.6 kb) was obtained from 10% of clones screened. C) Targeted clones are heterozygous as they gave rise to the PCR product to detect the WT allele. D) Partial sequences from the PCR product to detect the targeted allele showing a portion of the 5'HA and the CMV promoter integration. E) Isolated clones after FLP recombinase transfection were resistant to ganciclovir, and sensitive to hygromycin showing loss of the resistance cassette.

3.3 Discussion

In this chapter I successfully generated a dual reporter hPSC line (LHX6-mcherry/PV-GFP), by targeted insertion of a mcherry and GFP reporter to the *LHX6* and *PV* locus, respectively. The LHX6-mCherry reporter is designed to identify MGE-derived GABAergic cortical interneurons (derived from the MGE) (Liodis et al., 2007). The LHX6-mcherry/PVAL-gfp dual reporter line is expected to be a highly valuable tool for studying different aspects of the development and function of interneurons in health and diseases as cortical interneuron dysfunction has been implicated in the aetiology of NDDs (Coghlan et al., 2012; Wohr et al., 2015).

A NKX2.1-GFP hPSCs reporter has previously been developed with the aim of tracing the development of forebrain derivatives (Goulburn et al., 2011; Maroof et al., 2013). However the GFP^{+} neural progenitors derived from this reporter are not necessarily committed to GABAergic cortical interneurons due to the role of Nkx2.1 on cholinergic development (Lopes et al., 2012; Sandberg et al., 2016; Sussel et al., 1999). Moreover Nkx2.1 expression pattern suggest that in an advanced state of differentiation Nkx2.1 is indeed labelling striatal interneurons (Nobrega-Pereira et al., 2008; Sussel et al., 1999). In contrast, LHX6 expression is restricted to nascent cortical interneurons and its expression remains in these cells in their mature state (Du et al., 2008; Sandberg et al., 2016). Despite the accumulated literature suggesting that LHX6 might provide a better labelling for cortical interneurons, a detailed characterization of the specificity and expression profile of mCherry signal in progenitors and interneurons derived from the

LHX6-mCherry hPSCs is necessary in order to address whether the targeting of *LHX6* is a better strategy than NKX2.1-GFP for tracking cortical interneurons. It is also necessary to demonstrate the faithful labelling of MGE-derived interneurons as it has been reported that even when a reporter is driven by endogenous regulatory elements of targeted genes, the labelling of other populations may occur (Hu et al., 2013).

Although it is predicted that the LHX6-mcherry reporter will label the majority of MGE-derived interneurons, the identification of specific interneuron subtypes would require another marker or reporter (e. g. by targeting *PV* and *SST* genes). Unlike the vGAT-mCherry reporter published to date, which labels all GABAergic neurons (DeRosa et al., 2015), the hPSCs dual reporter described in this thesis was designed to specifically mark the PV subtype. Since PV and SST are the two major interneuron subtypes originated in the MGE, the reporter cell derived $mCherry^{+}$-GFP^{+} would be the PV subtype, while the $mCherry^{+}$_GFP^{-} mature neurons would likely be the SST^{+} subtype. However, since the expression of cortical interneuron subtype markers occurs late during foetal development (*PV mRNA* increases after 200 days of development whereas *SST* increases after 100 days, reported in the human brain transcriptome database (http://hbatlas.org/), and that hPSC-derived neurons are often immature, $mCherry^{+}$_GFP^{-} phenotype *in vitro* may represent immature MGE derived interneurons.

In contrast to classic strategies of homologous recombination, which required the use of longer homologous arms (beyond 1.5 kb) (Zwaka and Thomson, 2003), the use of CRISPR/cas9 technology in this work allowed the efficient targeting with homologous arms as short as 500 bp and 700 bp in two independent loci in hESCs. This is in line with published reports suggesting that short homology arms of 500-1000 bp in length are sufficient for CRISPR/Cas9 assisted gene targeting (Merkle et al., 2015; Zhu et al., 2015). Moreover, unlike traditional gene targeting method, which requires the delivery of up to 40 ug of targeting vector (Zwaka and Thomson, 2003); the CRISPR/Cas9 strategy in combination with modern methods of DNA delivery, such as nucleofection, allowed the use of smaller quantities of DNA (1-2 ug of Cas9/sgRNA along with 6-7 ug of targeting vector) delivered as circular plasmids. Additional advantages of the selected methods for deriving the dual reporter line was the possibility of using more than one sgRNA to target a locus. In this thesis, 3 sgRNAs were used for LHX6 targeting which lead to the generation of two homozygous clones, while one sgRNA was used in the case of *PV* locus

where all the targeted clones were heterozygous. Although targeting efficiency can be loci dependent, this result suggests that multiple gRNAs increases gene editing efficiency. This finding agrees with a previous study by Kabadi, et al. 2014; in which a higher level of target gene activation was achieved when multiple gRNAs were employed for targeting the promoter of a gene of interest in a CRISPR activator system (Black et al., 2016; Kabadi et al., 2014).

Regarding the functionality of the dual reporter, when designing the LHX6 targeting vector the drug selection gene was placed downstream of mCherry sequence (Figure 3.2A). This design allows mCherry to be expressed without the need to remove the selection cassette. However, I did not detect mCherry expression at day 45 of differentiation a stage when LHX6 is known to be expressed (Maroof et al., 2013). We postulated that the lack of mCherry signal may be due to interference by the *neomycin* resistance gene. Inhibition of the reporter expression by the drug selection unit, even when it is placed downstream of the reporter gene has also been recently observed in the derivation of an OCT4-GFP hPSCs reporter (Zhu et al., 2015). Interestingly, the opposite effect (increased intensity of fluorescence) as an effect of a retained selection cassette in a knock in mouse has also been documented (Scarff et al., 2003). In addition to above reports, several studies have suggested a potential interaction between the resistance cassette (specifically the PGK-neo) and the regulatory elements of the targeted gene (Pham et al., 1996; Scacheri et al., 2001). It has also been suggested that such interaction may vary a lot in different loci (Pham et al., 1996). Thus, the removal of the selection element is advisable as the effect of the retained selection unit is unpredictable. These reports, together with the absence of the LHX6-mcherry reporter signal prior to the excision of the selection cassette in my study, suggest that the removal of the selection cassette may be a necessary manipulation in order to visualise the expression of the reporter gene. Further functional characterization of the dual reporter will be presented in Chapter 4.

4. Faithful expression of the mCherry reporter during differentiation of hPSCs towards the MGE fate

4.1 Introduction

In contrast to transgenic integration of exogenous promoters, reporter cell lines generated by knock in approach offer advantages for containing all the required components of the endogenous gene regulatory units, such as promoters and enhancers. Thus, expression of the knock in reporters are more likely to faithfully mirror the dynamic transcription of the targeted gene (Rojas-Fernandez et al., 2015). Indeed, published data demonstrates that the fluorescent protein reporters in the existing hPSCs knock in lines exhibit expected expression patterns appropriate to the state of differentiation and the targeted gene, and are co-expressed with the protein produced by the target genes (Li et al., 2015b; Zhu et al., 2015). Combining the multi-lineage differentiation potential of hPSCs, cell type specific reporter lines serve as a powerful tool for investigations concerning cell fate decisions at molecular, cellular and physiological levels.

The success of using hPSC reporters relies on the full preservation of pluripotency and differentiation potential by these cells. Another key requirement is the faithful expression of the reporter to that of the targeted gene. From the plethora of accumulated knowledge from mouse models, it is known that Lhx6 is expressed in the MGE from E11.5 and is mostly localised in the sub-ventricular and sub-mantle zones of the MGE, marking post-mitotic neurons and potentially progenitors leaving the cell cycle (Grigoriou et al., 1998; Liodis et al., 2007). As mouse embryonic development proceeds, the expression of Lhx6 is further restricted to and preferentially expressed in PV and SST interneurons. Therefore, it is important to ascertain that the LHX6-mCherry reporter expression mirror the above pattern during MGE differentiation *in vitro.* This can be achieved by the combined use of small molecules and growth factors mimicking mouse forebrain development and instructs the cells towards the MGE-like fate, activating NKX2.1 expression that in turns activate LHX6 expression (Du et al., 2008; Maroof et al., 2013; Noakes et al., 2019), thus providing a cell population to assay mCherry expression pattern and fidelity.

One of the main applications of the LHX6-mcherry hPSCs reporter lines is to develop an improved interneuron differentiation protocol. In terms of interneuron differentiation, currently most of the published protocols successfully generate a large proportion of $NKX2.1^+$ cells, reflecting efficient acquisition of an MGE-like identity.

These $NKX2.1^+$ cells can be further differentiate into $GABA^+$ cells. However, as summarised in Sun et al. 2016, these protocols produce low percentages of SST^+ (1.53 % of total cells) and even lower percentages of PV^+ interneurons (less than 1% of total cells), although a pre-sorting step of $NKX2.1^+$ MGE progenitors could increase the yield (Maroof et al., 2013; Nicholas et al., 2013; Sun et al., 2016). The low yield of MGE-derived interneuron subtypes has been partially attributed due to the long timeline required for interneuron maturation (Nicholas et al., 2013). Higher yield of PV^+ has been reported in mice by direct reprogramming, but the PV^+ phenotype was not stable (Colasante et al., 2015). Therefore, further research is need to promote efficient *in vitro* generation of defined interneuron subtypes.

The complexity of the developmental mechanisms governing interneuron diversity makes challenging to develop improved differentiation paradigms. As the differentiation protocols seek to mimic the embryonic development of the MGE-derived interneurons, the optimisation of the differentiation protocols needs to take into account the intricate interaction of cell intrinsic control and environmental influences as well as temporal sequence of these regulatory mechanisms. Hence, a detailed understanding of the developmental trajectories of the interneuron subtypes will inform on the cues and timing required by hPSCs during *in vitro* differentiation.

The recent development of single cell RNA-seq technologies have uncovered exciting new information on such developmental mechanisms. This new technology allows the delineation of genes expressed at different phases of development of the MGE subpopulations, presumably fated to become SST^+ or PV^+ interneuron subtypes (Mayer et al., 2018; Mi et al., 2018). However, once these genes are identified, their functional role during interneuron differentiation and maturation must be tested in order to design new differentiation protocols that allow the generation of interneuron populations with mature phenotypes that serve as disease models, drug screening and regenerative medicine applications. Therefore, the generation and validation of hPSC reporters to track MGE-like cells fated to become interneurons is essential.

In this chapter, I present an extensive characterization of the LHX6-mcherry reporter and provide evidence of its potential as a screening platform for functionally identifying factors capable of regulating interneuron specification and maturation. However, I was unable to validate GFP expression in PV^+ neurons due to the very low yield of PV^+ cells under our differentiation protocol. Therefore, the dual reporter will be referred as LHX6-mCherry reporter thereafter in this thesis.

4.2 Results

4.2.1 The key features of hPSCs are preserved in LHX6-mCherry reporter cells

To start the characterization of the LHX6-mCherry reporter cells, the expression of the pluripotency marker OCT4 was verified by immunostaining. As shown in Figure 4.1A, under self-renewal conditions, the vast majority of cells were stained positive for OCT4. The colony morphology appeared flat and compact, which is typical for human pluripotent cells (Figure 4.1B). Karyotyping revealed that 82% of cells contained 46 chromosomes, the normal number for somatic human cells (Figure 4.1C). However, this analysis was restricted to preparing chromosomes for counting, following the procedure detailed in section 2.3.4. Therefore, genomic DNA was extracted from the dual reporter cell line and the H7 parental line. The core team of the MRC Centre for Neuropsychiatric Genetics and Genomic performed a CNV (copy number variation) analysis. The dual reporter displays two CNVs also found in the parental H7 cell line (a deletion in the 2q37.3 and a duplication in the 3q26.1), hence, these CNVs were not generated during the two rounds of targeting. Furthermore, the duplication in region 3(q26.33q27.2) has been found in advances passages of hESCs (Spits et al., 2008). Because of the close proximity with the duplication found in both the dual reporter and the parental line, it is possible that this duplication was caused by long-term culture. With regard to the deletion in 2q37.3, this has not been reported within the common abnormalities found in hESCs, the closest abnormality to this locus was a deletion in the position 2(q24q33), which was reported as a non-recurrent abnormalities found in hESCs (Taapken et al., 2011). Another CNV in locus 17p13.1 (deletion) was detected in the LHX6-mCherry/PV-

GFP, unlike the previous CNVs, this was not present in the parental cell line. After an extensive search, I could not find this CVN reported as common or rare CNVs previously identified in hESCs and further investigation will be necessary to address to which extent this CNV may affect the properties of the the LHX6-mCherry/PV-GFP reporter. The above results demonstrates that most of the key properties of PSCs were maintained following two rounds of gene editing.

The LHX6-mCherry cells where then induced to differentiate towards MGE-like fate, following a protocol modified from Maroof et al., 2013 (described in Noakes et al., 2019) (Figure 4.1D). Small molecule based dual SMAD inhibition was used to promote neuralisation. In this protocol, dual SMAD inhibition was performed by the combined action of LDN-193189 and SB-431542. WNT signalling inhibition was promoted with XAV939 to facilitate the acquisition of anterior/ventral fate. The cells were further ventralised by exposure to SHH and purmorphamine which is a SHH agonist (Maroof et al., 2013). In order to assay whether the gene editing process had any impact on the differentiation potential of the LHX6-mCherry reporter cells were differentiated alongside the H7 parental cells. It was found that at day 21 of differentiation, the major population of the culture expressed FOXG1, a key transcription factor important for telencephalon development and is considered a *bona fide* marker for telencephalon (Aguiar et al., 2014). At this stage, MGE markers such as NKX2.1, and OLIG2 were also detected at abundance (Figure 4.1E).

Counting the number of immune-reactive cells for telencephalic and MGE markers revealed similar percentages of cells positive for NKX2.1 (H7: 90.13±2.07, LHX6-mCherry: 88.26±2.80), OLIG2 (H7: 13.18±1.16, LHX6-mCherry: 12.66±1.06) and FOXG1 (H7: 72.32±2.98, LHX6-mCherry: 80.64.26±3.98) (Figure 4.1F); suggesting that differentiation potential was not affected after two rounds of gene targeting.

The above progenitors were further differentiated until day 65. At this stage, cells expressing MGE-derived neuronal markers, such as GAD67 and SST were found in the cultures (Figure 4.1G). However, no PV^+ cells were detected by immnunocytochemistry (Figure 4.2 A). A RT-PCR for detecting *PV* transcript was also performed, the transcript was barely upregulated along differentiation (Figure 4.2 B). I therefore concluded that PV cells were not present in those cultures by day 65 of differentiation. Furthermore, no GFP signal was observed in lived cells by fluorescent microscopy. Taking these results

together, I concluded that the lack of PV cells rather than the dysfunctionality of the GFP reporter was the cause of the absence of GFP signal. Although these results were obtained from two independent sets of differentiation, it is possible that the evaluation of PV^+ cells production and PV-GFP functionality will need the analysis of several differentiations and longer timeframe. This because it is known that the generation of PV^+ cells using our differentiation paradigm is not robust, as PV^+ neurons were detected in 50% of independent differentiations (Noakes et al., 2019).

In addition the timeline of PV^+ interneurons development is extended to postnatal stages in mouse (Mukhopadhyay et al., 2009), while the *in vitro* differentiation of hPSCs towards cortical interneurons resembles the extended timeline of cortical interneuron development in human (Nicholas et al., 2013). This highlights the need for extending the timeline of the analysis. Moreover, future validation of the PV-GFP reporter will require the use of a positive control each time that PV is assayed by immunostaining. In my experiments, the used PV antibody has proven to detect PV interneurons in other experiments; however, as change of experimental conditions may affect antibody performance, the use of a positive control is necessary to accurately determine whether PV is present or absent in the analysed cultures.

Interestingly numerous CR^+ cells (Figure 4.1G), a lineage mostly originated from the CGE (Kelsom and Lu, 2013), were identified. Although a small proportion of CR^+ interneurons that co-expressing SST are derived from the dorsal MGE (Fogarty et al., 2007), double staining for CR and SST detected few double positive interneurons. The lack of PV^+ cells has prohibited the functional validation of the PV-GFP reporter function. This highlights the need for a better understanding of interneuron subtype specification that would facilitate the design of efficient differentiation paradigms for defined interneuron subtypes.

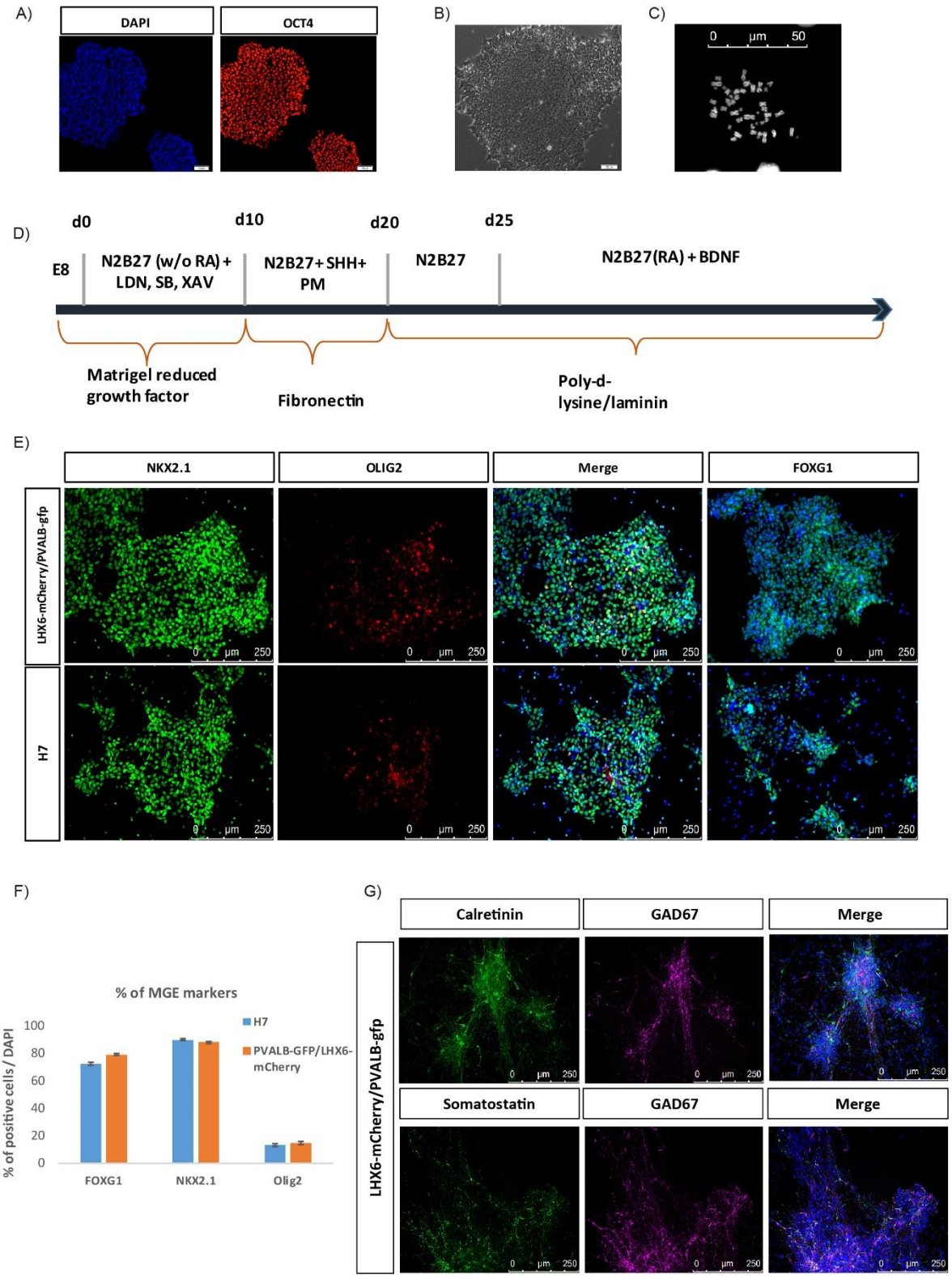

Figure 4.1| LHX6-mcherry/PV-gfp dual reporter cell line acquires MGE-like fate upon differentiation. A) The dual reporter cell line expresses the transcription factor OCT4 as a marker of pluripotency after two rounds of gene targeting, virtually all the cells in the culture are positive for OCT4 (red) assayed by immunocytochemistry. B) The colony morphology of the dual reporter cell line is characteristic of hPSCs. C) 82% of cells contains normal number of chromosomes. D) Diagram of the differentiation protocol to induce MGE-like fate. The diagram depicts media, factors, and substrate and time point of each stage of the differentiation. E) Upon differentiation, the dual reporter cell line is committed to a MGE-like fate, expressing distinctive transcription factors of MGE as NKX2.1 (green) and OLIG2 (red), >70% of cells is also expressing

FOXG1 showing their anterior character. F) Quantification of the percentage of MGE markers in the cultures, showing that the dual reporter cell line owns a comparable capability to the parental line H7 to acquire MGE-like fate. Bar graphs shows mean ± SEM. No statistical difference between the parental line H7 and the dual reporter cell line. (H7: n=9, dual reporter: n=9, P>0.05, 2-tailed t-test). G) After allowing maturation of the MGE-like cells, they acquire fates of MGE derivatives, such as calretinin (green), SST (green) and GAD67 (magenta). Scale Bar: A and B 20 µm, C 50 µm, E and G 250 µm.

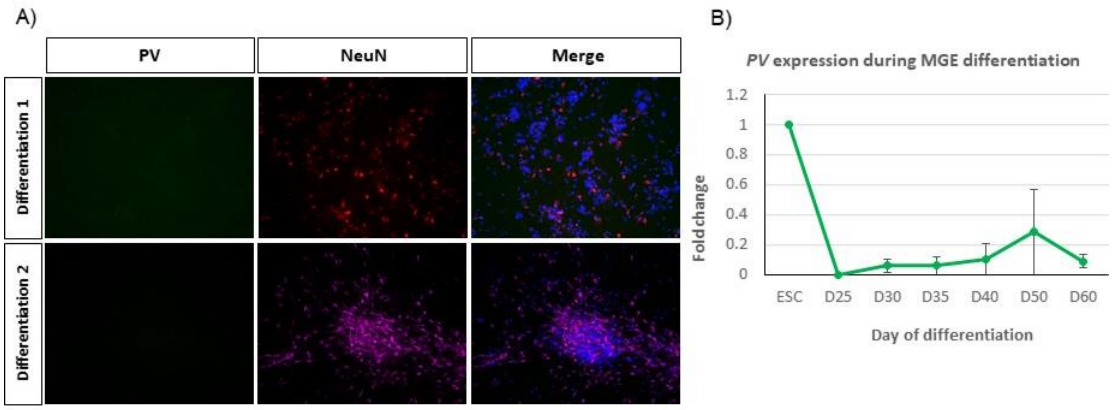

Figure 4.2| No PV$^+$ cells were detected by day 65 of the dual reporter differentiation. A) Immunocytochemistry for detecting PV$^+$ cells (green). No PV$^+$ cells were detected in spite that many cells were already NeuN$^+$ (red or magenta). B) Expression profile of *PV* along MGE differentiation. PV transcript was downregulated with respect to ESCs and it was not upregulated by day 60 of differentiation. Bar graphs shows mean ± SEM (n=2).

4.2.2 Kinetic of mCherry$^+$ cell population mirrors the expression pattern of LHX6 during MGE differentiation

LHX6 is known to be expressed in immature interneurons once MGE progenitors leaving the cell cycle and it is necessary for the development of SST and PV cortical interneurons (Du et al., 2008; Liodis et al., 2007). I therefore examined the generation of mCherry$^+$ cells during MGE differentiation, and their co-expression with LHX6. Firstly, I characterised the dynamics of *LHX6* transcript expression by qPCR during MGE differentiation protocol. I found that, although upregulated upon differentiation, *LHX6* transcription level was not remarkably increased, as its maximum fold change was 23.83±9.48 (4.3A). Secondly, I monitored the presence of mCherry$^+$ cells by flow cytometry, as well as by direct inspection under the fluorescence microscope. Flow cytometry detected mCherry$^+$ cells from day 20 and the number gradually increased to

its peak at day 35 (21.71 ± 1.82%, Figure 4.3B). According to studies in mice, LHX6 expression is maintained in mature neurons (Liodis et al., 2007), however, the percentage of mCherry$^+$ cells decrease after day 35.

The above observation was unexpected. Given that mCherry$^+$ cells are post-mitotic, the observed decrease in proportion of these cells could be due to the proliferation of mCherry$^-$ cells, which could contain precursors of mCherry$^+$ cells as well as those destined to other fates. To investigate whether such decrease was due to a diluting effect of the mCherry$^+$ population by the proliferative mCherry$^-$ cells, I treated the differentiation cultures with demecolcine, an inhibitor of microtubules polymerization, which prevents cell division through destabilization of the microtubule attachment to spindle poles (Yang et al., 2010).

Cultures were treated with 1µg/mL of demecolcine for 2 hours on day 35 of differentiation and the percentage of mCherry$^+$ cells was assayed by flow cytometry at days 40, 45, 50 and 60 (Figure 4.3C). I found that, instead of decreasing in number as in untreated cultures after day 35, the number of mCherry$^+$ cells in demecolcine treated cultures increased to its highest level of 38.92 ± 1.95% at day 40. The proportion of mCherry$^+$ cells dropped slightly to 31.5 ± 1.0% at day 45 and to 28.6 ± 0.9% at day 60 (the latest time point analysed). These results suggest that the decrease of mCherry$^+$ population observed previously was most likely due to expansion of mCherry$^-$ cells rather than a dramatic loss of mCherry$^+$ cells at the later phase of differentiation. The temporal profile of mCherry$^+$ cells under such condition mirrors the expression pattern expected for LHX6 during MGE development, which start in nascent MGE-derived neurons and maintained in cortical interneurons throughout life. However, few mCherry$^+$ cells were readily detectable by direct observation of the cultures under the fluorescent microscope (Figure 4.3D).

I then investigated whether mCherry$^+$ expression faithfully mirrors that of LHX6 protein by double immunostaining for mCherry and LHX6. Firstly I evaluated the specificity of the mCherry and LHX6 antibodies in medium spiny neuron (MSN) progenitors, a LGE-derived fate that lacks LHX6 expression (Fjodorova et al., 2015). MSN were derived from a line of hPSCs constitutively expressing mCherry (kindly provided by a fellow PhD student Francesca Keefe). Immunostaining of MSN progenitors did not show LHX6$^+$ cells whereas mCherry signal was evident (Figure 4.3E). A second set of negative control was

the undifferentiated parental H7 cells alongside the LHX6-mCherry reporter. All cells appeared LHX6$^+$, however a weak staining of mCherry was found only in the LHX6-mCherry hPSCs (Figure 4.3F). Then I proceeded to evaluate the co-localisation of mCherry and LHX6 in MGE-like progenitors, I found that 97.9 ± 0.46 % of LHX6$^+$ cells were mCherry$^+$, while 97.56 ± 1.10 % of the mCherry$^+$ cells were LHX6$^+$ (Figure 4.3G). This result suggests that the mCherry reporter faithfully marks the LHX6$^+$ cells.

However, immunostaining detected many more mCherry$^+$ than those by flow cytometry. 17.27± 1.67% mCherry$^+$ cells were detected at day 40 by flow cytometry whereas 89.48±2.76% mCherry$^+$ cells were detected at day 41 by immunocytochemistry. This inconsistence might be a consequence of the low levels of LHX6 expression during MGE differentiation as previously found by qPCR (Figure 4.3A). It is possible that such low levels of *LHX6-mCherry* transcription give rise to boarder line levels of mCherry protein for the sensitivity of flow cytometry (Figure 4.3B,C), and a level too low for the naked eye to detect under the microscope (Figure 4.3D). However, as the antibody amplifies the signal of LHX6 and mCherry during immunostaining thus higher percentages of mCherry$^+$/LHX6$^+$ cells were found by this method.

Overall, the results presented in this section show that mCherry reporter accurately labels LHX6$^+$ cells. The temporal kinetic of the mCherry$^+$ population during differentiation was consistent with the expected pattern for LHX6 expression in post-mitotic cortical interneurons *in vivo* (Figure 4.3C) and indeed mirror that of *LHX6* transcript profile detected by qPCR (Figure 4.3A).

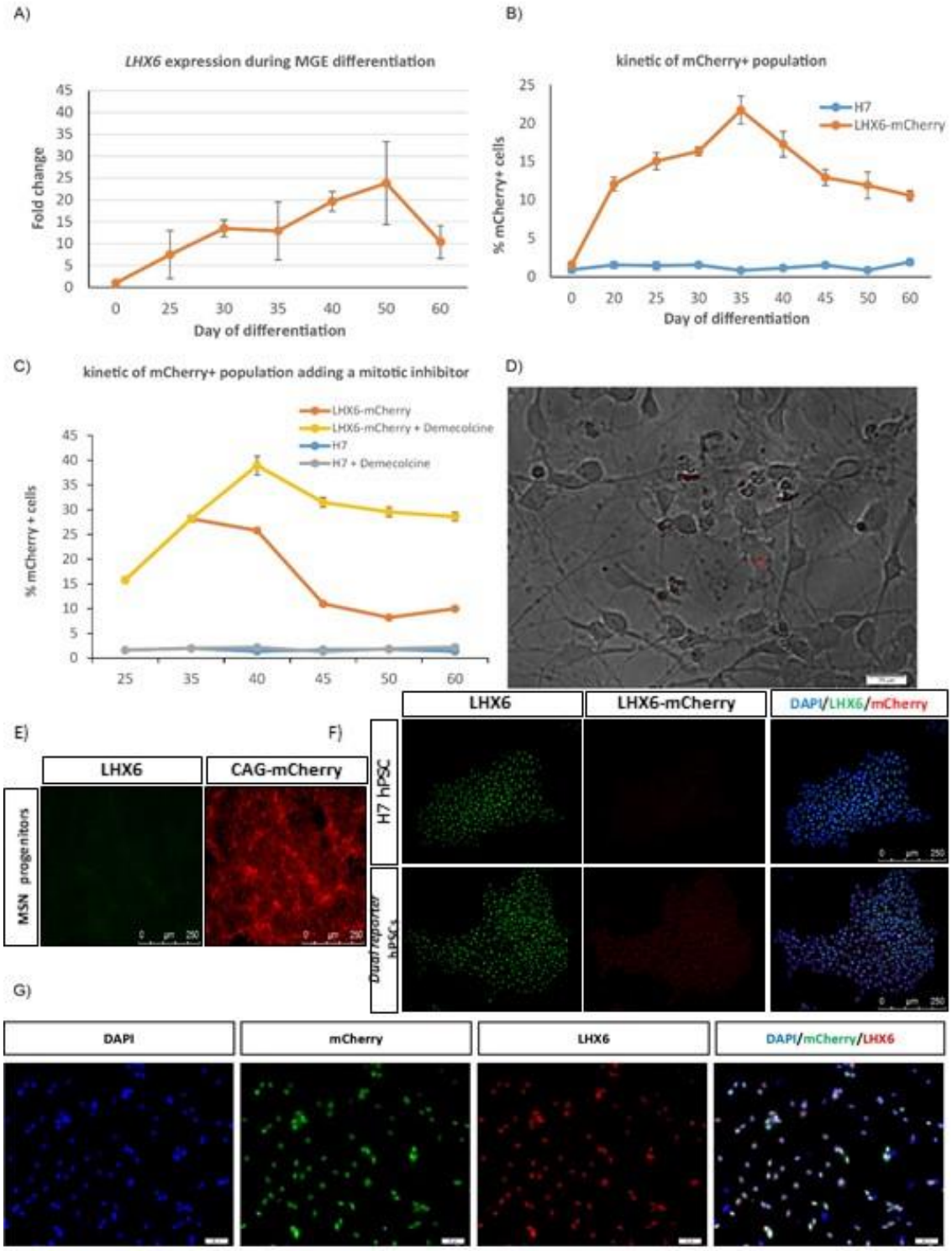

Figure 4.3| LHX6-mcherry/PV-gfp dual reporter cell line labels the LHX6^{+} population. A) Expression profile of LHX6 along MGE differentiation. This data shows a maximum fold change of *LHX6* transcript during the differentiation of the dual reporter was 23.84±9.48 (mean±SEM n=2), whereas the maximum fold change of *LHX6* transcript in H7 cells was 66.55±11.38 (Figure 5.5B). Therefore, the levels of expression of *LHX6* in the dual reporter is decreased by around the half in comparison to the parental cell line. Assaying the effectiveness of the multicistronic expression in the reporter might explain the difference in the LHX6 expression levels. B) Kinetic of the mCherry^{+} population along MGE *in vitro* differentiation. The dual reporter cell line peaks at 21.71 ± 1.82% at day 35 whereas H7 cell line maintains a percentage < 2% at each time point, likely due to auto-fluorescence (Data is presented as mean ± SEM, n=6). C) Comparison of the kinetic of mCherry^{+} population when treated with and without mitotic inhibitor (yellow and

orange line respectively). As in panel B, not treatment with mitotic inhibitor leads to a decrease in the percentage of the mCherry$^+$ population after peaked at day 35. Treatment with demecolcine shifts the kinetic of mCherry$^+$ cells, as it peaks at day 40 and the percentage remains stable from day 45 onwards. Suggesting that decrease in mCherry$^+$ populations is a consequence of dilution of proliferative mCherry- cells (Data is presented as mean ± SEM, n=3). D) mCherry expression observed by fluorescence microscopy in live cells. E, F) Antibodies for detecting LHX6 and mCherry are specificity as no signal for LHX6 is detected in MSN progenitors. LHX6 was detected in the pluripotent stage with a week co-expression of mCherry only in the reporter cell line. G) Immunocytochemistry showing co-expression of mCherry (green) with LHX6 (red) in MGE progenitors derived from the LHX6-mCherry reporter. Virtually all cell expressing mCherry are expressing LHX6 (merge mCherry/LHX6, yellow). D and G Scale bar 20µm. E and F scale bar 250 µm.

4.2.3 mCherry expression is restricted to the MGE-like cells

Another aspect to consider regarding the LHX6-mcherry reporter characterisation concerns regional specificity. To assess whether mCherry expression is restricted to cells of the MGE-fate, the LHX6-mCherry cells were induced to differentiate towards the cortical-fate, with the MGE differentiation as the positive control.

The generation of cortical cells was achieved by culturing cells in basal N2B27 medium following the dual Smad inhibition step (ie. the control condition as described in Arber et al., 2015) . To corroborate that the cells acquired the expected fate as designed by the protocol, cortical and MGE markers were assayed by immunocytochemistry. Both the cortical and MGE cells should express the pan-forebrain marker FOXG1 (Aguiar et al., 2014), while only cortical-like progenitors express PAX6, a transcription factor that is expressed in the radial glia of dorsal mouse telencephalon (Ypsilanti and Rubenstein, 2016) (Figure 4.4B, D). As expected, NKX2.1$^+$ and OLIG2$^+$ cells were absent in the cortically differentiated cultures (Figure 4.4B, right column and Figure 4.4C).

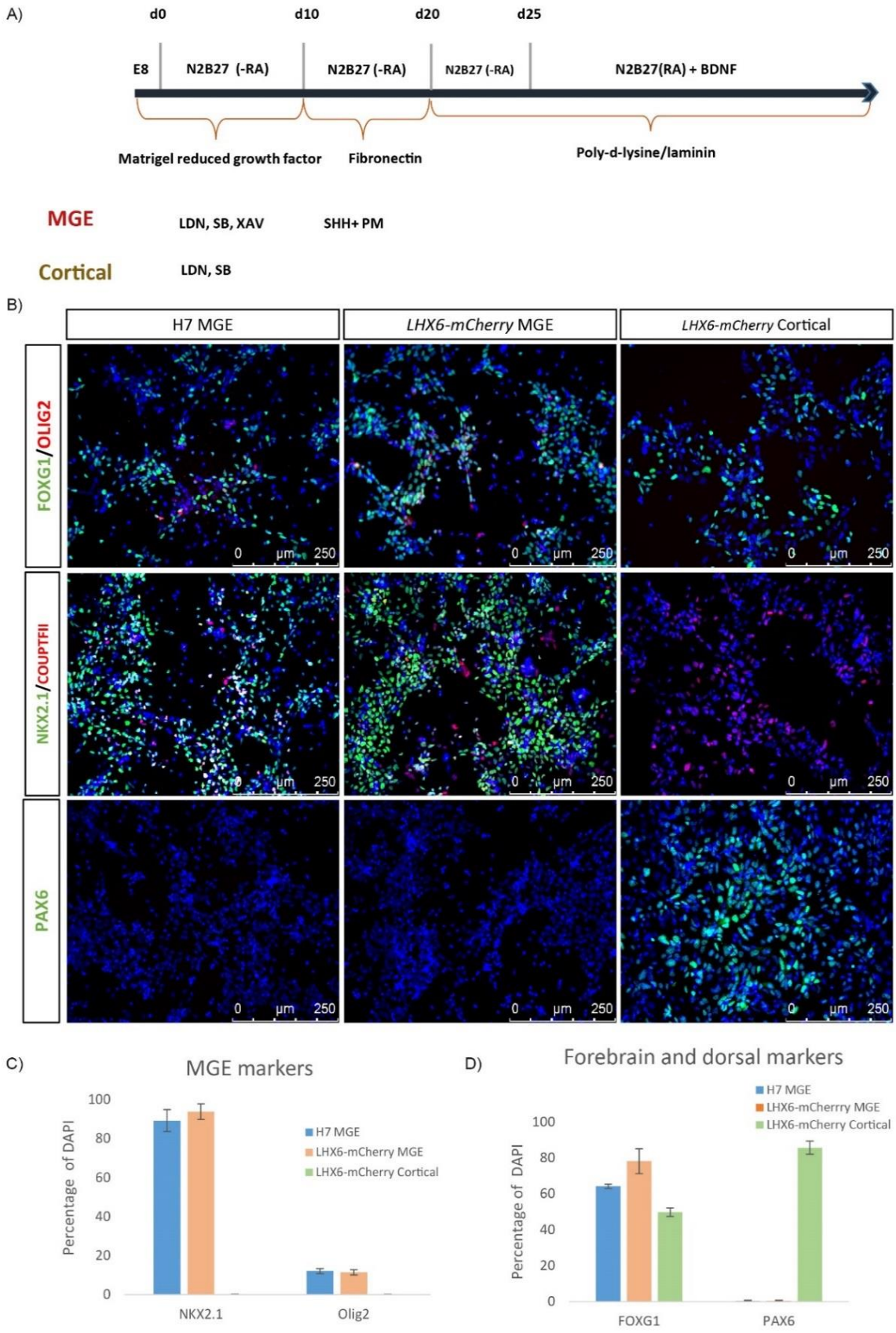

Figure 4.4| The reporter cell line displays the correct set of MGE or cortical makers. A) Comparison of the small molecules and growth factors employed to induce MGE and cortical fate. B) The H7 parental line and the dual reporter cell line induced to differentiate towards MGE fate give rise to FOXG1^{+}, NKX2.1^{+}, OLIG2^{+} , PAX6^{-} cell population, whereas the dual reported cell line induced to differentiate as cortical progenitors were FOXG1^{+}, NKX2.1^{-}, OLIG2^{-}, PAX6^{+} cell population. C) Percentage of positive cells for MGE makers in H7 and LHX6-mCherry found in

cells differentiated through MGE and cortical-differentiation paradigms. (Data is presented as mean±SEM, n=3) D) Percentage of positive cells for forebrain and dorsal markers in cell populations obtained through MGE and cortical protocols. (Data is presented as mean±SEM, n=3). B scale bar 250 µm.

In contrast, NKX2.1^{+}- OLIG2^{+}- PAX6^{-} cells were found in MGE cultures (Figure 4.4B left and middle column and Figures 4.4C, D). During human embryonic development, PAX6 is found in the CGE and LGE on the 15 gestation week but is absent in the human MGE (Mo and Zecevic, 2008). The absence of PAX6 in MGE-like cultures validated the robustness of the MGE differentiation paradigm, which was further confirmed with the quantitative outcome of the assayed markers in my cultures (Figure 4.4 C and D).

Lhx6 is known to be expressed in the ventral telencephalon but absent in the dorsal mouse developing forebrain (Grigoriou et al., 1998; Liodis et al., 2007). Additionally, there is evidence that LHX6 expression is absent during human cortical development (http://cortecon.neuralsci.org/). Therefore, mCherry signal is predicted to be uniquely detected in cells differentiated through the MGE protocol whilst absent in cortical differentiation.

By flow cytometry analysis, I found that mCherry signal was indeed absent in cortical cultures at day 25, 35 and 45, while detected in the MGE cultures at the 3 time points analysed (Figure 4.5A). Moreover, immunocytochemistry analysis of day 65 in cortical cultures confirmed the absence of SST^{+} cells (Figure 4.5B), while this cell type was evident in MGE cultures as predicted (Figure 4.5B), importantly these SST^{+} cells were mCherry^{+} (Figure 4.5C). The findings described in this section, demonstrates that mCherry signal, reporting LHX6 expression, is absent in other forebrain fates, thus mCherry expression is a reliable readout to assay culture conditions for the *in vitro* induction of MGE-like fate and its derivatives.

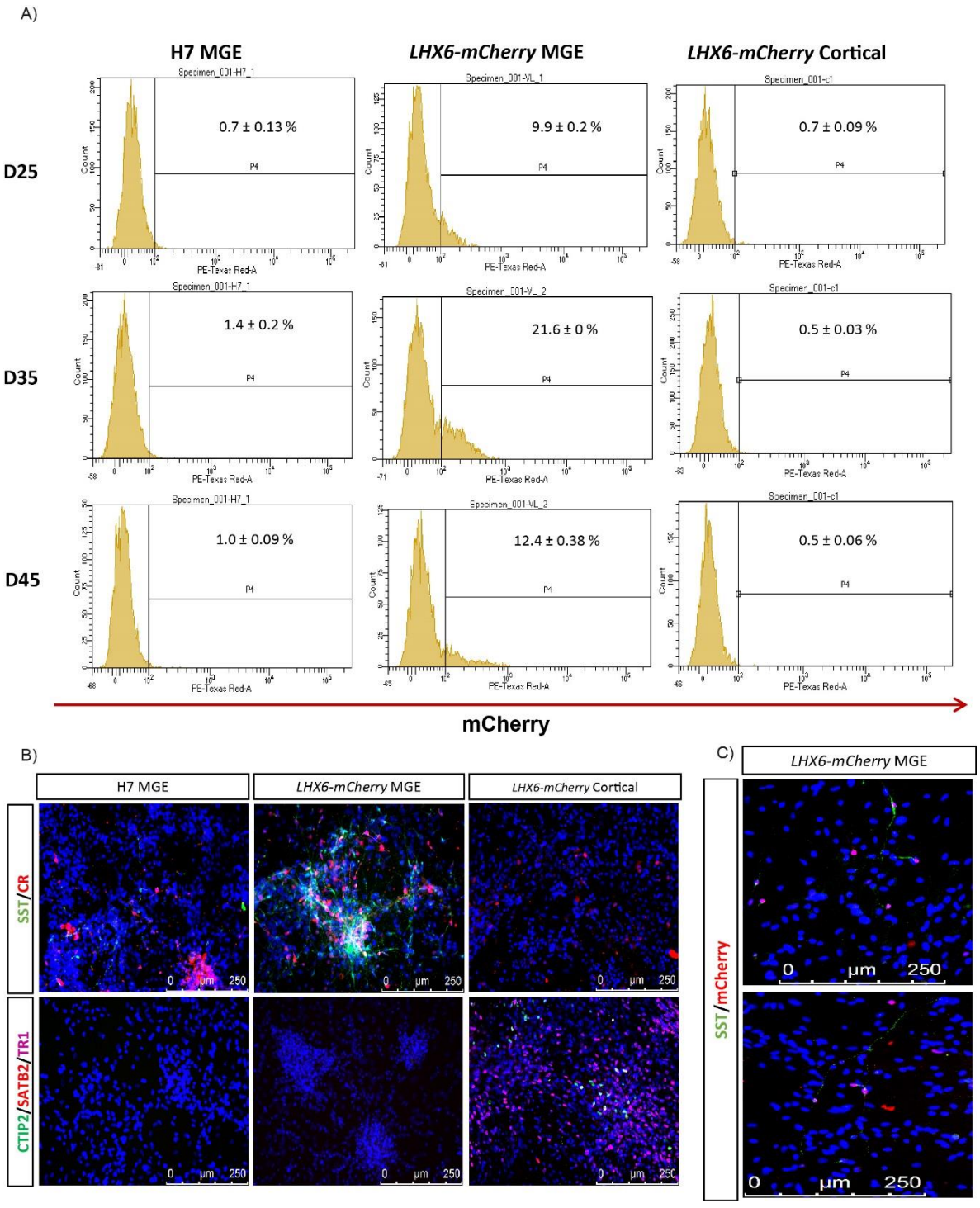

Figure 4.5| mCherry signal is a reliable readout of culture conditions to obtain MGE-derivatives. A) Flow cytometry at different time points along differentiation shows that mCherry signal is only detected during MGE differentiation, whilst mCherry fluorescence in cortical progenitors is comparable to the negative control (H7 parental cell line). B) Maturation of MGE-like population gave rise to SST^+ and CR^+ cells, whereas cortical-like progenitors matured as CR^+ but no SST^+ cells were found Conversely makers or cortical layers were absent in MGE-like mature cells and detected in cortical-like mature cells. C) mCherry is co-expressed in SST^+ interneurons obtained from in vitro MGE differentiation protocol. Thus, a proportion of $mCherry^+$ MGE-like progenitors develop as SST^+ interneurons. B and C scale bar 250 µm.

4.3 Discussion

In this chapter, the functionality of the LHX6-mCherry reporter cell line was evaluated and an extensive characterisation of the reporter cell line showed that, after two rounds of gene targeting, the LHX6-mcherry cells behaved similarly to that of the parental line in generating MGE-like cells, preserving OCT4 expression and normal number of chromosomes (Figure 4.1E, F).

Different approaches were employed to detect mCherry$^+$ cells, such as flow cytometry, immunostaining and direct visualisation of mCherry under the fluorescent microscope. From these different analyses, very few mCherry$^+$ cells were found by direct microscopic inspection of live cells (Figure 4.3D) and a pronounced difference of around 72.21% in the proportion of mCherry$^+$ cells was found by immunostaining and flow cytometry evaluated between day 40 and 41. The discrepancy found by distinct methods might be a consequence of low levels of upregulation of *LHX6* in our differentiation conditions, based on the expression profile obtained by qPCR, where the maximum *LHX6* fold change recorded was 23.83 ± 9.48. This could be hampering the accurate visual detection of mCherry$^+$ cells, which, depending on the expression levels could be only visualised by immunostaining and/or flow cytometry. Indeed the small fold change of *LHX6* detected by qPCR correlates with low intensity of fluorescence detected by flow cytometry. Low levels of *LHX6* expression during *in vitro* MGE differentiation has been also reported by Nicholas, et al., 2013; that through an embryoid body differentiation approach, reported 0.003 fold change (expressed as $2^{-\delta CT}$) of *LHX6* expression (Nicholas et al., 2013).

One of the main purposes to generating the LHX6-mcherry reporter is to identify cortical interneuron determinants. Therefore showing restriction of the mCherry signal to the MGE-lineage was also essential. My results showed that, mCherry expression is only expressed during the differentiation of the MGE lineage but not in pallial derivatives. Therefore, mCherry signal could be used as a readout to screen culture conditions and/or novel molecules and transcription factors able to induce MGE derivatives committed to become cortical interneurons. Even though, it was demonstrated that mCherry signal is not detected during pyramidal cortical differentiation, a lineage derived from the pallium, which does not express LHX6 (http://cortecon.neuralsci.org/),

this experiment do not exclude that mCherry could be inappropriately expressed in other lineages. Since differentiation through embryoid bodies promotes the derivation of cell types from the three germ layers(Brickman and Serup, 2017), differentiating the dual reporter through this approach might help to formally rule out whether mCherry could be wrongly expressed in other cell fates.

Overall, the results presented in this chapter suggest that targeting the *LHX6* gene is indeed a suitable approach to track MGE derivatives fated to become cortical interneurons, nevertheless one of the main limitations of the LHX6-mCherry reporter is the low intensity of the mCherry fluoresce along 60 days of MGE differentiation. It is not clear whether *LHX6* is physiologically low upregulated during MGE embryonic development or whether the low levels of *LHX6* transcript induced during in *vitro* differentiation paradigms are the consequence of the lack of signals to support a strong upregulation of *LHX6*. In either case, the derivation of a second-generation LHX6-mCherry reporter may improve the visual detection of $LHX6^{+}$ cells. Such a second generation of LHX6-mCherry reporter could be done by replacing the mCherry fluorescent protein by the emerald GFP, which has almost three times the quantum yield (fluorescent photons per absorbed photon) than mCherry, and hence may be three times brighter (Cranfill et al., 2016).

Another option to derive a second generation LHX6-reporter line is to adapt the genetic recombination approach used for lineage tracing in mouse models, reviewed in detail in Kretzschmar and Watt, 2012. Such approach consists of introducing the sequence of a recombinase (i. e. Cre or Flp) into the locus of a gene of interest, in our case Cre or Flp would be knocked in the *LHX6* locus. In parallel, a safe harbour is modified by using a targeting vector with the sequence of a constitutive and strong promoter driving the expression of a fluorescent protein. The expression of the fluorescent protein is prevented by placing a stop codon between the promoter and the fluorescent protein and the stop codon is flanked by Frt or LoxP sites, which promote site-specific recombination. Thus, when LHX6 is expressed, Flp or Cre recombinase will remove the stop codon to allow the expression of the fluorescent protein. As the fluorescent protein will be driven by a constitutive promoter it is expected that, all cells that once expressed the gene of interest, even transiently during development, will express the fluorescent protein with strong intensity throughout their life (Kretzschmar and Watt, 2012). The

development of a second generation LHX6-mCherry reporter hold promise as a powerful tool, which can be visually detected under the microscope or high throughput screening platforms to functionally testing and identifying unknown determinants of cortical interneurons.

Regarding the functional evaluation of the PV-GFP reporter, it was shown that after 65 days of *in vitro* differentiation, my cultures contained SST^+ and CR^+ interneurons, but no PV^+ interneurons were obtained, which limited the functional evaluation of PV-gfp reporter. The reasons behind the extremely low yield of PV^+ interneurons are not clear, however it is unlikely to be due to a poor MGE specification, as the original protocol reported by Maroof et al, 2013; using a NKX2.1-GFP reporter line around 60% of cells became GFP^+. In this report cultures were exposed to SHH and purmorphamine in a similar temporal window than in our modified protocol. Indeed, our modified protocol yielded 88.26±2.80 % of $NKX2.1^+$ cells in my experiments. Additionally, using the same protocol another member of our lab found 72.3 ± 3.5% of $NKX2.1^+$ cells and detected 1.5 ± 0.9% of PV^+ cells at day 60 of differentiation (Noakes et al., 2019). These results suggest that the initial MGE specification of our cultures is not compromised neither by the combination of patterning factors or by the temporal window in which those factors were applied. Moreover, Noakes' findings showed that MGE-like progenitors obtained with our modified protocol could differentiate as PV^+ cells.

A noticeable difference between our modified protocol and Maroof's protocol is the co-culture of MGE progenitors onto mouse embryonic cortical cells (E13.5) to promote maturation of interneurons. Under such conditions 5% of $NKX2.1^+$ cells became PV^+. The generation of PV^+ neurons obtained by Maroof supports increasing evidence that early neuron activity might act as either a permissive or an instructive cue to guide cortical interneuron maturation and survival, as extensively reviewed in (Lim et al., 2018; Wamsley and Fishell, 2017). This evidence might partially explain the practically null yield of PV^+ interneurons in my cultures, since no neuron activity was promoted. In contrast to Maroof's findings, Noakes et al., 2019 reported 1.5 ± 0.9% of PV^+ cells without a co-culture step. However, in this study PV^+ cells were detected in 3 out of 6 experiments. This suggest that the generation of PV^+ cells is not robust in our current differentiation paradigm and additional modifications are needed in order to overcome this limitation. The recent standardization of co-culture conditions in our laboratory

could be included into our differentiation paradigm, and may provide an alternative to assay the functionality of the PV-GFP reporter.

Otherwise, the use of the CRISPR/Vp64dcas9Vp64 system to promote transcriptional activation of a target gene (Colasante et al., 2015; Vierbuchen et al., 2010) is another promising strategy that might allow us to evaluate the PV-GFP functionality. The CRISPR/Vp64dcas9Vp64 system is based on the same principle as CRISPR/Cas9 but unlike it, a genetically modified Cas9 is used, this Cas9 has an inactive nuclease domain, referred as dCas9 (dead Cas9). This modified dCas9 is also fused to two trans-activator domains (named Vp64dcas9Vp64). Thus, gRNAs can be designed to direct the Vp64dcas9Vp64 to the promoter of a gene of interest, where instead of promoting a double strand break, it will promote the transcription of the target gene. Through this strategy, gRNAs can be designed not only to evaluate the functionality of the PV-GFP reporter by targeting the *PV* promoter, but also to interrogate the role of specific candidate genes on different phases of interneuron development.

Despite the accumulated knowledge about MGE development in mouse, the existence of some differences between mouse and human forebrain development have also been documented. For instance, a transient FOXA2^{+} population is found during *in vitro* differentiation of hPSCs as well as in human embryos, whereas a FOXA2^{+} population was not found in the developing ventral forebrain in mice (Maroof et al., 2013). In addition, although LHX6 expression is found in GABAergic cells into the monkey cortex, it is also reported some differences in the expression or combination of expression patters of LIM proteins (Such as LHX6) between mouse and primates (Abellan et al., 2010). The differences between mouse, primates and human forebrain development, highlight the relevance of studying human-specific mechanisms orchestrating the development of cortical interneurons. Our current and future experiments, using the LHX6-mCherry cell line, will provide insights on human-specific developmental mechanisms of cortical interneurons, such knowledge will be highly valuable to optimise differentiation protocols to obtain clinically-relevant populations of interneurons as PV and SST subtypes, as well as to study interneuron differentiation mechanisms in health and in disease.

5. The role of TGFβ signalling on cell cycle length regulation during the differentiation of MGE-like progenitors

5.1 Introduction

Gaining a deep understanding of how the intrinsic and extrinsic signals work in concert to govern cortical interneuron development is an area of intense research and will facilitate the development of improved strategies for in *vitro* generation of defined interneuron subtypes, which in turn provide a powerful model for studying molecular mechanisms of human diseases and drug screening. Following the generation of the LHX6 interneuron reporter line, the next aim of my thesis is to functionally testing potential modulators of MGE differentiation.

In this chapter, I investigated the effects of the modulation of TGFβ signalling during *in vitro* MGE differentiation. TGFβ signalling was investigated due to previous reports suggesting it as feasible regulator of MGE differentiation. The first report came up in 2010 by Maira and co-workers, who through a microarray analysis, found expression of members of TGFβ superfamily in the developing mouse subpallium at E15.5 (Maira et al., 2010). Expression of TGFβ and BMP family members were detected at RNA level. Additionally activation of Smad2 (effector of the TGFβ branch) through phosphorylation at serines 465 and 467, was detected by immunocytochemistry at E12.5 and E15.5. Interestingly, phosphorylated smad2 (pSmad2) was found to be co-expressed and interacting with Dlx2. This transcription factor, together with Dlx1, have been related to controlling the migration of cortical interneurons towards the cortex (Le et al., 2007).

Furthermore, by chromatin immunoprecipitation experiments, Dlx2, Smad1, Smad2/3 and Smad4 were found localised at the enhancers of Dlx1/2, Dlx5/6 and Arx in the developing telencephalon at E15.5, suggesting a role for Dlx2/pSmad2 as transcriptional regulators of those genes. Indeed, transient co-expression of Smad2 and DLX5 in COS cells led to an increased transcriptional activation of a lacZ reporter driven by the Dlx5/6 intergenic enhancer (Maira et al., 2010), further supporting a role for Smad2/Dlx-proteins on the transcriptional control of genes related to MGE development.

Moreover, TGFβ signalling inhibition using a dominant negative form of Smad4 showed a role for TGFβ signalling in controlling the migration of sub-pallial cells towards the cortex in E12.5 forebrain explants. Considering that pSmad2 interacts with Dlx2, a discovery of the effects of TGFβ signalling on interneuron migration is in line with the previous identified role for Dlx1/2 on cortical interneuron migration (Le et al., 2007). Thus the work presented by Maira et al., provided the first evidence that functional interaction between TGFβ signalling and Dlx play a role in the development of telencephalic GABAergic neurons.

A second report came up in 2016 by Sandberg et al. who through a combination of genetic and genomic approaches proposed a mechanism by which Nkx2.1 controls the network of transcription factors orchestrating the development of the mouse MGE and its GABAergic derivatives. Briefly, using a conditional *Nkx2.1* knockout mouse (Nkx2.1 KO), Sandberg and co-workers characterized the epigenetic state of regulatory elements of dysregulated genes in the knockout. The epigenetic state of those dysregulated genes was compared with the epigenetic state in the wild type mice. They found that Nkx2.1 acts mainly as a repressor in the MGE, whereas in combination with Lhx6, it mediates the epigenetic transition into a transcriptionally active chromatin at regulatory elements to promote gene expression in MGE derivatives.

In the study above, *Tgfβ3* was found to be downregulated at mRNA level in the Nkx2.1 KO MGE. Furthermore, binding elements for Nkx.2.1 and Lhx6 were found in the putative enhancer of *Tgfβ3.* These results pointed to *Tgfβ3 gene* as a putative transcriptional target of Nkx2.1 and Lhx6, both known to be major players in the specification of the MGE and cortical interneurons. In addition, the activity of *Tgfβ3* putative enhancer was validated in the developing MGE by generating a transgenic mouse driving the expression of lacZ under the control of the putative *Tgfβ3* enhancer, as a result β-gal activity was found in the SVZ and MZ of the MGE at E12.5. Moreover, through a luciferase reporter assay, opposing transcriptional changes were detected when Nkx2.1 and/or Lhx6 motifs were mutated in the *Tgfβ3* enhancer. These experiments confirmed the transcriptional regulation of *Tgfβ3* by Lhx6 and Nkx2.1.

Considering the evidence of TGFβ signalling activation in the developing MGE, and the broad spectrum of its actions, I hypothesized that TGFβ signalling might participate in other aspects of MGE and interneuron differentiation. In this chapter, employing the

LHX6-mCherry reporter along with activation and pharmacological inhibition of TGFβ signalling respectively, I asked the next questions: 1) Does TGFβ signalling affects interneuron production?; if so 2)which are the cellular mechanisms by which TGFβ exert its effects during the differentiation of human MGE-like derivatives?

5.2 Results

5.2.1 TGFβ signalling inhibition leads to a decreased production of LHX6-mCherry^{+} cells

In order to directly test a role for TGFβ signalling in MGE development and interneuron differentiation, I inhibited TGFβ signalling during the patterning stage of our differentiation paradigm using the small molecule inhibitor LY2109761, a dual kinase TβRI/II inhibitor which leads to a decrease of pSmad2 levels (Melisi et al., 2008).

I firstly tested the temporal window by which TGβ inhibition affects interneuron differentiation by applying the LY2109761 inhibitor (referred to as LY hereafter) from differentiation day 11 to 20 (named condition 2 or C2) or day 16 to 20 (condition 3 or C3), fully covering the patterning stage (day 11 to 20) by SHH and purmorphamine. In the control conditions (condition 1 or C1), the vehicle DMSO was added instead of the inhibitor in the same time windows (Figure 5.1A). After LY treatment, the differentiation continued as normally, and cultures were analysed by immunocytochemistry at day 21 and flow cytometry at day 25, 35 and 45.

Immunocytochemistry at differentiation day 21 was performed to detect markers related to telencephalic identity such as FOXG1, and MGE-fate (NKX2.1 and OLIG2). Positive cells for each marker were counted followed by statistical analysis. This analysis revealed that only OLIG2^{+} proportion was affected in the C2 (LY 11-20) treated cultures (C1: 19. 02 ± 5.12 %, C2: 4.35 ± 1.42 %); while NKX2.1 (C1: 94.08 ± 1.0%, C2: 89.15 ± 2.91%) and FOXG1 (C1: 92.06 ± 2.27 %, C2: 89.49 ± 2.5 %) were not significantly affected (Figure 5.1B).

Counting and statistical analysis of the proportion of MGE markers in the cultures differentiated through condition C3 did not display any significant change: NKX2.1 (C1: 91.31 ± 1.24 %, C3: 85.81 ± 2.12 %), FOXG1 (C1: 87.88 ± 3.44 %, C3: 87.29 ± 3.53 %), OLIG2 (C1: 4.51 ± 0.86 %, C3: 3.91± 0.87%). These results were also the case for the H7 parental line, as in both cell lines, only the proportion of $OLIG2^{+}$ cells was decreased in the C2 (H7 C1: 21.76 ± 3.28 %, C2: 6.84 ± 1.95 %), while no changes were detected in the proportion of positive cells for other makers treated with LY compared with cultures treated with the vehicle (Figure 5.2D).

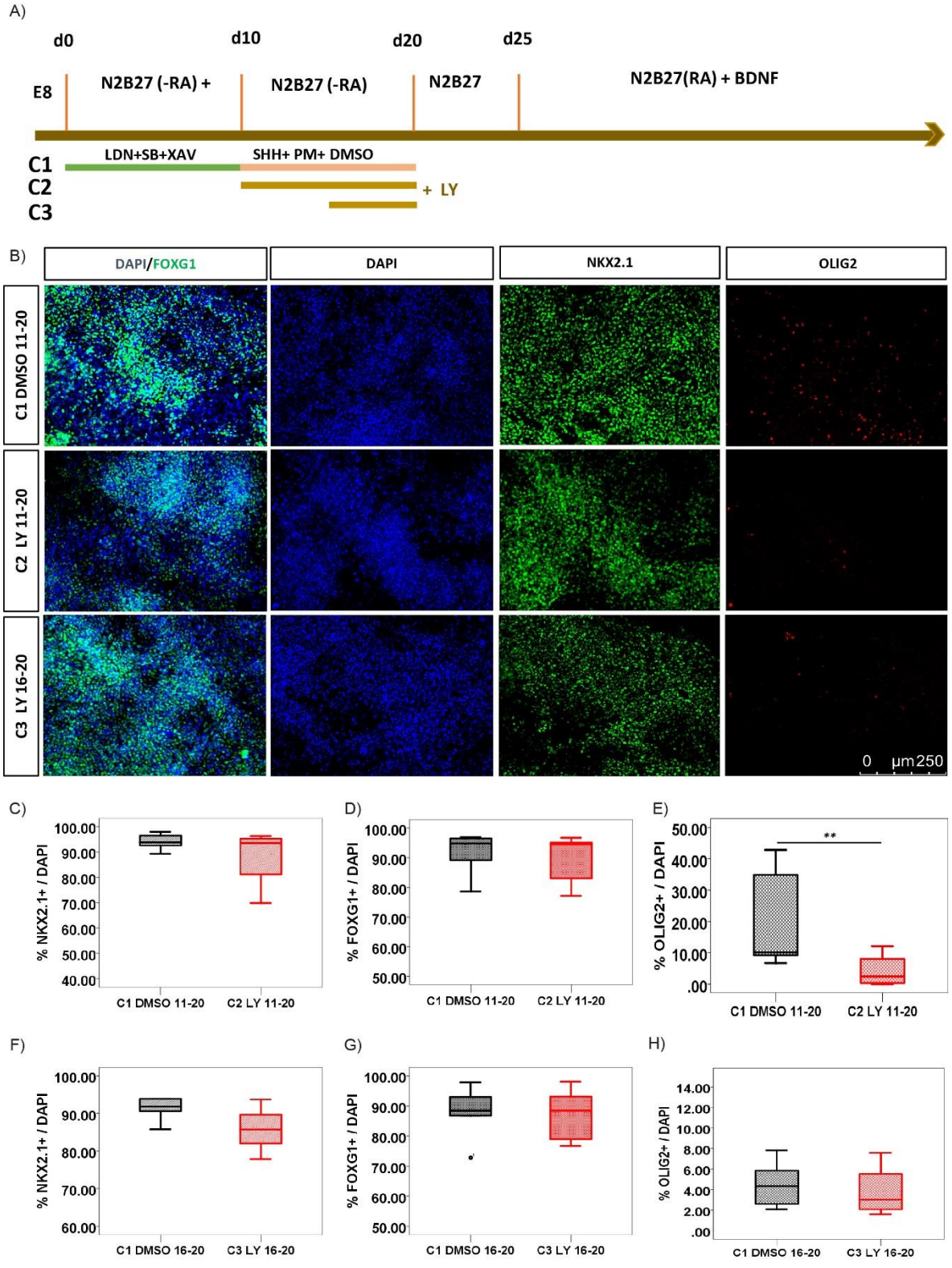

Figure 5.1| TGFβ inhibition leads to a decrease of OLIG2^{+} cells in LHX6-mCherry reporter. A) Graphic description of the differentiation conditions to assay TGFβ inhibition effects. C1 control condition following the standard differentiation paradigm, the vehicle DMSO was added during the patterning stage. C2 in addition to the standard differentiation LY was added from days 11-20. C3 additionally to standard differentiation LY was added from day 16-20. B) Staining for detecting MGE markers in cultures under the above differentiation conditions. C-E) Quantification of the proportion of positive cells for MGE markers in cultures in control C1 and C2 LY 11-20 condition. Data is presented as the median percentage with the 1st and 3rd quartiles

from 3 independent experiments. NKX2.1: C1 n= 8, C2 n=10, no significant difference P>0.05, two tailed t-test equal variances assumed; FOXG1: C1 n= 8, C2 n=10, no significant difference P>0.05, two tailed t-test, equal variances assume; OLIG2: C1 n=9, C2 n=10, ** P<0.01 compared by the Mann Whitney U test for independent samples. F-H) Quantification of positive cells for MGE markers in LY 16-20 condition. Data is presented as the median percentage with the 1st and 3rd quartiles from 3 independent experiments. NKX2.1: C1 n= 6, C2 n=7, no significant difference P>0.05, two tailed t-test; FOXG1: C1 n= 6, C2 n=6, no significant difference P>0.05, two tailed t-test, OLIG2: C1 n=6, C2 n=7. No significant difference P>0.05, two- tailed t test. Equal variances assumed. B scale bar 250 µm.

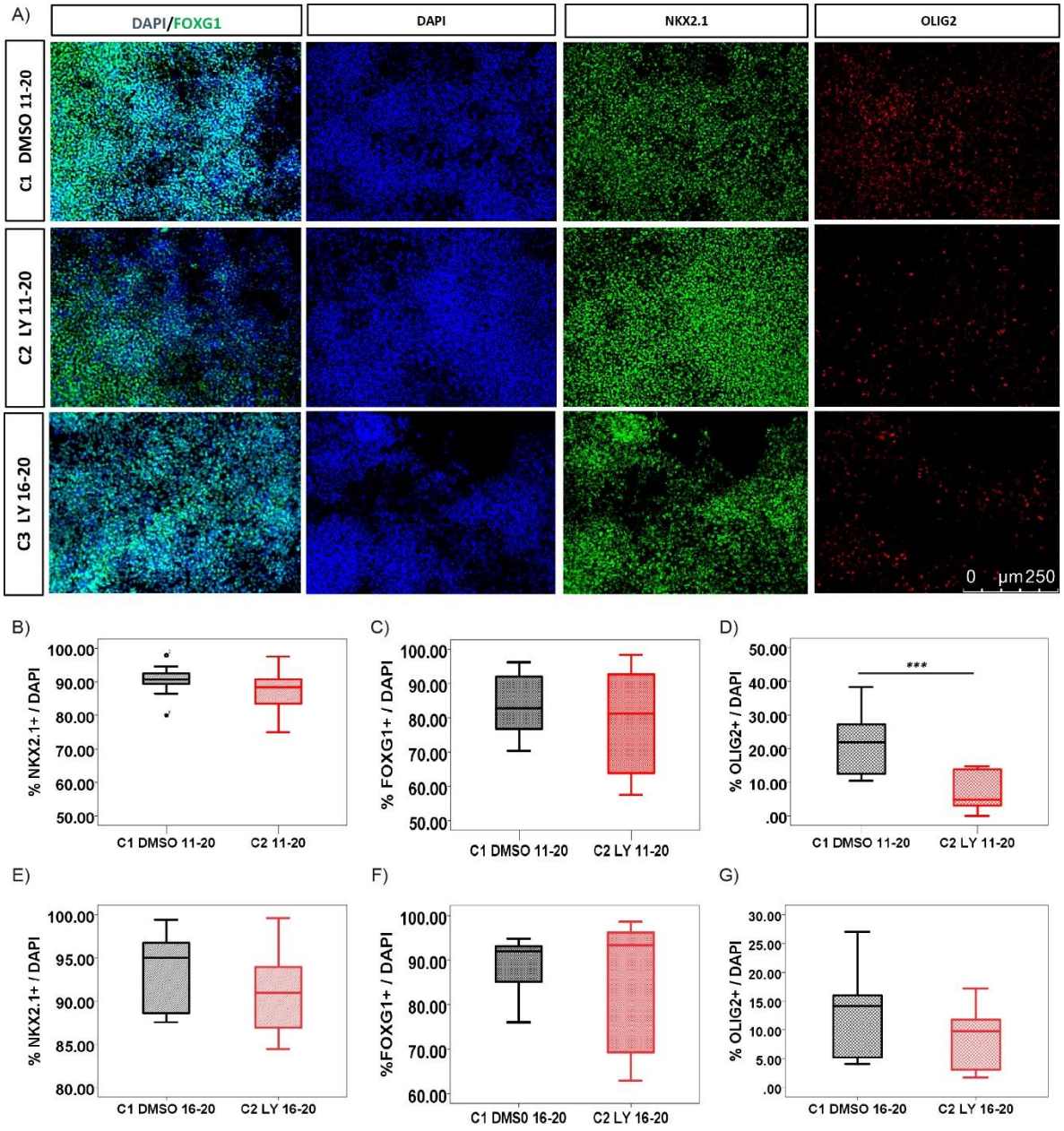

Figure 5.2| TGFβ inhibition leads to a decrease of OLIG2+ cells in H7 line A) Staining for detecting MGE markers in cultures under the differentiation conditions in Figure 5.1A. B-D) Quantification of the proportion of positive cells for MGE markers in cultures in LY 11-20 condition. Data is presented as the median percentage with the 1st and 3rd quartiles from 3 independent experiments. NKX2.1: C1 n= 9, C2 n=9, no significant difference P>0.05, two tailed t-test equal variances assumed; FOXG1: C1 n= 9, C2 n=9, no significant difference P>0.05, two tailed t-test,

equal variances assume; OLIG2: C1 n=9, C2 n=9, *** P=0.001 two- tailed t test. Equal variances assumed for the three markers. E-G) Quantification of positive cells for MGE markers in LY 16-20 condition. Data is presented as the median percentage with the 1st and 3rd quartiles from 3 independent experiments. NKX2.1: C1 n=7, C2 n=7, no significant difference P>0.05, two tailed t-test equal variances assumed; FOXG1: C1 n=7, C2 n=7, no significant difference P>0.05, two tailed t-test, equal variances assume; OLIG2: C1 n=7, C2 n=7, no significant P>0.05, two- tailed t test. Equal variances assumed for NKX2.1 and OLIG2. Not equal variances assumed for FOXG1. A scale bar 250 µm. C1 control condition following the standard differentiation paradigm, the vehicle DMSO was added during the patterning stage. C2 in addition to the standard differentiation LY was added from days 11-20. C3 additionally to standard differentiation LY was added from day 16-20.

To address whether the TGFβ inhibition affects further differentiation stages, progenitors differentiated through conditions above described were dissociated as single cells and analysed by flow cytometry at day 35 (around mCherry$^+$ cells peak). Significant reductions in the proportion of mCherry$^+$ cells were found in both inhibition conditions (Figure 5.3A). However, statistical analysis revealed a more severe reduction in condition LY 11-20, thus considering these results along with the decrease of OLIG2$^+$ cells, subsequent experiments were performed on this condition.

I then investigated the effects of LY 11-20 treatment on the kinetic of mCherry$^+$ cells during 60 days of differentiation by flow cytometry with the first analysis point at day 25 (Figure 5.3B). There was no evident difference on the proportion of mCherry$^+$ cells at day 25 between the LY treated and control cultures (Control 7.1 ± 0.23 %, LY 7.58 ± 0.40 %). However, the proportion of mCherry$^+$ cells became different as differentiation progressed leading to a maximum of 45% reduction in cultures treated with LY fold change reduction in cultures treated with LY at day 45 (control 44.72 ± 1.06 %, LY 24.62 ± 1.11 %). This difference was almost unchanged at day 60 in LY condition (Control 20.33 ± 1.24, LY 11.23 ± 0.72, 44.76% reduction).

Next, I investigated whether the observed reduction of mCherry$^+$ cells translates to a decrease in GABAergic interneuron subtypes. Immunocytochemistry was performed on cultures fixed at day 65 of differentiation. The vast majority of the cells were GAD67$^+$ indicating their GABAergic identity (Figure 5.3C), SST$^+$ neurons were found in cultures under both differentiation conditions (Figure 5.3 C), whereas no PV$^+$ cells were detected (Figure 5.3D left panel).

Since NKX2.1$^+$ population gives rise to LHX6$^+$ cells (committed to become GABAergic interneurons) and LHX8$^+$ cells (committed to become cholinergic interneurons) (Lopes et al., 2012; Sussel et al., 1999), I wondered whether the decrease in the percentage of mCherry$^+$ cells at day 60 was due to a shift on the differentiation potential of the MGE-like cultures. I therefore performed an immunocytochemistry to detect ChAT (choline acetyltransferase), the enzyme that catalyses the synthesis of acetylcholine in cholinergic neurons (Oda, 1999), which are also derived in the MGE from NKX2.1$^+$ cells (Fragkouli et al., 2009; Sussel et al., 1999). I did not detect any ChAT$^+$ neurons in cultures from both differentiation conditions (Figure 5.3D right panel).

Quantification of SST stained cultures from 3 independent differentiations revealed that, although there was a decrease in the proportion of SST$^+$ neurons in the LY 11-20 condition, this reduction was not statistically different (two tailed t test). I also determined the generation of CR$^+$ neurons, which is the other major subtype of interneurons in the cultures, no significant difference was found (two tailed t test). These results is somewhat surprising, given that LHX6 is post-mitotically expressed, I hypothesised that MGE-like cultures treated with LY are maintained in the progenitor state for longer, thus when LY-treated progenitors finally proceed to the mitotic state they give rise to a similar number of SST$^+$ neurons to the control cultures.

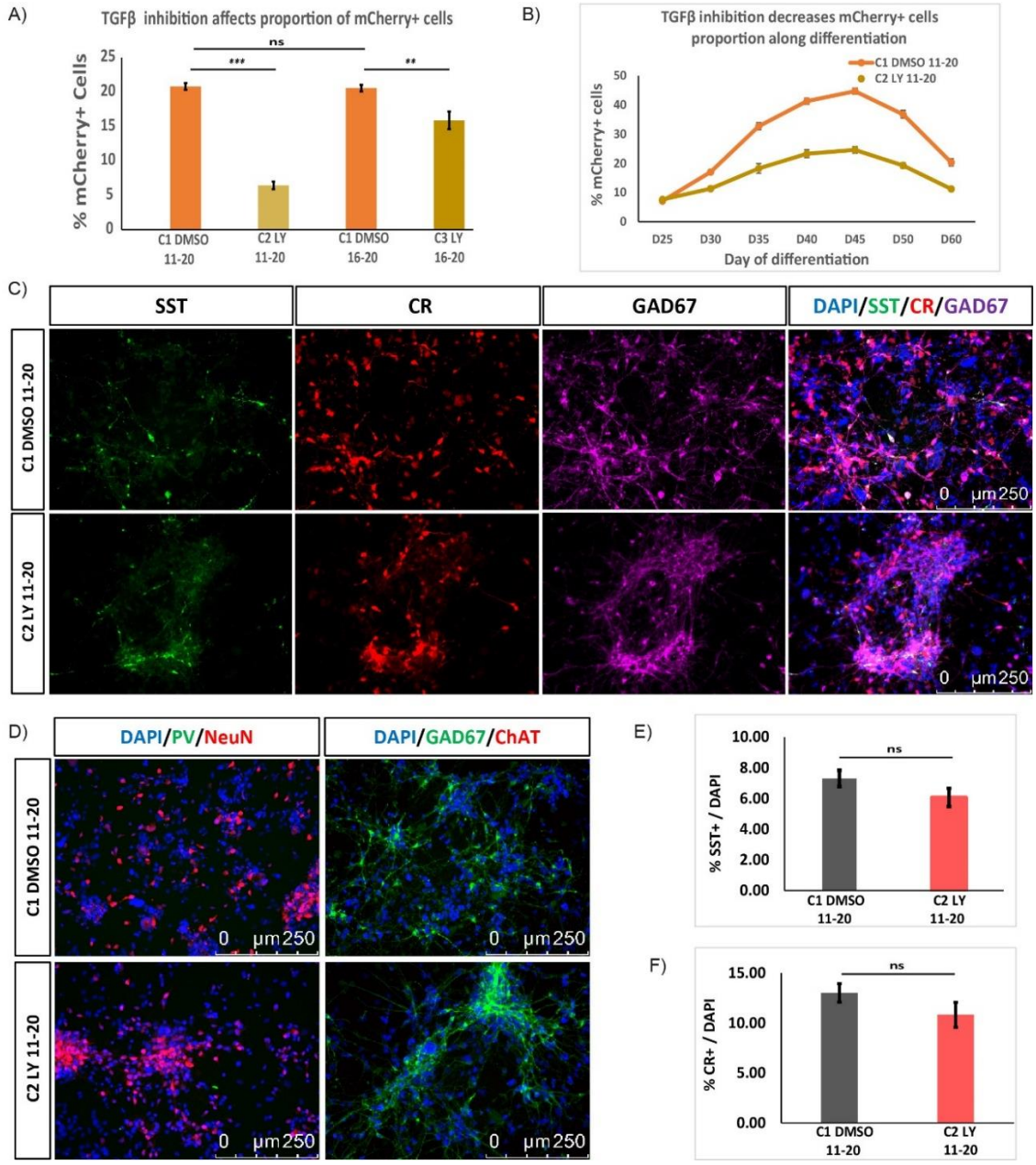

Figure 5.3| TGFβ inhibition decreases mCherry⁺ cells but does not affect differentiation potential. A) Graph comparing the proportion of mCherry⁺ cells at day 35. Data presented as mean percentage ± SEM from 2 independent experiments. C1 (11-20) n=6, C2 n=6, C1 (16-20) n=6, C3 n=6, ns (no significant difference) P>0.05, ** P<0.01, *** P<0.001; one way ANOVA with post-hoc Tukey. B) mCherry⁺ cells proportion is decreased in LY treated cultures along 60 days of differentiation. Data shows mean percentage ± SEM from 2 independent experiments (C1: n=6, C2: n=6). E) Representative immunostaining of interneuron markers at day differentiation day 65. D) Representative images of PV and ChAT immunocytochemistry. E) Quantification of

SST^+ cells. Data is presented as mean percentage ± SEM from 3 independent experiments (C1: n=23, C2: n=24). No significant difference was found P>0.05 two- tailed t test. Equal variances assumed. F) Quantification of CR^+ cells. Data is presented as mean percentage ± SEM from 3 independent experiments (C1: n=14, C2: n=15). No significant difference was found P>0.05 two-tailed t test. Equal variances assumed. C and D scale bar 250 µm. C1 control condition following the standard differentiation paradigm, the vehicle DMSO was added during the patterning stage. C2 in addition to the standard differentiation LY was added from days 11-20. C3 additionally to standard differentiation LY was added from day 16-20.

5.2.2 TGFβ signalling blockade delays differentiation of MGE-like progenitors

To test the above hypothesis, I firstly investigated whether LY treatment affects EdU incorporation of $NKX2.1^+$ cells, as an indication of proliferative capacity. At day 22, I administrated an EdU pulse for 2 hours to cultures in the LY 11-20 and control conditions, followed by double immunostaining to detect NKX2.1 and EdU (Figure 5.4A). I found that cultures treated with LY contained a higher proportion of $NKX2.1^+$ cells that incorporated EdU than those in the control conditions (Figure 5.4B).

To gain further support of the above findings, I performed RT-PCR analysis on genes whose expression has been associated to either proliferating progenitors (*TOP2A* and *FABP7*) or post-mitotic cells (*STMN2, GAD1, SOX6* and *LHX6*) in the mouse MGE (Mi et al., 2018). These genes were reported to be highly expressed by the MGE cells as determined by single cell RNA-seq. Samples from LY 11-20 and control cultures were collected at the pluripotent state (day 0) and at differentiation days 20, 30, 35 40, 45, 50, 55 and 60.

I found that MGE progenitor associated gene transcripts were detected at higher levels in the LY treated cultures from day 30 onwards compared to the control cultures; and their expression sustained higher at later time points than in control conditions (Figure 5.4C).

Conversely, genes expressed in post-mitotic MGE-derivatives such as *LHX6* , SOX6 and *GAD1*, were detected at a higher level in control than in LY-treated cultures during day 30-45, although the increase of *STMN2* transcript in LY treated cultures was not consistent across all time points analysed (Figure 5.4D). A similar trend of LY-mediated

gene expression changes was also found for H7 cells differentiated under control and LY 11-20 conditions (Figure 5.5).

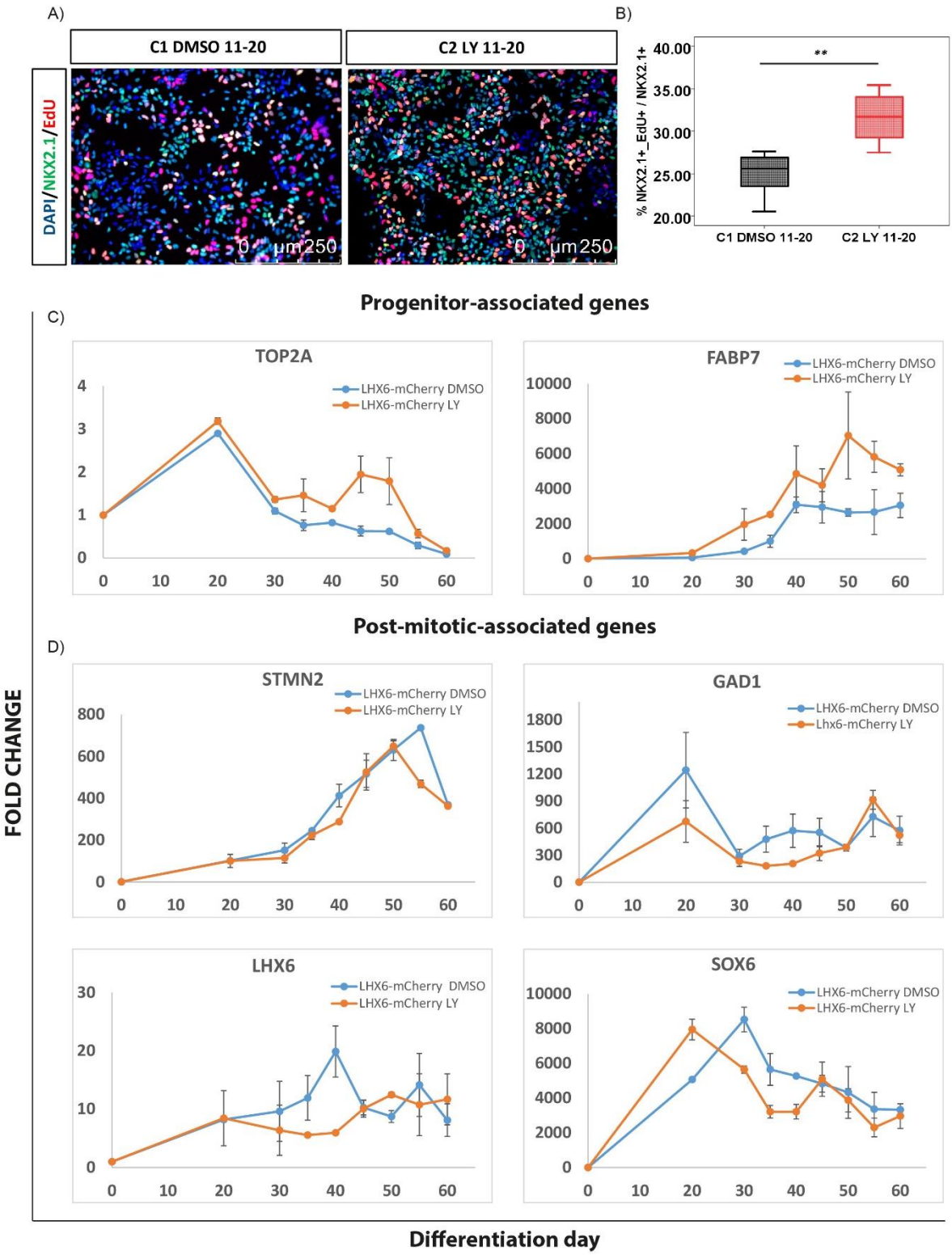

Figure 5.4| TGFβ inhibition promotes the maintenance of MGE-like cells as progenitors in LHX6-mCherry reporter. A) Representative immunostaining for detecting NKX2.1^{+} cells incorporating EdU. Scale bar 250 µ. B) Proportion of NKX2.1^{+}_EdU^{+} in control and LY treated cultures. Data presented as mean percentage ± SEM from 2 independent experiments (C1: n=6, C2: n=6). ** P<0.01, two tailed t-test. Equal variances assumed. C) Expression profile of MGE-progenitors

associated genes *TOP2* and *FABP7* in control (blue) and LY-treated cultures (orange). Data is presented as the mean fold change ± SEM from two independent experiments. (DMSO: n=2, LY: n=2, at each time point). D) Expression profile of genes associated to post-mitotic MGE derivatives in control (blue) and LY-treated cultures (orange).). Data is presented as the mean fold change ± SEM from two independent experiments. (DMSO: n=2, LY: n=2, at each time point). C1 control condition following the standard differentiation paradigm, the vehicle DMSO was added during the patterning stage. C2 in addition to the standard differentiation LY was added from days 11-20.

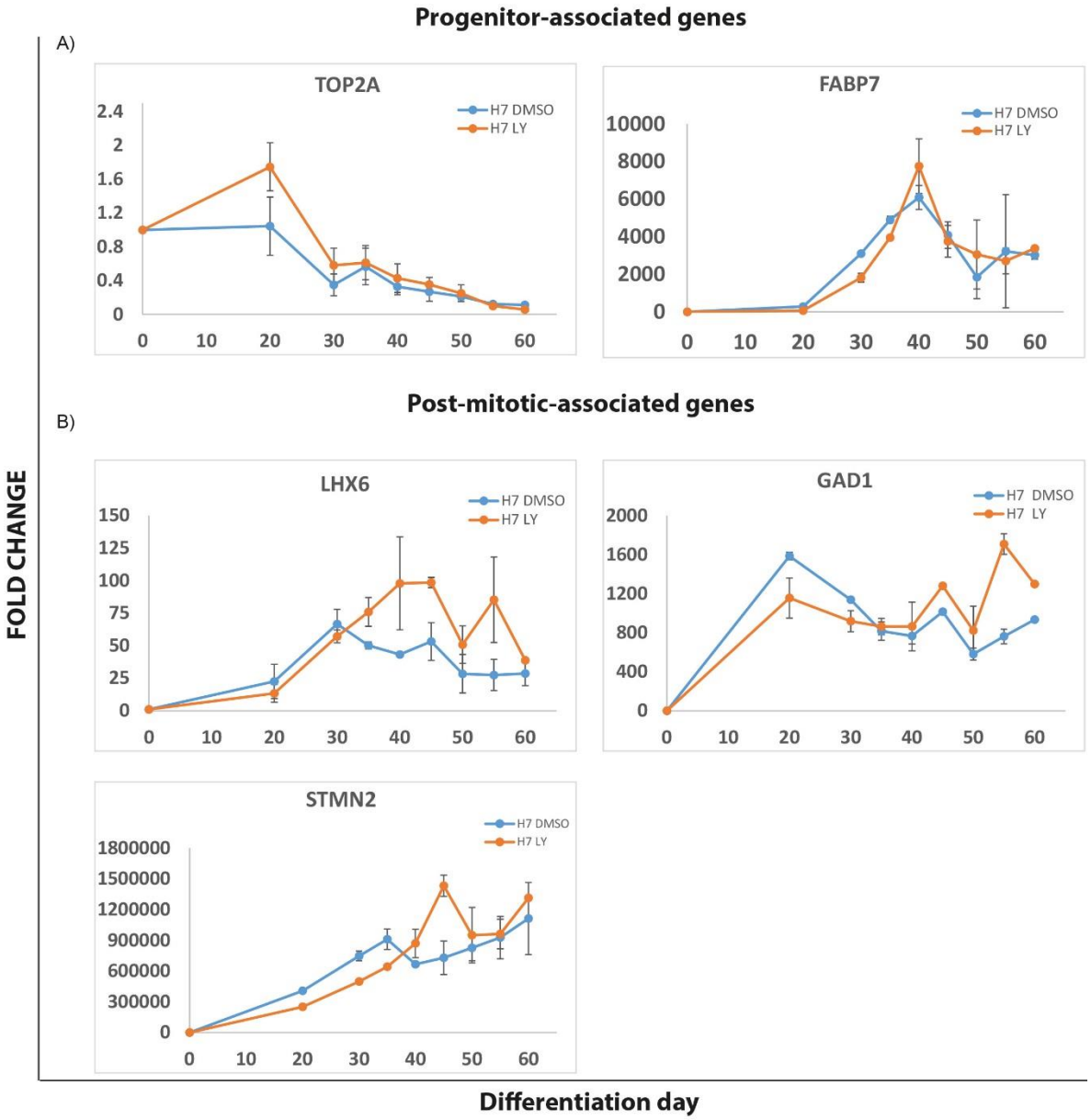

Figure 5.5| TGFβ inhibition promotes the maintenance of MGE-like cells as progenitors in H7 line. A) Expression profile of MGE-progenitors associated genes *TOP2* and *FABP7* in control (blue) and LY-treated cultures (orange) Data is presented as the mean fold change ± SEM from two independent experiments. (DMSO: n=2, LY: n=2, at each time point). B) Expression profile of genes associated to post-mitotic MGE derivatives in control (blue) and LY-treated cultures

(orange). Data is presented as the mean fold change ± SEM from two independent experiments. (DMSO: n=2, LY: n=2, at each time point). Control condition following the standard differentiation paradigm, the vehicle DMSO was added during the patterning stage. LY: in addition to the standard differentiation LY was added from days 11-20.

Interestingly, for most of the analysed genes their expression levels became similar in control and LY treated conditions by day 60 of differentiation. These results support the hypothesis that cultures treated with LY are retained in the progenitor state, resulting in a protracted terminal differentiation, hence a decrease in the proportion of post-mitotic LHX6$^+$ cells. However, LY mediated action cease eventually, allowing LY-treated cells to proceed towards terminal differentiation.

5.2.3 Inhibition of TGFβ signalling lengthened the cell cycle of MGE-like progenitors

It is intriguing why the proportion of NKX2.1$^+$ cells was not increased in the LY treated condition, despite an increase in EdU incorporation in these cells. Moreover, a hypothetic increase of NKX2.1$^+$ cells would eventually lead to an increase of LHX6$^+$ cells which subsequently would give rise to a higher proportion of SST$^+$ cells, none of the results support this scenario.

One potential mechanism that attribute to the seeming contradictive findings is a reduced proliferation rate due to changes in cell cycle. I therefore investigated TGFβ signalling inhibition leads to a lengthening of the cell cycle in MGE-like progenitors. A cumulative EdU study was performed in control and LY 11-20 conditions. The principle of this assay is originally described by Nowakowski et al., 1989 , and since it has been used in other studies to determine cell cycle length of neural progenitors (Arai et al., 2011; Estivill-Torrus et al., 2002).

Briefly, this method considers that the proliferative population, named growth fraction (GF) is asynchronously distributed along the cell cycle and is growing in a steady state, hence the number of cells in each phase is proportional to the length of that phase.

Therefore, giving pulses of a DNA –intercalating agent for increasing periods of time- will eventually mark all the proliferating cells in the culture. The proportion of labelled cells increases linearly along time and can be applied to obtain the time of cell cycle (tc) and the time of S-phase (ts) (the correlation referred to as the Nowakowski equation) (Figure 5.6C) (Nowakowski et al., 1989).

MGE-like cells were exposed to EdU for increasing periods of time up to 24 hours, followed by immunostaining for detecting NKX2.1 and EdU. To distinguish potential differential cell cycle length changes in $NKX2.1^+$ and $NKX2.1^-$ cell populations, I counted EdU^+ cells in both populations ($EdU^+/NKX2.1^+$ and $EdU^+/NKX2.1^-$) at each time point. These proportions were plotted against time to obtain the equation describing the linear correlation between time and proportion of EdU^+ labelled cells for each population (Figure 5.6 A, B). The slope and intersection values were employed to calculate the time of cell cycle and time in S-phase, following the model equation presented in Figure 5.6C. I found that LY treatment did not affect the Tc or Ts of the $NKX2.1^-$ cell population. However, LY exposure did resulted in a longer cell cycle (45.35 h) in $NKX2.1^+$ cells than those in control conditions (39.61 h). LY-induced increase in the cell cycle length in $NKX2.1^+$ cells was concomitant with the increase in the length of S phase, which lengthened from 16.14 h in control conditions to 21.37 h in LY treatment. No cell cycle lengthening was found in $NKX2.1^-$ cells between control and LY treated cultures (45.81h in both cases).

These results suggest that a lengthening of the cell cycle, caused by temporal inhibition of TGFβ signalling, prolongs the progenitor stage of MGE- like cells in a time window prior to day 60, leading to a decrease in the proportion of $mCherry^+$ cells. However, these $NKX2.1^+$ cells retain their differentiation potential and were able to progress towards post-mitotic neurons once the LY effect faded.

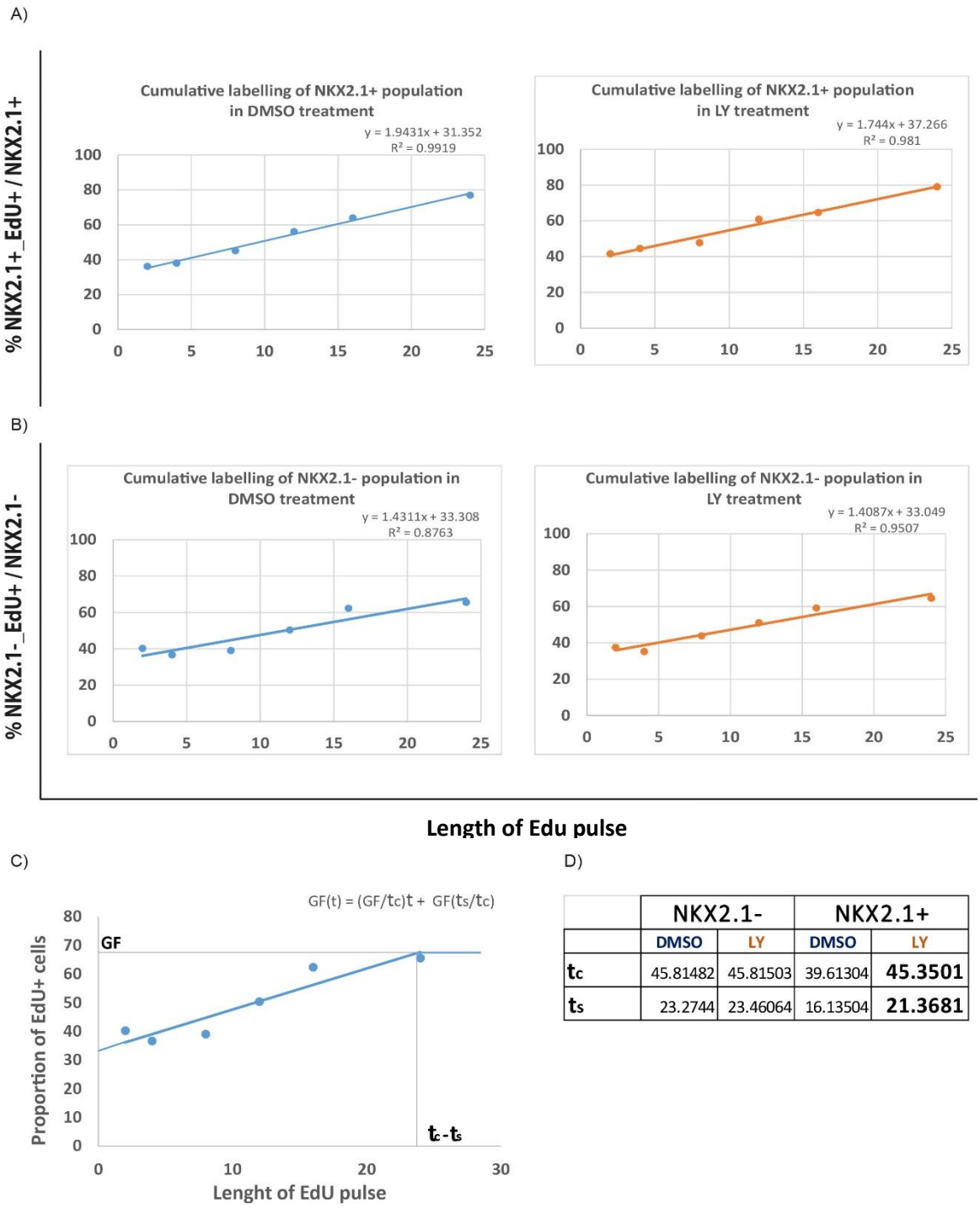

C)

D)

	NKX2.1-		NKX2.1+	
	DMSO	LY	DMSO	LY
t_c	45.81482	45.81503	39.61304	**45.3501**
t_s	23.2744	23.46064	16.13504	**21.3681**

Figure 5.6| TGFβ inhibition lengthened cell cycle of NKX2.1$^+$ population. A) Graphs of EdU incorporation along time for NKX2.1$^+$ population. Data is presented as the percentage of double positive cells NKX2.1$^+$_Edu$^+$ out the total NKX2.1$^+$ population ± SEM, n=6 at any time-point. B) Graphs of EdU incorporation along time for NKX2.1$^-$ population. Data is presented as the percentage of double positive cells NKX2.1$^-$_Edu$^+$ out the total NKX2.1$^-$ population ± SEM, n=6 at any time-point. C) Graphical description of the Nowakowski equation. D) Table sumarising the tc and ts for NKX2.1$^+$ and NKX2.1$^-$ population after DMSO and LY treatment. C1 control condition following the standard differentiation paradigm, vehicle DMSO was added during the patterning stage. C2 in addition to the standard differentiation LY was added from days 11-20.

5.2.4 Cell cycle inhibitors accelerates the progression to post-mitotic state and recovers the proportion of mCherry$^+$ cells upon TGFβ inhibition

I then investigated whether a forced cell cycle exit could accelerate neuronal differentiation and hence recover the proportion of mCherry$^+$ cells in LY treated cultures. With this purpose, I followed the kinetic of mCherry$^+$ population in control and LY- treated cultures. From day 35, around the peak time of mChery$^+$ cell production, I added a combination of two cell cycle inhibitors (CCI), 10 µM DAPT (a γ-secretase inhibitor) and 2 µM PD0332991 (a CDK4/6 inhibitor) (Telezhkin et al., 2016).

In contrast to previous experiments (Figure 5.3B) and control conditions without adding CCI (Figure 5.7A), forced exit of the cell cycle gradually recovers the proportion of mCherry$^+$ population after TGFβ inhibition, at day 60 the proportion of mCherry$^+$ cells was virtually equal to those in the control conditions (Figure 5.7B). By day 65 both conditions gave rise to similar proportion of SST$^+$ and CR$^+$ neurons (Figure 5.7 C-B). These results provide further support that the forced exit of the cell cycle accelerates the progression towards the post-mitotic state of MGE-like cells, in cultures previously retained as progenitors upon the inhibition of TGFβ.

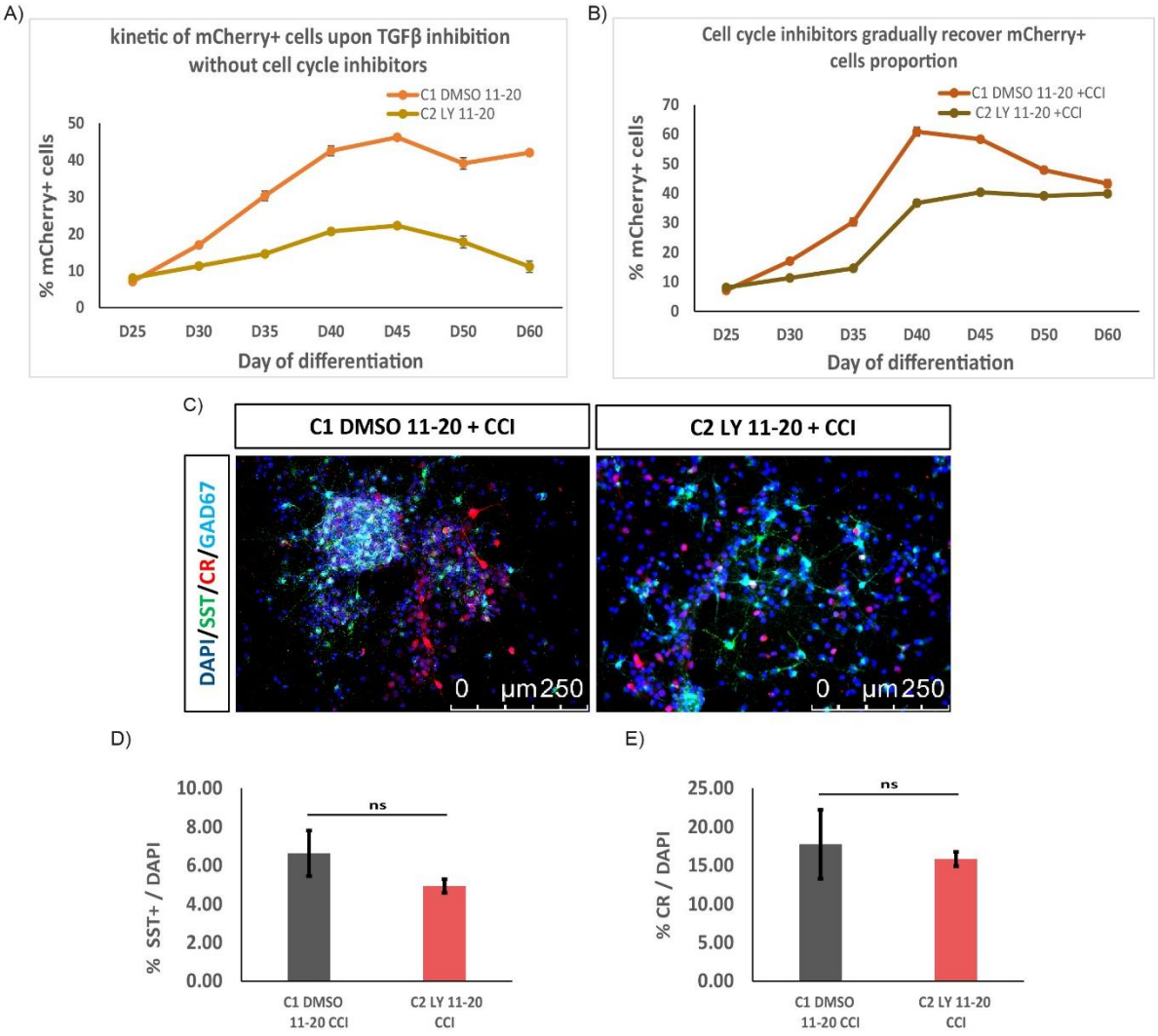

Figure 5.7| Forced exit of cell cycle recovers mCherry⁺ cells proportion. A) Control kinetic of mCherry⁺ population in control and LY-treated cultures without cell cycle inhibitors. Data was obtained by flow cytometry and presented as the mean percentage ± SEM, C1: n=3 at any time-point, C1: n=3 at any time-point. B) Kinetic of mCherry⁺ population upon the addition of cell cycle inhibitors in control and LY-treated cultures. . Data was obtained by flow cytometry and presented as the mean percentage ± SEM, C1: n=3 at any time-point, C1: n=3 at any time-point. C) Representative immunostaining for SST, CR and GAD67 in cultures treated with cell cycle inhibitors. Scale bar 250 µ. D) Quantification of SST⁺ cells in control and LY-treated cultures upon cell cycle inhibitor addition. Data is presented as mean percentage ± SEM from 2 independent experiments, C1: n=6, C2: n=10. No significant difference was found P>0.05 two- tailed t test. Non equal variances assumed. E) Quantification of CR⁺ cells in control and LY-treated cultures upon cell cycle inhibitor addition. Data is presented as mean percentage ± SEM from 2 independent experiments, C1: n=6, C2: n=10. No significant difference was found P>0.05 two-tailed t test. Equal variances assumed. C1 control condition following the standard differentiation paradigm, the vehicle DMSO was added during the patterning stage. C2 in addition to the standard differentiation LY was added from days 11-20.

5.2.5 TGFβ3 promotes the generation of mCherry$^+$ cells

I then asked whether addition of TGFβ3 during MGE differentiation would elicit the opposite effect as observed on TGFβ signalling inhibition. TGFβ3 was added at day 14 to 20 (Condition 2 or C2) during interneuron differentiation and compared to standard differentiation (Condition 1 or C1) (Figure 5.8A). Immunocytochemical analysis of pan-forebrain (FOXG1 C1: 92.71 ± 2.17 %, C2: 94.06 ± 1.06 %) and MGE progenitor markers NKX2.1 (C1: 93.23 ± 1.56 %, C2: 94.28 ± 2.11%) and OLIG2 (C1: 49.11 ± 4.63%, C2: 48.73 ± 4.15%) on day 21 revealed no significant difference on the proportion of any of these populations, suggesting that the acquisition of MGE fate was not affected by the addition of TGFβ3 (Figure 5.8B-E).

I next analysed, by flow cytometry the proportion of mCherry$^+$ cells in control and TGFβ3-treated cultures at days 25, 35 and 45. I found that TGFβ3-treated cultures had a trend to contain a higher proportion of mCherry$^+$, however, statistical significant increase was only found at day 25 (Figure 5.8F). Further differentiation of TGFβ3 and control cultures, gave rise to similar percentages of SST$^+$ and CR$^+$ neurons (Figure 5.8G-I).

Overall, these results seem to support and complement the findings caused by the inhibition of TGFβ signalling, as an opposite change on the proportion of mCherry$^+$ population was found by adding TGFβ3. This result indicates that TGFβ signalling might regulate the progression from progenitor to post-mitotic state of MGE-like cells by modulating the cell cycle length. Since mCherry signal reports the expression of LHX6, a transcription factor whose expression is associated to post-mitotic cells in the MGE, therefore, changes in the proportion of mCherry$^+$ and time at which this changes happen, suggest a shift on the kinetic to which MGE-like progenitors exit the cell cycle. This transition to the post-mitotic state seems to depend on the levels of activity of TGFβ signalling.

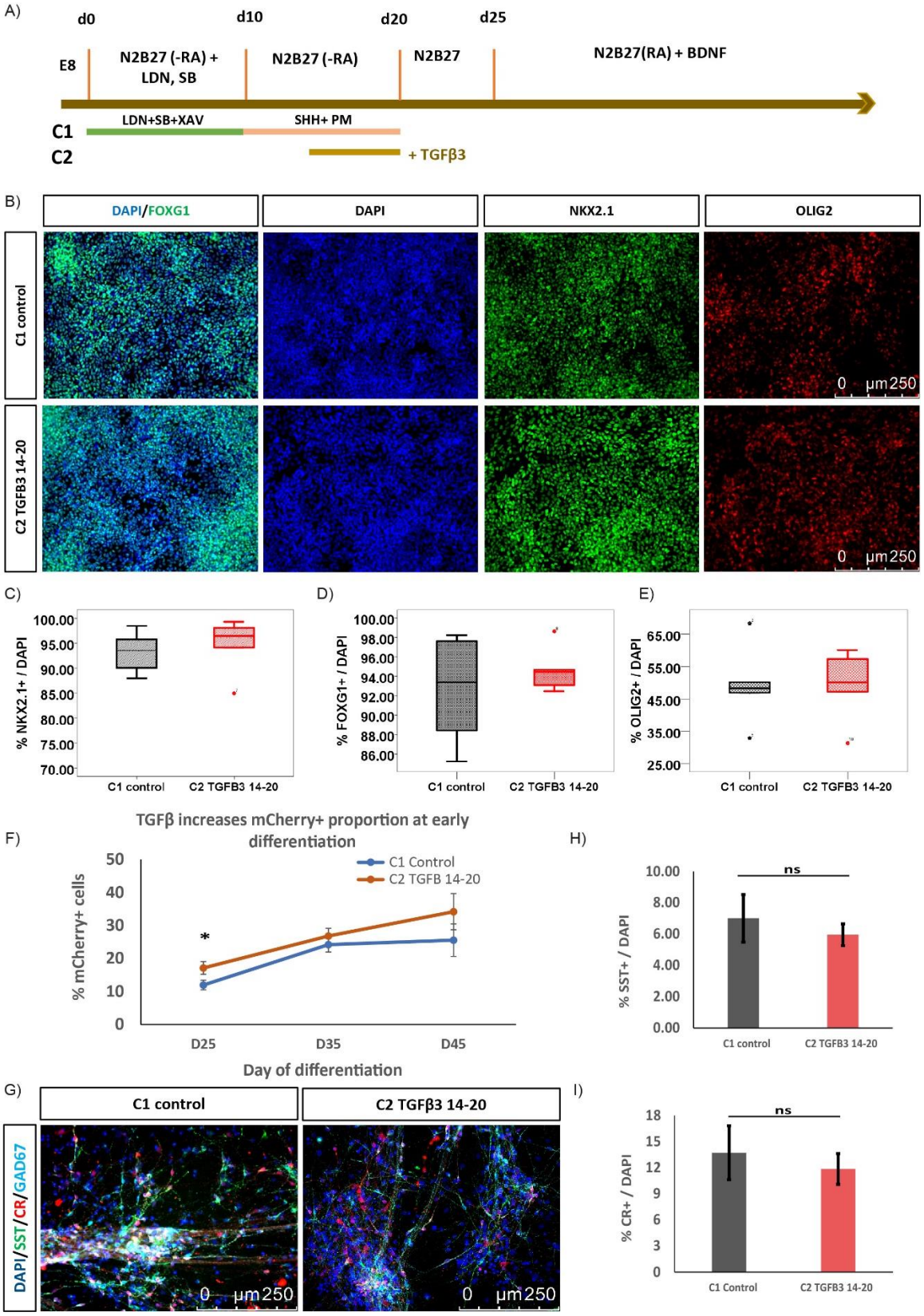

Figure 5.8| TGFβ3 addition increases mCherry^{+} percentage at day 25. A) Diagram of the differentiation conditions used for TGFβ3 addition. B) Representative images of the immunostaining for detecting MGE markers. C) Quantification of the proportion of NKX2.1^{+} cells. Data is presented as the median percentage with the 1st and 3rd quartiles, from two independent experiments, C1: n=6, C2: n=6. No significant difference was found P>0.05 two- tailed t test. Equal variances assumed. D) Quantification of the proportion of FOXG1^{+} cells. Data is presented as the median percentage with the 1st and 3rd quartiles, from two independent experiments, C1:

n=6, C2: n=6. No significant difference was found P>0.05 two- tailed t test. Not equal variances assumed. E) Quantification of the proportion of $OLIG2^+$ cells. Data is presented as the median percentage with the 1st and 3rd quartiles, from two independent experiments, C1: n=6, C2: n=6. No significant difference was found P>0.05 two- tailed t test. Equal variances assumed. F) Graph comparing the proportion of $mCherry^+$ cells at days 25, 35, and 45. Data was obtained by flow cytometry and presented as mean percentage ± SEM from 3 independent experiments, C1: n=9, C2: n=9, except at day 45 C1: n=6, C2: n=9. Significant difference was found at day 25 P<0.05 two- tailed t test. No significant difference P>0.05 was found at day 35 and 45. G) Representative image of the immunocytochemistry for SST, CR and GAD67 in control and TGFβ3 conditions. H) Quantification of SST^+ cells. Data is presented as mean percentage ± SEM from 2 independent experiments, C1: n=8, C2: n=11. No significant difference P>0.05 was found, two tailed t-test. Equal variances assumed. I) Quantification of CR^+ cells. Data is presented as mean percentage ± SEM from 2 independent experiments, C1: n=6, C2: n=9. No significant difference P>0.05 was found, two tailed t-test. Equal variances assumed. B, G) Scale bar 250 µ. C1 control condition following the standard differentiation paradigm. C2 in addition to the standard differentiation TGFβ3 was added from days 14-20.

5.3 Discussion

Since in our differentiation paradigm, the addition of SHH and purmorphamine activated NKX2.1 expression, which in turn would activate LHX6 expression, and it is predicted that by the combined action of these transcription factors *TGFβ3* is transcriptionally regulated, in this chapter, I have studied the effects of TGFβ signalling inhibition on MGE differentiation of hPSCs. My findings suggest that TGFβ signalling plays a role on cell cycle regulation of NKX2.1 cells, affecting the progression these progenitors to post-mitotic neurons. Inhibition of TGFβ signalling retains the MGE-like cells as progenitors by lengthening the cell cycle. Once they exit the cell cycle, MGE-like cells resumed their differentiation to $LHX6^+$ cells that subsequently gave rise to SST^+ neurons, indicating that TGFβ signalling inhibition during the patterning did not affect cell fate.

A TGFβ signalling- dependent control in cell proliferation and cell cycle-exit has been previously demonstrated in other regions of the brain, such as the dorsal midbrain and the cortex (Falk et al., 2008; Seoane et al., 2004). In the cortex, TGFβ signalling induces a cytostatic effect by directly promoting transcriptional activation of the cyclin-dependent kinase inhibitor p21, this activity is mediated by the action of Smad2/3 and FoxO, and leads to a cell cycle arrest at G1 (Seoane et al., 2004). While the inhibition of TGFβ signalling by ablation of Tβr2 lead to an increased proliferation and decreased cell-cycle exit in the dorsal midbrain (Falk et al., 2008).

Consistent with the current, the above mentioned reports, activation of TGFβ pathway has been reported to induce the transcriptional activation of p21 and p27 while promoting cyclin D1 suppression, which together facilitate the exit of the cell cycle. In contrast, inhibition of TGFβ signalling blocks the activation of p21, and maintains neural progenitors in cell cycle (Garcia-Campmany and Marti, 2007; Seoane et al., 2004; Siegenthaler and Miller, 2005). However, the effects of TGFβ signalling manipulation on cell cycle length varies among these studies. While activation of the signalling by Tgfβ1 ligand caused the exit of the cell cycle without modifying its length (Siegenthaler and Miller, 2005), the inhibition of TGFβ signalling by loss of function of Tβr2 triggered ectopic activation of Wnt1/β-catenin and Fgf8 which promoted increased proliferation, inhibition of cell cycle exit and shortening of the cell cycle (Falk et al., 2008). The different effects of TGFβ signalling manipulation on cell cycle length regulation by these and my studies might be explained by context-dependent mechanisms, which remain to be characterised.

Although my results show a clear trend towards the lengthening of the cell cycle (Figure 5.6D), the cell cycle time obtained by my study may not be accurate. This is because that estimation of the cell cycle time depends on the precise determination of the growth fraction in the cell population of interest, which in turn depends on the plateau of the proportion of cells labelled with EdU (Nowakowski et al., 1989). However, a plateau of EdU^+ was not reached in my experiment. The cell cycle length needs to be further validated by collecting cell samples with longer EdU pulse.

The cumulative EdU labelling assay also allows the estimation of the S-phase length (Figure 5.6D). Interestingly, my results suggest that the increase in the S-phase duration (5.23 h lengthened) attributes to the overall lengthening of the cell cycle (5.74 h lengthened). A longer S-phase has been related to apical and basal cortical progenitors dividing to expand the progenitor pool compared to the progenitors undergoing neurogenic division (Arai et al., 2011; Spella et al., 2011). This finding supports that TGFβ signalling inhibition retains MGE-like cells in the progenitor identity, which is further supported by the fact that forcing the exit of the cell cycle gradually recovers the proportion of $mCherry^+$ cells in cultures treated with LY (Figure 5.7 A and B). The exiting of the cell cycle was promoted by the combined effect of DAPT (a γ-secretase inhibitor) and PD0332991 (a CDK4/6 inhibitor) (Telezhkin et al., 2016), while the last specifically

targets cell cycle regulators, the effect of inhibiting NOTCH signalling by DAPT might be more complex. NOTCH inhibition enhances neuronal differentiation, however, the exit of the cell cycle is necessary to boost neuronal differentiation (Crawford and Roelink, 2007; Telezhkin et al., 2016). This raises the question of whether such effect could affect the neuronal cell fate. While the answer to this interrogation would need to include in the comparisons the proportion of interneuron subtypes obtained after treating the cells only with PD0332991; it is unlikely that the initial specification of progenitors is changed in response to DAPT. Since it has been shown that, the *in vitro* differentiation of other caudally–derived ventral neuronal types (motoneurons and interneurons) were not affected with the inclusion of DAPT while Shh was also activated. Therefore, in absence of Notch signalling, the already Shh-induced neurons only acquired a more mature phenotype precociously (Crawford and Roelink, 2007).

However, it has been also proposed that, during *in vitro* differentiation of cortical interneurons from mESCs, the administration of DAPT further enhances the generation of Sst^+ interneurons at the expenses of Pv^+, using culture conditions that were already biased to become Sst^+ (Tischfield et al., 2017). In contrast to the experiments from Tischfield and colleagues, the addition of DAPT and PD0332991 did not enhanced the derivation of SST^+ interneurons. Therefore, it is possible that the apparent increase of SST^+ interneuros, seen by Tischfield, was an effect of the quicker acquisition of more mature phenotypes, which is also favoured by the fact that during development SST^+ interneurons arisen before than PV^+ interneurons (Mukhopadhyay et al., 2009). A more formal answer to this question might be provided by the study of interneuron development in a conditional notch mutant, where the effects of the downregulation of notch around the neurogenesis in the MGE can be tested.

TGFβ3 at 1ng/ml was added to the cultures with the aim of testing whether the opposite outcomes to the inhibition could be promoted. A slight but significant effect was observed on the proportion of $mCherry^+$ cells only at day 25. This effect could be increased by using higher concentration of TGFβ3, as some of the effects on cell cycle exit of another member of the TGFβ family, TGFβ1 were induced by using 40 ng/ml (Siegenthaler and Miller, 2005). Alternatively, the restricted increase of $mCherry^+$ cells to day 25 could be simply due to this effect cannot last longer. The pronounced decrease of $mCherry^+$ cells in the LY treatment contrasts with the slight increase with the addition

of TGFβ3. This might be related to the presence of FOXG1, which is broadly expressed in MGE-like cultures. FOXG1 has been reported to repress the action of Smad2/3 and FoxO complex to activate p21 (Seoane et al., 2004), this might interfere with the transduction of TGFβ signalling to exit the cell cycle meaning a small increase of $mCherry^+$ cells. In contrast to the addition of TGFβ3, the presence of FOXG1 in the cultures might potentiate the effect of LY, leading to a strong inactivation of p21, therefore keeping cells in cell cycle with an evident decrease on the production of $mCherry^+$ cells. With regard to interneuron subtype, no significant difference was found on the proportion of SST^+ or CR^+ neurons, indicating that addition of TGFβ did not bias the acquisition of the interneuron subtype fate.

With caveats that one of the major interneuron subtypes were almost absent in my culture, my results indicate that TGFβ signalling is unlikely a major regulator of interneuron subtype fate specification. However, during interneuron development the exit of the cell cycle is not coupled to the beginning of SST or PV expression (Nicholas et al., 2013; Wamsley and Fishell, 2017). Indeed, this uncoupled process opens debate about the time at which the interneuron subtype fate is acquired. Two main hypothesis are in discussion. One proposing that subtype fate is determined soon after the exit of cell cycle whereas the second view suggests that the fate is stablished when the interneuron settle in its final position in the brain; where cues of the surrounding environment finally determine interneuron subtype (Hu et al., 2017b; Lim et al., 2018; Wamsley and Fishell, 2017)

Due to the debate on the time at which interneuron subtype is acquired and the lack of PV^+ in my cultures, it is not possible to rule out an effect on the interneuron fate specification as a consequence of TGFβ signalling modulation. Indeed it is very intriguing that independently on the proportion of $LHX6^+$ cells obtained in each of the culture conditions used in this work, only a portion of the $LHX6^+$ cells became SST^+ neurons (ranging from 4.94 to 7.30 %.) Similar percentages were found in Noakes et al., 2019. These low percentages of SST^+ and PV^+ interneurons might be suggesting that relevant cues are lacking or not sufficient in the cultures to promote a more efficient terminal differentiation of the $LHX6^+$ cells, which have been conceived as a proto- interneuron state (Flames and Marin, 2005). A more accurate answer to whether TGFβ signalling

regulates interneuron specification could be obtained by studying interneuron specification in a knockout mouse for *TGFβ3* in the MGE.

In summary, findings described in this chapter present evidence on the role of TGFβ signalling in regulating neurogenesis of hPSC-derived MGE-like cells by modulating cell cycle length. These findings are in line with the TGFβ3 expression pattern in the mouse MGE, where TGFβ3 is highly expressed in the subventricular zone and mantle zone of the MGE (Sandberg et al., 2016). Further characterization of the cell cycle regulators implicated in the control of the cell cycle length of MGE-like cells is necessary to delineate the specific mechanisms through which TGFβ exert its effects on MGE-like progenitors.

6. General discussion

6.1 Summary of findings

In this thesis, I generated a hPSC reporter cell line for tracking hPSC-derived cortical interneurons. The key properties of pluripotency and differentiation potential to MGE-like progenitors were validated. I provide evidence that the knock in mCherry faithfully labelled LHX6$^+$ cells and that mCherry expression was maintained in the SST$^+$ interneurons upon further differentiation *in vitro*. Moreover, mCherry expression recapitulated the expected temporal and spatial expression pattern of LHX6 during differentiation into different neuronal subtypes, demonstrating a restricted expression to the MGE-like lineage. Thus, my findings highlight the potential of this reporter line as a valuable experimental platform for identifying new determinants of interneuron fates. This cell line was designed as a dual reporter to also identify the PV+- interneuron subtype. However, the low efficiency to generate these interneurons (Nicholas et al., 2013; Noakes et al., 2019; Sun et al., 2016) prevented the validation of PV-GFP reporter in the current study.

Using the LHX6 reporter line, I investigated a role for TGFβ signalling in MGE/interneuron differentiation. Pharmacological inhibition of TGFβ signalling prolonged the MGE progenitor stage by lengthening the cell cycle, with no effect on the production of CR$^+$ and SST$^+$ neurons. In contrast, addition of exogenous TGFβ3 resulted in an early production of mCherry$^+$ cells, possibly due to a higher percentage of MGE-progenitors exited the cell cycle at earlier stages of differentiation. The results presented in Chapter 5 suggest that TGFβ signalling controls the progression from progenitors to post-mitotic neurons in human MGE-like (NKX2.1$^+$) cells through the modulation of the cell cycle length.

6.2 LHX6-mCherry reporter in the identification of new determinants of human MGE-derived interneurons

In vitro differentiation of MGE-derived cortical interneurons begins with the induction of NKX2.1^{+} neural progenitors. These cells can be produced highly efficiently in this study and previously published works (Maroof et al., 2013; Nicholas et al., 2013; Noakes et al., 2019). However, only a proportion of these NKX2.1+ progenitors seems to progress to LHX6^{+} immature interneurons in my culture. Furthermore, the yield of defined MGE derived interneuron subtypes (SST^{+} of PV^{+}) remains low (Maroof et al., 2013; Nicholas et al., 2013; Noakes et al., 2019; Sun et al., 2016) or the phenotype might not be stable (Colasante et al., 2015). The lack of efficient interneuron differentiation protocol is due largely to our limited understanding on the control of interneuron diversity and subtype fate specification. This limitation is further complicated by the protracted acquisition of subtype identity both in mice (Mukhopadhyay et al., 2009), and during hPSC differentiation (Nicholas et al., 2013).

Given the significance of PV and SST interneurons in neuropsychiatric and neurodegenerative diseases, it is important to develop better paradigms for generating these cells *in vitro* from hPSCs. The optimisation of a differentiation protocol could be achieved by using a high throughput-screening platform that allows the analysis of several potential determinants at the time. The implementation of this screening platform would need the use of a reporter that can be easily detected under the microscope. Since the LHX6-mCherry reporter has been shown to be functional and specific but mCherry signal is too low, then the design and derivation of a second generation reporter that can be directly visualised under the fluorescent microscope holds an enormous potential for the identification of new interneuron determinants. The strategies for deriving a second-generation reporter were discussed in section 4.3.

With regard to potential determinants to be screened, valuable information has become available from recent publications exploiting the use of single-cell RNA-seq technology, and by integration of genetic and genomic data of the genes downstream of Nkx2.1. With respect to single cell RNA-seq studies, the first published data was done by Mayer et al., 2018, where the authors presented evidence of specification of SST^{+} and PV^{+} interneurons in post-mitotic cells within mouse developing MGE at E13.5. These sub-

populations could be identified by the expression of a set of genes whose expression is conserved in adulthood. *Mef2c*, *Erbb4* and *Plcxd3* were proposed as early marker genes for PV^+ interneurons whilst *Sst, Tspan7* and *Satb1* would be early markers for SST^+ neurons (Mayer et al., 2018). In this study the role of *Mef2c* was further investigated. It was found that its conditional deletion caused specific loss of PV^+ interneurons, highlighting this gene as a potential determinant of PV-fate.

Another single cell RNA-seq study was published a few months later, also finding that PV or SST populations can be distinguished as early as E12.5. Mice-MGE cells were identified as an early PV^+ population when expressing *Ccnd2* and *St18*, while the early SST^+ population was marked by the expression of *Epha5*, *Cdk14* and *Maf*. To validate these results, the authors overexpressed *Maf* in the MGE, finding that SST^+ population increased at the expenses of PV^+ (Mi et al., 2018).

Additionally, from the genetic and genomic data presented in Sandberg et al, 2016, a set of genes were identified as potential targets of Lhx6 and Nkx2.1. In this work, a broad analysis of the function of Nkx2.1 was carried out to understand how this transcription factor controls gene networks to guide the development of MGE-derived interneurons. From the information derived from Sandberg's work, I shortlisted possible genes with a role in MGE development following the next criteria. First, I considered genes that the authors reported to be potential targets of Lhx6 and Nkx2.1. Next, I limited to genes whose expression has been documented in the developing MGE and finally, these genes shown to be downregulated in the conditional Nkx2.1 knockout mouse. Based on these criteria, Tgfβ3, Etv1 and Sox6 were highlighted as relevant genes. Another candidate is Nhxp1, since it was described to be expressed in the mantle zone of the MGE at E13.5 and its expression preserved in cortical interneurons (Sandberg et al., 2016). In this thesis, I have begun the investigation of the role of TGFβ signalling in human MGE-like cells, however, it would be interesting to extend the investigation to SOX6, ETV1 and NXPH1.

Even though the above genes have been independently shown to contribute to different developmental stages of cortical interneurons, their ability to instruct interneuron subtypes from hPSCs has not been assayed. For instance, it is known that Sox6 functions downstream of Lhx6 and its loss of function caused a decrease in the number of PV^+ and SST^+ interneurons, defects on interneurons position and maturation that led to an

epileptic phenotype at P15 (Azim et al., 2009; Batista-Brito et al., 2009). ETV1 has been reported not being required for specification or migration of PV interneurons, however seems to have a role on transcriptionally controlling the expression of Kv1.1 (a potassium channel voltage dependent), which lately impacts on the electrophysiological properties of PV interneurons (Dehorter et al., 2015). Less information is available about NXPH1 role in mammalian interneuron development. However, it is known that *nxph1* is expressed in the sub-pallium during zebrafish development and its expression is confined to interneurons. Interestingly, this gene was found to be downregulated in the *mib* (an E3 ubiquitin ligase) zebrafish mutant, which develops seizure activity (Thomas-Jinu and Houart, 2013). Furthermore, *NXPH1* gene was found to be close to a duplication CNV identified in ASD families, consequently suggested as a potential gene of risk for autism (Salyakina et al., 2011).

The above evidence shows involvement of these genes in the development and function of cortical interneurons. Nonetheless, any of these studies have tested whether their over-expression (alone or in combination) can elicit a determinant function of interneuron subtypes. Therefore, developing a system for overexpressing these genes in a second generation LHX6-mCherry reporter will help us to functionally evaluate their potential as determinants of cortical interneuron development.

6.3 Mechanisms and crosstalk of TGFβ signalling in MGE neurogenesis

A deeper analysis of TGFβ mechanisms in the MGE is needed in order to determine whether shared mechanisms converge to mediate its functions in different regions of the brain (Falk et al., 2008; Garcia-Campmany and Marti, 2007; Seoane et al., 2004; Siegenthaler and Miller, 2005). For instance, it is known that TGFβ signalling interacts with Wnt signalling in the dorsal-caudal midbrain in mouse to cooperate in the regulation of proliferation over neuronal differentiation. In this region the inhibition of TGFβ signalling by ablation of Tgfbr2 caused an ectopic expression of Wnt1 and increased β-catenin nuclear accumulation, which through its target Cyclin D1 promoted increased proliferation in neuroprogenitors (Falk et al., 2008). Interestingly WNT/β-Catenin signalling has been recently shown to have a role on the maintenance of the MGE progenitors derived from hPSCs, where the activation of WNT signalling maintain human MGE-like progenitors in an undifferentiated state, while its ablation led to an

early exit of the cell cycle and accelerated neurogenesis (Ma et al., 2019). Future studies should be directed to understand whether the effects, here reported for TGFβ signalling in the human MGE-like neurogenesis are linked to or dependent on WNT signalling.

In addition to the identification of signalling pathways involved in the maintenance of human MGE-like progenitors, a key question that remains to be addressed is whether the manipulation of these signalling pathways influences the acquisition of the interneuron subtype fate. From a plethora of studies concerning the development of MGE-derived cortical interneurons, it is known that there is a highly regulated temporality at which PV or SST interneurons are born. SST^+ have a tendency to be born earlier than PV^+ interneurons (Fertuzinhos et al., 2009; Mayer et al., 2018; Nicholas et al., 2013), hence, the time at which a progenitor exit the cell cycle might determine its competence to become a specific interneuron subtype.

The investigation of a potential interaction between TGFβ and WNT signalling is especially relevant since it was recently reported that Wnt signalling participates on interneuron subtype specification in mice (McKenzie et al., 2019). In this report was shown that Wnt signalling shifts from the regulation of proliferation to specification, the later was mediated by non-canonical Wnt signalling via the activation of Ryk receptor. Interestingly, the canonical pathway was also activated (McKenzie et al., 2019). How these two parallel pathways are regulated and how they might interact with other signals to regulate proliferation, neurogenesis and specification, are questions to address for deciphering how these developmental processes are orchestrated during interneuron differentiation. The understanding of these mechanisms will open the possibility of manipulating these pathways to bias the interneuron subtype of MGE progenitors.

In this thesis, I presented evidence that TGFβ signalling is implicated in the regulation of the progression from progenitors to pots-mitotic neurons in human MGE-like progenitors. This result, along with a previous report showing that the forced exit of the cell cycle of GABAergic progenitors accelerates neuron maturation at electrophysiological level (Telezhkin et al., 2016), raise the question of whether TGFβ signalling could promote cortical interneuron maturation. Indeed, Tgfβr1 mutant has been shown to decrease the number, migration and dendritic arborisation of new-born neurons in adult mouse hippocampus (He et al., 2014); therefore further

characterisation of the effects of TGFβ3 is needed to determine whether this signalling guides interneuron maturation.

The findings reported here provide new contribution to our understanding on the control of neurogenesis of human MGE progenitors. This knowledge may be used to modulate the speed of human interneuron production *in vitro*.

6.4 Conclusions

In this thesis, I successfully generated a functional LHX6-mCherry reporter that could be used for studying the control of human MGE-derived interneuron development. Upon differentiation of the LHX6-mCherry hPSCs, mCherry signal recapitulated LHX6 expression pattern and faithfully labels LHX6^{+} interneurons while showing lineage restriction. These characteristics allowed me to use the reporter to gain insights into the role of TGFβ signalling on MGE-like progenitor's differentiation. I found that this signalling pathway participates in the decision of proliferation versus differentiation of MGE-like progenitors by regulating cell cycle length with no apparent effects on interneuron subtype fate. Ultimately, the reporter line generated in this thesis provides a tool as a screening platform to discover new factors involved in the acquisition of interneuron fate and interneuron-subtype specification.

References

Abellan, A., Menuet, A., Dehay, C., Medina, L., and Retaux, S. (2010). Differential expression of LIM-homeodomain factors in Cajal-Retzius cells of primates, rodents, and birds. Cerebral cortex *20*, 1788-1798.

Aguiar, D.P., Sghari, S., and Creuzet, S. (2014). The facial neural crest controls fore- and midbrain patterning by regulating Foxg1 expression through Smad1 activity. Development *141*, 2494-2505.

Ambasudhan, R., Talantova, M., Coleman, R., Yuan, X., Zhu, S., Lipton, S.A., and Ding, S. (2011). Direct reprogramming of adult human fibroblasts to functional neurons under defined conditions. Cell stem cell *9*, 113-118.

Arai, Y., Pulvers, J.N., Haffner, C., Schilling, B., Nusslein, I., Calegari, F., and Huttner, W.B. (2011). Neural stem and progenitor cells shorten S-phase on commitment to neuron production. Nat Commun *2*, 154.

Arber, C., Precious, S.V., Cambray, S., Risner-Janiczek, J.R., Kelly, C., Noakes, Z., Fjodorova, M., Heuer, A., Ungless, M.A., Rodriguez, T.A.*, et al.* (2015). Activin A directs striatal projection neuron differentiation of human pluripotent stem cells. Development *142*, 1375-1386.

Arif, S.H. (2009). A Ca(2+)-binding protein with numerous roles and uses: parvalbumin in molecular biology and physiology. Bioessays *31*, 410-421.

Azim, E., Jabaudon, D., Fame, R.M., and Macklis, J.D. (2009). SOX6 controls dorsal progenitor identity and interneuron diversity during neocortical development. Nature neuroscience *12*, 1238-1247.

Batista-Brito, R., Rossignol, E., Hjerling-Leffler, J., Denaxa, M., Wegner, M., Lefebvre, V., Pachnis, V., and Fishell, G. (2009). The cell-intrinsic requirement of Sox6 for cortical interneuron development. Neuron *63*, 466-481.

Black, J.B., Adler, A.F., Wang, H.G., D'Ippolito, A.M., Hutchinson, H.A., Reddy, T.E., Pitt, G.S., Leong, K.W., and Gersbach, C.A. (2016). Targeted Epigenetic Remodeling of Endogenous Loci by CRISPR/Cas9-Based Transcriptional Activators Directly Converts Fibroblasts to Neuronal Cells. Cell stem cell *19*, 406-414.

Boergermann, J.H., Kopf, J., Yu, P.B., and Knaus, P. (2010). Dorsomorphin and LDN-193189 inhibit BMP-mediated Smad, p38 and Akt signalling in C2C12 cells. Int J Biochem Cell Biol *42*, 1802-1807.

Brandenberger, R., Wei, H., Zhang, S., Lei, S., Murage, J., Fisk, G.J., Li, Y., Xu, C., Fang, R., Guegler, K.*, et al.* (2004). Transcriptome characterization elucidates signaling networks that control human ES cell growth and differentiation. Nature biotechnology *22*, 707-716.

Brickman, J.M., and Serup, P. (2017). Properties of embryoid bodies. Wiley Interdiscip Rev Dev Biol *6*.

Cai, Y., Zhang, Q., Wang, C., Zhang, Y., Ma, T., Zhou, X., Tian, M., Rubenstein, J.L., and Yang, Z. (2013). Nuclear receptor COUP-TFII-expressing neocortical interneurons are derived from the medial and lateral/caudal ganglionic eminence and define specific subsets of mature interneurons. The Journal of comparative neurology *521*, 479-497.

Cambray, S., Arber, C., Little, G., Dougalis, A.G., de Paola, V., Ungless, M.A., Li, M., and Rodriguez, T.A. (2012). Activin induces cortical interneuron identity and differentiation in embryonic stem cell-derived telencephalic neural precursors. Nat Commun *3*, 841.

Chambers, S.M., Fasano, C.A., Papapetrou, E.P., Tomishima, M., Sadelain, M., and Studer, L. (2009). Highly efficient neural conversion of human ES and iPS cells by dual inhibition of SMAD signaling. Nature biotechnology *27*, 275-280.

Chan, H.Y., V, S., Xing, X., Kraus, P., Yap, S.P., Ng, P., Lim, S.L., and Lufkin, T. (2011). Comparison of IRES and F2A-based locus-specific multicistronic expression in stable mouse lines. PloS one *6*, e28885.

Choudhry, Z., Rikani, A.A., Choudhry, A.M., Tariq, S., Zakaria, F., Asghar, M.W., Sarfraz, M.K., Haider, K., Shafiq, A.A., and Mobassarah, N.J. (2014). Sonic hedgehog signalling pathway: a complex network. Ann Neurosci *21*, 28-31.

Coghlan, S., Horder, J., Inkster, B., Mendez, M.A., Murphy, D.G., and Nutt, D.J. (2012). GABA system dysfunction in autism and related disorders: from synapse to symptoms. Neuroscience and biobehavioral reviews *36*, 2044-2055.

Colasante, G., Lignani, G., Rubio, A., Medrihan, L., Yekhlef, L., Sessa, A., Massimino, L., Giannelli, S.G., Sacchetti, S., Caiazzo, M.*, et al.* (2015). Rapid Conversion of Fibroblasts into Functional Forebrain GABAergic Interneurons by Direct Genetic Reprogramming. Cell Stem Cell *17*, 719-734.

Corbin, J.G., and Butt, S.J. (2011). Developmental mechanisms for the generation of telencephalic interneurons. Developmental neurobiology *71*, 710-732.

Cranfill, P.J., Sell, B.R., Baird, M.A., Allen, J.R., Lavagnino, Z., de Gruiter, H.M., Kremers, G.J., Davidson, M.W., Ustione, A., and Piston, D.W. (2016). Quantitative assessment of fluorescent proteins. Nat Methods *13*, 557-562.

Crawford, T.Q., and Roelink, H. (2007). The notch response inhibitor DAPT enhances neuronal differentiation in embryonic stem cell-derived embryoid bodies independently of sonic hedgehog signaling. Developmental dynamics : an official publication of the American Association of Anatomists *236*, 886-892.

Cruz-Santos, M.C., Aragon-Raygoza, A., Espinal-Centeno, A., Arteaga-Vazquez, M., Cruz-Hernandez, A., Bako, L., and Cruz-Ramirez, A. (2016). The Role of microRNAs in Animal Cell Reprogramming. Stem cells and development *25*, 1035-1049.

Dakhore, S., Nayer, B., and Hasegawa, K. (2018). Human Pluripotent Stem Cell Culture: Current Status, Challenges, and Advancement. Stem cells international *2018*, 7396905.

Danesin, C., Peres, J.N., Johansson, M., Snowden, V., Cording, A., Papalopulu, N., and Houart, C. (2009). Integration of telencephalic Wnt and hedgehog signaling center activities by Foxg1. Developmental cell *16*, 576-587.

Danjo, T., Eiraku, M., Muguruma, K., Watanabe, K., Kawada, M., Yanagawa, Y., Rubenstein, J.L., and Sasai, Y. (2011). Subregional specification of embryonic stem cell-derived ventral telencephalic tissues by timed and combinatory treatment with extrinsic signals. The Journal of neuroscience : the official journal of the Society for Neuroscience *31*, 1919-1933.

Davis-Dusenbery, B.N., Williams, L.A., Klim, J.R., and Eggan, K. (2014). How to make spinal motor neurons. Development *141*, 491-501.

Dehorter, N., Ciceri, G., Bartolini, G., Lim, L., del Pino, I., and Marin, O. (2015). Tuning of fast-spiking interneuron properties by an activity-dependent transcriptional switch. Science *349*, 1216-1220.

Del Pino, I., Garcia-Frigola, C., Dehorter, N., Brotons-Mas, J.R., Alvarez-Salvado, E., Martinez de Lagran, M., Ciceri, G., Gabaldon, M.V., Moratal, D., Dierssen, M.*, et al.* (2013). Erbb4 deletion from fast-spiking interneurons causes schizophrenia-like phenotypes. Neuron *79*, 1152-1168.

DeRosa, B.A., Belle, K.C., Thomas, B.J., Cukier, H.N., Pericak-Vance, M.A., Vance, J.M., and Dykxhoorn, D.M. (2015). hVGAT-mCherry: A novel molecular tool for analysis of GABAergic neurons derived from human pluripotent stem cells. Molecular and cellular neurosciences *68*, 244-257.

Donnelly, M.L.L., Hughes, L.E., Luke, G., Mendoza, H., Ten Dam, E., Gani, D., and Ryan, M.D. (2001). The 'cleavage' activities of foot-and-mouth disease virus 2A site-directed mutants and naturally occurring '2A-like' sequences. J Gen Virol *82*, 1027-1041.

Du, T., Xu, Q., Ocbina, P.J., and Anderson, S.A. (2008). NKX2.1 specifies cortical interneuron fate by activating Lhx6. Development *135*, 1559-1567.

Dvorak, P., Dvorakova, D., Koskova, S., Vodinska, M., Najvirtova, M., Krekac, D., and Hampl, A. (2005). Expression and potential role of fibroblast growth factor 2 and its receptors in human embryonic stem cells. Stem cells *23*, 1200-1211.

Estivill-Torrus, G., Pearson, H., van Heyningen, V., Price, D.J., and Rashbass, P. (2002). Pax6 is required to regulate the cell cycle and the rate of progression from symmetrical to asymmetrical division in mammalian cortical progenitors. Development *129*, 455-466.

Falk, S., Wurdak, H., Ittner, L.M., Ille, F., Sumara, G., Schmid, M.T., Draganova, K., Lang, K.S., Paratore, C., Leveen, P.*, et al.* (2008). Brain area-specific effect of TGF-beta signaling on Wnt-dependent neural stem cell expansion. Cell stem cell *2*, 472-483.

Fertuzinhos, S., Krsnik, Z., Kawasawa, Y.I., Rasin, M.R., Kwan, K.Y., Chen, J.G., Judas, M., Hayashi, M., and Sestan, N. (2009). Selective depletion of molecularly defined cortical interneurons in human holoprosencephaly with severe striatal hypoplasia. Cerebral cortex *19*, 2196-2207.

Filice, F., Vorckel, K.J., Sungur, A.O., Wohr, M., and Schwaller, B. (2016). Reduction in parvalbumin expression not loss of the parvalbumin-expressing GABA interneuron subpopulation in genetic parvalbumin and shank mouse models of autism. Molecular brain *9*, 10.

Fjodorova, M., Noakes, Z., and Li, M. (2015). How to make striatal projection neurons. Neurogenesis *2*, e1100227.

Flames, N., and Marin, O. (2005). Developmental mechanisms underlying the generation of cortical interneuron diversity. Neuron *46*, 377-381.

Fogarty, M., Grist, M., Gelman, D., Marin, O., Pachnis, V., and Kessaris, N. (2007). Spatial genetic patterning of the embryonic neuroepithelium generates GABAergic interneuron diversity in the adult cortex. J Neurosci *27*, 10935-10946.

Fragkouli, A., van Wijk, N.V., Lopes, R., Kessaris, N., and Pachnis, V. (2009). LIM homeodomain transcription factor-dependent specification of bipotential MGE progenitors into cholinergic and GABAergic striatal interneurons. Development *136*, 3841-3851.

Garcia-Campmany, L., and Marti, E. (2007). The TGFbeta intracellular effector Smad3 regulates neuronal differentiation and cell fate specification in the developing spinal cord. Development *134*, 65-75.

Gerrard, L., Rodgers, L., and Cui, W. (2005). Differentiation of human embryonic stem cells to neural lineages in adherent culture by blocking bone morphogenetic protein signaling. Stem cells *23*, 1234-1241.

Goulburn, A.L., Alden, D., Davis, R.P., Micallef, S.J., Ng, E.S., Yu, Q.C., Lim, S.M., Soh, C.L., Elliott, D.A., Hatzistavrou, T.*, et al.* (2011). A targeted NKX2.1 human embryonic stem cell reporter line enables identification of human basal forebrain derivatives. Stem cells *29*, 462-473.

Grigoriou, M., Tucker, A.S., Sharpe, P.T., and Pachnis, V. (1998). Expression and regulation of Lhx6 and Lhx7, a novel subfamily of LIM homeodomain encoding genes, suggests a role in mammalian head development. Development *125*, 2063-2074.

Gurdon, J.B. (1962). The developmental capacity of nuclei taken from intestinal epithelium cells of feeding tadpoles. J Embryol Exp Morphol *10*, 622-640.

Hansen, D.V., Lui, J.H., Flandin, P., Yoshikawa, K., Rubenstein, J.L., Alvarez-Buylla, A., and Kriegstein, A.R. (2013). Non-epithelial stem cells and cortical interneuron production in the human ganglionic eminences. Nature neuroscience *16*, 1576-1587.

He, Y., Zhang, H., Yung, A., Villeda, S.A., Jaeger, P.A., Olayiwola, O., Fainberg, N., and Wyss-Coray, T. (2014). ALK5-dependent TGF-beta signaling is a major determinant of late-stage adult neurogenesis. Nature neuroscience *17*, 943-952.

Hebert, J.M., and Fishell, G. (2008). The genetics of early telencephalon patterning: some assembly required. Nature reviews Neuroscience *9*, 678-685.

Hladnik, A., Dzaja, D., Darmopil, S., Jovanov-Milosevic, N., and Petanjek, Z. (2014). Spatio-temporal extension in site of origin for cortical calretinin neurons in primates. Front Neuroanat *8*, 50.

Hu, H., Cavendish, J.Z., and Agmon, A. (2013). Not all that glitters is gold: off-target recombination in the somatostatin-IRES-Cre mouse line labels a subset of fast-spiking interneurons. Front Neural Circuits *7*, 195.

Hu, J.S., Vogt, D., Lindtner, S., Sandberg, M., Silberberg, S.N., and Rubenstein, J.L.R. (2017a). Coup-TF1 and Coup-TF2 control subtype and laminar identity of MGE-derived neocortical interneurons. Development *144*, 2837-2851.

Hu, J.S., Vogt, D., Sandberg, M., and Rubenstein, J.L. (2017b). Cortical interneuron development: a tale of time and space. Development *144*, 3867-3878.

Huang, S.M., Mishina, Y.M., Liu, S., Cheung, A., Stegmeier, F., Michaud, G.A., Charlat, O., Wiellette, E., Zhang, Y., Wiessner, S.*, et al.* (2009). Tankyrase inhibition stabilizes axin and antagonizes Wnt signalling. Nature *461*, 614-620.

Huse, M., Muir, T.W., Xu, L., Chen, Y.G., Kuriyan, J., and Massague, J. (2001). The TGF beta receptor activation process: an inhibitor- to substrate-binding switch. Mol Cell *8*, 671-682.

Inan, M., Welagen, J., and Anderson, S.A. (2012). Spatial and temporal bias in the mitotic origins of somatostatin- and parvalbumin-expressing interneuron subgroups and the chandelier subtype in the medial ganglionic eminence. Cerebral cortex *22*, 820-827.

Jaeger, I., Arber, C., Risner-Janiczek, J.R., Kuechler, J., Pritzsche, D., Chen, I.C., Naveenan, T., Ungless, M.A., and Li, M. (2011). Temporally controlled modulation of FGF/ERK signaling directs midbrain dopaminergic neural progenitor fate in mouse and human pluripotent stem cells. Development *138*, 4363-4374.

James, D., Levine, A.J., Besser, D., and Hemmati-Brivanlou, A. (2005). TGFbeta/activin/nodal signaling is necessary for the maintenance of pluripotency in human embryonic stem cells. Development *132*, 1273-1282.

Kabadi, A.M., Ousterout, D.G., Hilton, I.B., and Gersbach, C.A. (2014). Multiplex CRISPR/Cas9-based genome engineering from a single lentiviral vector. Nucleic acids research *42*, e147.

Kelsom, C., and Lu, W. (2013). Development and specification of GABAergic cortical interneurons. Cell & bioscience *3*, 19.

Kim, C.H., Oda, T., Itoh, M., Jiang, D., Artinger, K.B., Chandrasekharappa, S.C., Driever, W., and Chitnis, A.B. (2000). Repressor activity of Headless/Tcf3 is essential for vertebrate head formation. Nature *407*, 913-916.

Kim, J.H., Lee, S.R., Li, L.H., Park, H.J., Park, J.H., Lee, K.Y., Kim, M.K., Shin, B.A., and Choi, S.Y. (2011). High cleavage efficiency of a 2A peptide derived from porcine teschovirus-1 in human cell lines, zebrafish and mice. PloS one *6*, e18556.

Kim, T.G., Yao, R., Monnell, T., Cho, J.H., Vasudevan, A., Koh, A., Peeyush, K.T., Moon, M., Datta, D., Bolshakov, V.Y.*, et al.* (2014). Efficient specification of interneurons from human pluripotent stem cells by dorsoventral and rostrocaudal modulation. Stem cells *32*, 1789-1804.

Kretzschmar, K., and Watt, F.M. (2012). Lineage tracing. Cell *148*, 33-45.

Lavdas, A.A., Grigoriou, M., Pachnis, V., and Parnavelas, J.G. (1999). The medial ganglionic eminence gives rise to a population of early neurons in the developing cerebral cortex. The Journal of neuroscience : the official journal of the Society for Neuroscience *19*, 7881-7888.

Le, T.N., Du, G., Fonseca, M., Zhou, Q.P., Wigle, J.T., and Eisenstat, D.D. (2007). Dlx homeobox genes promote cortical interneuron migration from the basal forebrain by direct repression of the semaphorin receptor neuropilin-2. J Biol Chem *282*, 19071-19081.

Li, S., Xue, H., Long, B., Sun, L., Truong, T., and Liu, Y. (2015a). Efficient generation of hiPSC neural lineage specific knockin reporters using the CRISPR/Cas9 and Cas9 double nickase system. Journal of visualized experiments : JoVE, e52539.

Li, S., Xue, H., Wu, J., Rao, M.S., Kim, D.H., Deng, W., and Liu, Y. (2015b). Human Induced Pluripotent Stem Cell NEUROG2 Dual Knockin Reporter Lines Generated by the CRISPR/Cas9 System. Stem cells and development *24*, 2925-2942.

Lim, L., Mi, D., Llorca, A., and Marin, O. (2018). Development and Functional Diversification of Cortical Interneurons. Neuron *100*, 294-313.

Liodis, P., Denaxa, M., Grigoriou, M., Akufo-Addo, C., Yanagawa, Y., and Pachnis, V. (2007). Lhx6 activity is required for the normal migration and specification of cortical interneuron subtypes. The Journal of neuroscience : the official journal of the Society for Neuroscience *27*, 3078-3089.

Liu, W.B., Jiang, X., Han, F., Li, Y.H., Chen, H.Q., Liu, Y., Cao, J., and Liu, J.Y. (2013). LHX6 acts as a novel potential tumour suppressor with epigenetic inactivation in lung cancer. Cell Death Dis *4*, e882.

Liu, Z., Zhang, Z., Lindtner, S., Li, Z., Xu, Z., Wei, S., Liang, Q., Wen, Y., Tao, G., You, Y.*, et al.* (2019). Sp9 Regulates Medial Ganglionic Eminence-Derived Cortical Interneuron Development. Cerebral cortex *29*, 2653-2667.

Lopes, R., Verhey van Wijk, N., Neves, G., and Pachnis, V. (2012). Transcription factor LIM homeobox 7 (Lhx7) maintains subtype identity of cholinergic interneurons in the mammalian striatum. Proceedings of the National Academy of Sciences of the United States of America *109*, 3119-3124.

Ma, L., Wang, Y., Hui, Y., Du, Y., Chen, Z., Feng, H., Zhang, S., Li, N., Song, J., Fang, Y.*, et al.* (2019). WNT/NOTCH Pathway Is Essential for the Maintenance and Expansion of Human MGE Progenitors. Stem cell reports *12*, 934-949.

Ma, T., Wang, C., Wang, L., Zhou, X., Tian, M., Zhang, Q., Zhang, Y., Li, J., Liu, Z., Cai, Y.*, et al.* (2013). Subcortical origins of human and monkey neocortical interneurons. Nature neuroscience *16*, 1588-1597.

Maira, M., Long, J.E., Lee, A.Y., Rubenstein, J.L., and Stifani, S. (2010). Role for TGF-beta superfamily signaling in telencephalic GABAergic neuron development. Journal of neurodevelopmental disorders *2*, 48-60.

Marin, O. (2012). Interneuron dysfunction in psychiatric disorders. Nature reviews Neuroscience *13*, 107-120.

Maroof, A.M., Keros, S., Tyson, J.A., Ying, S.W., Ganat, Y.M., Merkle, F.T., Liu, B., Goulburn, A., Stanley, E.G., Elefanty, A.G.*, et al.* (2013). Directed differentiation and functional maturation of cortical interneurons from human embryonic stem cells. Cell stem cell *12*, 559-572.

Massague, J. (2012). TGFbeta signalling in context. Nat Rev Mol Cell Biol *13*, 616-630.
Mayer, C., Hafemeister, C., Bandler, R.C., Machold, R., Batista Brito, R., Jaglin, X., Allaway, K., Butler, A., Fishell, G., and Satija, R. (2018). Developmental diversification of cortical inhibitory interneurons. Nature *555*, 457-462.

McKenzie, M.G., Cobbs, L.V., Dummer, P.D., Petros, T.J., Halford, M.M., Stacker, S.A., Zou, Y., Fishell, G.J., and Au, E. (2019). Non-canonical Wnt Signaling through Ryk Regulates the Generation of Somatostatin- and Parvalbumin-Expressing Cortical Interneurons. Neuron *103*, 853-864 e854.

Melisi, D., Ishiyama, S., Sclabas, G.M., Fleming, J.B., Xia, Q., Tortora, G., Abbruzzese, J.L., and Chiao, P.J. (2008). LY2109761, a novel transforming growth factor beta receptor type I and type II dual inhibitor, as a therapeutic approach to suppressing pancreatic cancer metastasis. Mol Cancer Ther *7*, 829-840.

Merkle, F.T., Neuhausser, W.M., Santos, D., Valen, E., Gagnon, J.A., Maas, K., Sandoe, J., Schier, A.F., and Eggan, K. (2015). Efficient CRISPR-Cas9-mediated generation of knockin human pluripotent stem cells lacking undesired mutations at the targeted locus. Cell Rep *11*, 875-883.

Meyers, E.A., and Kessler, J.A. (2017). TGF-beta Family Signaling in Neural and Neuronal Differentiation, Development, and Function. Cold Spring Harb Perspect Biol *9*.

Mi, D., Li, Z., Lim, L., Li, M., Moissidis, M., Yang, Y., Gao, T., Hu, T.X., Pratt, T., Price, D.J., *et al.* (2018). Early emergence of cortical interneuron diversity in the mouse embryo. Science *360*, 81-85.

Minskaia, E., and Ryan, M.D. (2013). Protein coexpression using FMDV 2A: effect of "linker" residues. Biomed Res Int *2013*, 291730.

Mo, Z., and Zecevic, N. (2008). Is Pax6 critical for neurogenesis in the human fetal brain? Cerebral cortex *18*, 1455-1465.

Mukhopadhyay, A., McGuire, T., Peng, C.Y., and Kessler, J.A. (2009). Differential effects of BMP signaling on parvalbumin and somatostatin interneuron differentiation. Development *136*, 2633-2642.

Murry, C.E., and Keller, G. (2008). Differentiation of embryonic stem cells to clinically relevant populations: lessons from embryonic development. Cell *132*, 661-680.

Nicholas, C.R., Chen, J., Tang, Y., Southwell, D.G., Chalmers, N., Vogt, D., Arnold, C.M., Chen, Y.J., Stanley, E.G., Elefanty, A.G., *et al.* (2013). Functional maturation of hPSC-derived forebrain interneurons requires an extended timeline and mimics human neural development. Cell stem cell *12*, 573-586.

Noakes, Z., Keefe, F., Tamburini, C., Kelly, C.M., Cruz Santos, M., Dunnett, S.B., Errington, A.C., and Li, M. (2019). Human Pluripotent Stem Cell-Derived Striatal Interneurons: Differentiation and Maturation In Vitro and in the Rat Brain. Stem cell reports *12*, 191-200.

Nobrega-Pereira, S., Kessaris, N., Du, T., Kimura, S., Anderson, S.A., and Marin, O. (2008). Postmitotic Nkx2-1 controls the migration of telencephalic interneurons by direct repression of guidance receptors. Neuron *59*, 733-745.

Nolbrant, S., Heuer, A., Parmar, M., and Kirkeby, A. (2017). Generation of high-purity human ventral midbrain dopaminergic progenitors for in vitro maturation and intracerebral transplantation. Nat Protoc *12*, 1962-1979.

Nowakowski, R.S., Lewin, S.B., and Miller, M.W. (1989). Bromodeoxyuridine immunohistochemical determination of the lengths of the cell cycle and the DNA-synthetic phase for an anatomically defined population. J Neurocytol *18*, 311-318.

Nusslein-Volhard, C., and Wieschaus, E. (1980). Mutations affecting segment number and polarity in Drosophila. Nature *287*, 795-801.

Oda, Y. (1999). Choline acetyltransferase: the structure, distribution and pathologic changes in the central nervous system. Pathol Int *49*, 921-937.

Pera, E.M., Acosta, H., Gouignard, N., Climent, M., and Arregi, I. (2014). Active signals, gradient formation and regional specificity in neural induction. Experimental cell research *321*, 25-31.

Pham, C.T., MacIvor, D.M., Hug, B.A., Heusel, J.W., and Ley, T.J. (1996). Long-range disruption of gene expression by a selectable marker cassette. Proc Natl Acad Sci U S A *93*, 13090-13095.

Porter, J.A., Ekker, S.C., Park, W.J., von Kessler, D.P., Young, K.E., Chen, C.H., Ma, Y., Woods, A.S., Cotter, R.J., Koonin, E.V.*, et al.* (1996a). Hedgehog patterning activity: role of a lipophilic modification mediated by the carboxy-terminal autoprocessing domain. Cell *86*, 21-34.

Porter, J.A., Young, K.E., and Beachy, P.A. (1996b). Cholesterol modification of hedgehog signaling proteins in animal development. Science *274*, 255-259.

Reubinoff, B.E., Pera, M.F., Fong, C.Y., Trounson, A., and Bongso, A. (2000). Embryonic stem cell lines from human blastocysts: somatic differentiation in vitro. Nature biotechnology *18*, 399-404.

Rojas-Fernandez, A., Herhaus, L., Macartney, T., Lachaud, C., Hay, R.T., and Sapkota, G.P. (2015). Rapid generation of endogenously driven transcriptional reporters in cells through CRISPR/Cas9. Scientific reports *5*, 9811.

Ruiz i Altaba, A., Palma, V., and Dahmane, N. (2002). Hedgehog-Gli signalling and the growth of the brain. Nature reviews Neuroscience *3*, 24-33.

Sakuma, T., Nishikawa, A., Kume, S., Chayama, K., and Yamamoto, T. (2014). Multiplex genome engineering in human cells using all-in-one CRISPR/Cas9 vector system. Scientific reports *4*, 5400.

Salyakina, D., Cukier, H.N., Lee, J.M., Sacharow, S., Nations, L.D., Ma, D., Jaworski, J.M., Konidari, I., Whitehead, P.L., Wright, H.H.*, et al.* (2011). Copy number variants in extended autism spectrum disorder families reveal candidates potentially involved in autism risk. PloS one *6*, e26049.

Sandberg, M., Flandin, P., Silberberg, S., Su-Feher, L., Price, J.D., Hu, J.S., Kim, C., Visel, A., Nord, A.S., and Rubenstein, J.L.R. (2016). Transcriptional Networks Controlled by NKX2-1 in the Development of Forebrain GABAergic Neurons. Neuron *91*, 1260-1275.

Scacheri, P.C., Crabtree, J.S., Novotny, E.A., Garrett-Beal, L., Chen, A., Edgemon, K.A., Marx, S.J., Spiegel, A.M., Chandrasekharappa, S.C., and Collins, F.S. (2001). Bidirectional transcriptional activity of PGK-neomycin and unexpected embryonic lethality in heterozygote chimeric knockout mice. Genesis *30*, 259-263.

Scarff, K.L., Ung, K.S., Sun, J., and Bird, P.I. (2003). A retained selection cassette increases reporter gene expression without affecting tissue distribution in SPI3 knockout/GFP knock-in mice. Genesis *36*, 149-157.

Seoane, J., Le, H.V., Shen, L., Anderson, S.A., and Massague, J. (2004). Integration of Smad and forkhead pathways in the control of neuroepithelial and glioblastoma cell proliferation. Cell *117*, 211-223.

Shi, Y., and Massague, J. (2003). Mechanisms of TGF-beta signaling from cell membrane to the nucleus. Cell *113*, 685-700.

Shi, Z., Zhang, J., Chen, S., Li, Y., Lei, X., Qiao, H., Zhu, Q., Hu, B., Zhou, Q., and Jiao, J. (2016). Conversion of Fibroblasts to Parvalbumin Neurons by One Transcription Factor, Ascl1, and the Chemical Compound Forskolin. The Journal of biological chemistry *291*, 13560-13570.

Siegenthaler, J.A., and Miller, M.W. (2005). Transforming growth factor beta 1 promotes cell cycle exit through the cyclin-dependent kinase inhibitor p21 in the developing cerebral cortex. The Journal of neuroscience : the official journal of the Society for Neuroscience *25*, 8627-8636.

Sinha, S., and Chen, J.K. (2006). Purmorphamine activates the Hedgehog pathway by targeting Smoothened. Nat Chem Biol *2*, 29-30.

Spella, M., Kyrousi, C., Kritikou, E., Stathopoulou, A., Guillemot, F., Kioussis, D., Pachnis, V., Lygerou, Z., and Taraviras, S. (2011). Geminin regulates cortical progenitor proliferation and differentiation. Stem cells *29*, 1269-1282.

Spits, C., Mateizel, I., Geens, M., Mertzanidou, A., Staessen, C., Vandeskelde, Y., Van der Elst, J., Liebaers, I., and Sermon, K. (2008). Recurrent chromosomal abnormalities in human embryonic stem cells. Nature biotechnology *26*, 1361-1363.

Steinhart, Z., and Angers, S. (2018). Wnt signaling in development and tissue homeostasis. Development *145*.

Streit, A., Berliner, A.J., Papanayotou, C., Sirulnik, A., and Stern, C.D. (2000). Initiation of neural induction by FGF signalling before gastrulation. Nature *406*, 74-78.

Sun, A.X., Yuan, Q., Tan, S., Xiao, Y., Wang, D., Khoo, A.T., Sani, L., Tran, H.D., Kim, P., Chiew, Y.S.*, et al.* (2016). Direct Induction and Functional Maturation of Forebrain GABAergic Neurons from Human Pluripotent Stem Cells. Cell Rep *16*, 1942-1953.

Sussel, L., Marin, O., Kimura, S., and Rubenstein, J.L. (1999). Loss of Nkx2.1 homeobox gene function results in a ventral to dorsal molecular respecification within the basal telencephalon: evidence for a transformation of the pallidum into the striatum. Development *126*, 3359-3370.

Taapken, S.M., Nisler, B.S., Newton, M.A., Sampsell-Barron, T.L., Leonhard, K.A., McIntire, E.M., and Montgomery, K.D. (2011). Karotypic abnormalities in human induced pluripotent stem cells and embryonic stem cells. Nature biotechnology *29*, 313-314.

Takahashi, K., and Yamanaka, S. (2006). Induction of pluripotent stem cells from mouse embryonic and adult fibroblast cultures by defined factors. Cell *126*, 663-676.

Tao, Y., and Zhang, S.C. (2016). Neural Subtype Specification from Human Pluripotent Stem Cells. Cell stem cell *19*, 573-586.

Telezhkin, V., Schnell, C., Yarova, P., Yung, S., Cope, E., Hughes, A., Thompson, B.A., Sanders, P., Geater, C., Hancock, J.M*., et al.* (2016). Forced cell cycle exit and modulation of GABAA, CREB, and GSK3beta signaling promote functional maturation of induced pluripotent stem cell-derived neurons. Am J Physiol Cell Physiol *310*, C520-541.

Thomas-Jinu, S., and Houart, C. (2013). Dynamic expression of neurexophilin1 during zebrafish embryonic development. Gene expression patterns : GEP *13*, 395-401.

Thomas, K.R., Deng, C., and Capecchi, M.R. (1992). High-fidelity gene targeting in embryonic stem cells by using sequence replacement vectors. Molecular and cellular biology *12*, 2919-2923.

Thomas, K.R., Folger, K.R., and Capecchi, M.R. (1986). High frequency targeting of genes to specific sites in the mammalian genome. Cell *44*, 419-428.

Thomson, J.A., Itskovitz-Eldor, J., Shapiro, S.S., Waknitz, M.A., Swiergiel, J.J., Marshall, V.S., and Jones, J.M. (1998). Embryonic stem cell lines derived from human blastocysts. Science *282*, 1145-1147.

Tischfield, D.J., Kim, J., and Anderson, S.A. (2017). Atypical PKC and Notch Inhibition Differentially Modulate Cortical Interneuron Subclass Fate from Embryonic Stem Cells. Stem cell reports *8*, 1135-1143.

Tremblay, R., Lee, S., and Rudy, B. (2016). GABAergic Interneurons in the Neocortex: From Cellular Properties to Circuits. Neuron *91*, 260-292.

Tyson, J.A., Goldberg, E.M., Maroof, A.M., Xu, Q., Petros, T.J., and Anderson, S.A. (2015). Duration of culture and sonic hedgehog signaling differentially specify PV versus SST cortical interneuron fates from embryonic stem cells. Development *142*, 1267-1278.

Vieira, C., Pombero, A., Garcia-Lopez, R., Gimeno, L., Echevarria, D., and Martinez, S. (2010). Molecular mechanisms controlling brain development: an overview of neuroepithelial secondary organizers. The International journal of developmental biology *54*, 7-20.

Vierbuchen, T., Ostermeier, A., Pang, Z.P., Kokubu, Y., Sudhof, T.C., and Wernig, M. (2010). Direct conversion of fibroblasts to functional neurons by defined factors. Nature *463*, 1035-1041.

Vogt, D., Hunt, R.F., Mandal, S., Sandberg, M., Silberberg, S.N., Nagasawa, T., Yang, Z., Baraban, S.C., and Rubenstein, J.L. (2014). Lhx6 directly regulates Arx and CXCR7 to determine cortical interneuron fate and laminar position. Neuron *82*, 350-364.

Wamsley, B., and Fishell, G. (2017). Genetic and activity-dependent mechanisms underlying interneuron diversity. Nature reviews Neuroscience *18*, 299-309.

Wang, Y., Dye, C.A., Sohal, V., Long, J.E., Estrada, R.C., Roztocil, T., Lufkin, T., Deisseroth, K., Baraban, S.C., and Rubenstein, J.L. (2010). Dlx5 and Dlx6 regulate the development

of parvalbumin-expressing cortical interneurons. The Journal of neuroscience : the official journal of the Society for Neuroscience *30*, 5334-5345.

Wang, Y., Wang, F., Wang, R., Zhao, P., and Xia, Q. (2015). 2A self-cleaving peptide-based multi-gene expression system in the silkworm Bombyx mori. Scientific reports *5*, 16273.
Wilmut, I., Schnieke, A.E., McWhir, J., Kind, A.J., and Campbell, K.H. (1997). Viable offspring derived from fetal and adult mammalian cells. Nature *385*, 810-813.

Wilson, S.W., and Houart, C. (2004). Early steps in the development of the forebrain. Developmental cell *6*, 167-181.

Wohr, M., Orduz, D., Gregory, P., Moreno, H., Khan, U., Vorckel, K.J., Wolfer, D.P., Welzl, H., Gall, D., Schiffmann, S.N*., et al.* (2015). Lack of parvalbumin in mice leads to behavioral deficits relevant to all human autism core symptoms and related neural morphofunctional abnormalities. Translational psychiatry *5*, e525.

Wonders, C.P., Taylor, L., Welagen, J., Mbata, I.C., Xiang, J.Z., and Anderson, S.A. (2008). A spatial bias for the origins of interneuron subgroups within the medial ganglionic eminence. Developmental biology *314*, 127-136.

Xu, Q., Cobos, I., De La Cruz, E., Rubenstein, J.L., and Anderson, S.A. (2004). Origins of cortical interneuron subtypes. The Journal of neuroscience : the official journal of the Society for Neuroscience *24*, 2612-2622.

Xu, Q., Wonders, C.P., and Anderson, S.A. (2005). Sonic hedgehog maintains the identity of cortical interneuron progenitors in the ventral telencephalon. Development *132*, 4987-4998.

Xue, H., Wu, S., Papadeas, S.T., Spusta, S., Swistowska, A.M., MacArthur, C.C., Mattson, M.P., Maragakis, N.J., Capecchi, M.R., Rao, M.S*., et al.* (2009). A targeted neuroglial reporter line generated by homologous recombination in human embryonic stem cells. Stem cells *27*, 1836-1846.

Yamaguchi, T.P. (2001). Heads or tails: Wnts and anterior-posterior patterning. Curr Biol *11*, R713-724.

Yang, H., Ganguly, A., and Cabral, F. (2010). Inhibition of cell migration and cell division correlates with distinct effects of microtubule inhibiting drugs. The Journal of biological chemistry *285*, 32242-32250.

Ypsilanti, A.R., and Rubenstein, J.L. (2016). Transcriptional and epigenetic mechanisms of early cortical development: An examination of how Pax6 coordinates cortical development. The Journal of comparative neurology *524*, 609-629.

Zhu, Z., Verma, N., Gonzalez, F., Shi, Z.D., and Huangfu, D. (2015). A CRISPR/Cas-Mediated Selection-free Knockin Strategy in Human Embryonic Stem Cells. Stem cell reports *4*, 1103-1111.

Zwaka, T.P., and Thomson, J.A. (2003). Homologous recombination in human embryonic stem cells. Nature biotechnology *21*, 319-321.